PB83-145318

NSF/CEE-82044

STRUCTURAL RESEARCH STUDIES
Department of Civil Engineering

MOMENT-ROTATION CHARACTERISTICS OF SEMI-RIGID STEEL BEAM-COLUMN CONNECTIONS

by
W.G. Altman, Jr.
A. Azizinamini
J.H. Bradburn
and
J.B. Radziminski

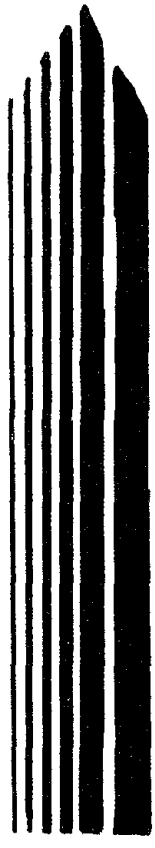

A REPORT OF AN INVESTIGATION CONDUCTED
by
THE DEPARTMENT OF CIVIL ENGINEERING
UNIVERSITY OF SOUTH CAROLINA

Supported by
EARTHQUAKE HAZARD MITIGATION PROGRAM
DIVISION OF CIVIL AND ENVIRONMENTAL ENGINEERING
NATIONAL SCIENCE FOUNDATION
Grant No. PFR - 7923520

UNIVERSITY OF SOUTH CAROLINA
COLUMBIA, SOUTH CAROLINA
JUNE, 1982

Final Report

MOMENT-ROTATION CHARACTERISTICS

OF

SEMI-RIGID STEEL BEAM-COLUMN CONNECTIONS

by

W. G. Altman, Jr.
A. Azizinamini
J. H. Bradburn
and
J. B. Radziminski

A Report of an Investigation Conducted
by

The Civil Engineering Department
University of South Carolina

supported by
Earthquake Hazards Mitigation Program
Division of Civil and Environmental Engineering
National Science Foundation
Grant No. PFR-79-23520

University of South Carolina
Columbia, South Carolina
June 1982

50272-101

REPORT DOCUMENTATION PAGE	1. REPORT NO. NSF/CEE-82044	2.	3. Recipient's Accession No. PB83 145318
4. Title and Subtitle Moment-Rotation Characteristics of Semi-Rigid Steel Beam-Column Connections, 1982 Final Report			5. Report Date June 1982 6.
7. Author(s) W.G. Altman, Jr., A. Azizinamini, J.H. Bradburn, J.B. Radziminski			8. Performing Organization Rept. No.
9. Performing Organization Name and Address University of South Carolina Department of Civil Engineering Columbia, SC 29208			10. Project/Task/Work Unit No. 11. Contract(C) or Grant(G) No. (C) (G) PFR7923520
12. Sponsoring Organization Name and Address Directorate for Engineering (ENG) National Science Foundation 1800 G Street, N.W. Washington, DC 20550			13. Type of Report & Period Covered 14.

15. Supplementary Notes
Submitted by: Communications Program (OPRM)
National Science Foundation
Washington, DC 20550

16. Abstract (Limit: 200 words)

The potential of semi-rigid beam-to-column connections in contributing to the integrity of steel frame building structures in an earthquake was evaluated. Experimental studies were conducted of bolted connections comprised of top and seat beam flange angles and double web angles to determine moment-rotation behavior under static loading and to measure energy absorption capability under cyclic loading. The cyclic tests consisted of subjecting the beam-column connections to several stages of full reversal, controlled amplitude displacements of progressively increasing magnitude. The connections exhibited ductile behavior, with generally stable moment-rotation hysteresis loops being established at each displacement amplitude up to the time that testing was discontinued. The tests culminated in the formation and subsequent propagation of fatigue cracks at the toe of the fillet in one or more of the beam flange angles. The cycle tests have demonstrated that the effectiveness of beam-to-column connections under seismically induced loading may be limited by low-cycle fatigue of the connection elements.

17. Document Analysis a. Descriptors

Earthquakes
Buildings
Beams (supports)
Columns (supports)
Joints (junctions)
Flanges
Steel construction
Earthquake resistant structures
Cyclic loads
Structural analysis

b. Identifiers/Open-Ended Terms

Gound motion

J.B. Radziminski, /PI

c. COSATI Field/Group

18. Availability Statement	19. Security Class (This Report)	21. No. of Pages
NTIS	20. Security Class (This Page)	22. Price

ABSTRACT

The purpose of the investigation has been to evaluate the potential of semi-rigid beam to column connections in contributing to the integrity of steel frame building structures in an earthquake environment. Experimental studies were conducted of bolted connections comprised of top and seat beam flange angles, and double web angles, to determine moment-rotation behavior under monotonic (static) loading, and to measure energy absorption capability under cyclic loading. From the static tests, geometric parameters which affect connection performance have been quantified, and compared with analytical models formulated to predict the initial stiffness and complete non-linear response of the connections.

The cyclic tests consisted of subjecting the beam-column connections to several stages of full reversal, controlled amplitude displacements of progressively increasing magnitude. The connections exhibited ductile behavior, with generally stable moment-rotation hysteresis loops being established at each displacement amplitude up to the time that testing was discontinued. The tests culminated in the formation and subsequent propagation of fatigue cracks at the toe of the fillet in one or more of the beam flange angles. The cyclic tests have demonstrated that the effectiveness, under seismically induced loading, of connections of the type studied herein may be limited by low-cycle fatigue of the connection elements.

TABLE OF CONTENTS

Page

I. INTRODUCTION.....1

1.1 Background, Research Objectives.....1
1.2 Scope of Investigation.....2
1.3 Acknowledgements.....4

II. DESCRIPTION OF TEST PROGRAM.....6

2.1 Materials.....6
2.2 Description of Test Specimens.....6
2.3 Testing Equipment and Test Procedures.....8

2.3.1 Static Tests.....9
2.3.2 Cyclic Tests.....11

III. EXPERIMENTAL INVESTIGATION.....14

3.1 Static Tests.....14

3.1.1 Scope of Investigation.....14
3.1.2 Tests Results.....15
3.1.3 Discussion of Static Test Results...19
3.1.4 Summary of Static Test Results.....27

3.2 Cyclic Tests.....28

3.2.1 Scope of Investigation.....28
3.2.2 Test Results.....28

3.2.2.1 Specimen 14C1.....30
3.2.2.2 Specimen 14C2.....31
3.2.2.3 Specimen 8C1.....32
3.2.2.4 Specimen 8C2.....33

3.2.3 Discussion of Moment-Rotation Hysteresis Loops.....34
3.2.4 Connection Hysteretic Energy Capacity.....39

IV. ANALYTICAL INVESTIGATION.....41

4.1 Static Tests.....41

4.1.1 Models of Beam-Column Connections.....41

4.1.1.1 Beam Models for Initial Stiffness.....41
4.1.1.2 Modified Beam Models for Complete Moment-Rotation Prediction.....46
4.1.1.3 Two Dimensional Finite Element Model.....48
4.1.1.4 Dual Spring Model.....49
4.1.1.5 Three Dimensional Finite Element Model.....50
4.1.1.6 Empirical Model.....51

4.1.2 Prediction of Moment-Rotation Behavior.....54

4.1.2.1 Initial Stiffness.....54
4.1.2.2 Post-Elastic Behavior.....55

4.2 Cyclic Tests.....60

4.2.1 Spring-Rigid Region Model for Cyclic M-ϕ Curve.....60
4.2.2 Tri-Linear Model for Cyclic M-ϕ Curve.....62

V. SUMMARY AND CONCLUSIONS.....64

5.1 Static Tests.....64
5.2 Cyclic Tests.....66

REFERENCES.....69

APPENDIX A Nomenclature.....73

APPENDIX B Three Dimensional Finite Element Model...77

TABLES.....81

FIGURES.....91

LIST OF TABLES

Table		Page
2.1	Mechanical Properties of Test Material	81
2.2	Schedule of Test Specimens	82
3.1	Summary of Static Test Results	83
3.2	Summary of Cyclic Test Results - Specimen 14C1	84
3.3	Summary of Cyclic Test Results - Specimen 14C2	86
3.4	Summary of Cyclic Test Results - Specimen 8C1	88
3.5	Summary of Cyclic Test Results - Specimen 8C2	89
4.1	Comparison of Initial Stiffness Predicted by Model II with Test Results	90

LIST OF FIGURES

Figure		Page
2.1	General Configurations of Test Specimens	91
2.2	Details of Connection for W8X21 Beam	92
2.3	Details of Connection for W14X38 Beam	93
2.4	Schematic of Loading System for Test Beams	94
2.5	Beam Supports for Test Specimens	95
2.6	Lateral Support System for Test Specimens	96
2.7	Loading Frame and Test Set-Up	97
2.8	Close-Up of Test Connection	97
2.9	Schematic of Testing and Recording Equipment	98
2.10	Location of Strain Gages on Tension Flange Angles	99
2.11	LVDT Mounting Apparatus	100
2.12	Typical Time-Displacement History for Cyclic Tests	101
3.1	Comparison of Moment-Rotation Curves Obtained from LVDT Measurements with Curve Obtained from Actuator Displacements	102
3.2	Data from Strain Gage Recordings - Specimen 14S2	103
3.3	Rotation of Beam Relative to Stub Column - Static Loading	104
3.4	Deformation Patterns in Beam-Column Connection Elements	105
3.5	Flange Angle from Specimen 14S2 After Test	106
3.6	Web Angles from Specimen 14S2 After Test	106
3.7	Effect of Flange Angle Thickness on Static Moment-Rotation Behavior - W14X38 Beam Connection	107
3.8	Effect of Web Angle Thickness on Static Moment-Rotation Behavior - W14X38 Beam Connection	108
3.9	Effect of Web Angle Length on Static Moment-Rotation Behavior - W14X38 Beam Connection	109
3.10a	Effect of Flange Angle Thickness on Static Moment-Rotation Behavior - W8X21 Beam Connection (Angle Gage = 2")	110
3.10b	Effect of Flange Angle Thickness on Static Moment-Rotation Behavior - W8X21 Beam Connection (Angle Gage = 2 1/2")	111
3.11a	Effect of Flange Angle Gage on Static Moment-Rotation Behavior - W8X21 Beam Connection (Angle Thickness = 3/8")	112

3.11b Effect of Flange Angle Gage on Static Moment-Rotation Behavior - W8X21 Beam Connection (Angle Thickness = 5/16").....113
3.12 Effect of Flange Angle Length on Static Moment-Rotation Behavior - W8X21 Beam Connection.....114
3.13 Comparison of Static Moment-Rotation Behavior of W14X38 and W8X21 Beam Connections.....115
3.14 Flange Angle from Specimen 14C1 after Cyclic Test.....116
3.15 Flange and Web Angles from Specimen 14C1 after Cyclic Test.....117
3.16 Stable Hysteresis Loops for Specimen 14C1.....118
3.17 Stable Hysteresis Loops for Specimen 14C2.....119
3.18 Stable Hysteresis Loops for Specimen 8C1.....120
3.19 Stable Hysteresis Loops for Specimen 8C2.....121
3.20 Typical Moment-Rotation Hysteresis Loop - Cyclic Tests.....122
3.21 Typical Time - Actuator Displacement Cycle.....122
3.22 Configurations of Connection During One-Half Cycle.....123
4.1a Assumed Behavior of Beam-to-Column Connection..124
4.1b Beam Model for Web Angles.....125
4.2a Idealized Beam Model for Flange Angle.....126
4.2b Idealized Beam Model for Web Angles.....126
4.3 Refined Beam Model for Flange Angle.....127
4.4 Refined Beam Model for Web Angles.....127
4.5 Assumed Material Behavior for Model III.....128
4.6 Model IV - Plane Stres Finite Element Model....128
4.7 Load Versus Displacement Curve for Flange Angle for Model IV.....129
4.8 Model V - Dual Spring Model.....129
4.9 Half Model of Beam-to-Column Connection Model VI.....130
4.10 Moment-Rotation Curves for Two Values of The Parameter P_i.....131
4.11 Relationship Between Beam Shear, F, and Relative End Displacement, Δ, for Flange and Web Angles.....131
4.12 Comparison of Model III and Model IV with Test Results for Specimen 14S2.....132
4.13 Results of Model V Analysis of Specimen 14S2 Flange Angle.....133
4.14 Overall Connection Model Using Model V for Analysis by ANSYS.....134
4.15 Comparison of Test Results with Moment-Rotation Behavior Predicted by Model V.....135

4.16 Comparison of Test Results with Moment-Rotation Behavior Predicted by Model VI.....135
4.17a Comparison of Model VII with Test Results for Specimen 14S1.....136
4.17b Comparison of Model VII with Test Results for Specimen 14S2.....137
4.17c Comparison of Model VII with Test Results for Specimen 14S4.....138
4.17d Comparison of Model VII with Test Results for Specimen 8S1.....139
4.17e Comparison of Model VII with Test Results for Specimen 8S2.....140
4.17f Comparison of Model VII with Test Results for Specimen 8S3.....141
4.17g Comparison of Model VII with Test Results for Specimen 8S7.....142
4.17h Comparison of Model VII with Test Results for Specimen 8S5.....143
4.17i Comparison of Model VII with Test Results for Specimen 8S6.....144
4.18 Tri-Linearized Moment-Rotation Hysteresis Loop.....145
4.19 Comparison of Tri-linearized Hysteresis Loop with Specimen 14C2 Test Results.....146

I. INTRODUCTION

1.1 Background, Research Objectives

The satisfactory performance of ductile, moment-resisting steel frame building structures in an earthquake environment has been well established. The integrity of such structures is dependent upon the ability of the beam-to-column connections to provide the rigid frame behavior and attendant energy absorption capacity necessary to resist the seismically induced lateral forces. Considerable experimental evidence has been generated on the static and cyclic moment-rotation characteristics of rigid connections, (1-31) which has demonstrated that they provide adequate strength and ductility to insure the required performance of the structural system. Similar documentation is available on the behavior of flexible connections (32-35) commonly referred to as "simple framing."

It is common practice, particularly in certain low seismic risk areas of the United States, to utilize A.I.S.C. Type 2 construction in building design. The beam-column connections are considered, for design purposes, to be flexible under gravity loading, and are required to develop only enough moment capacity to provide resistance to lateral forces (36). It is easily recognized, however, that such framing systems may be appropriately considered as being comprised of "semi-rigid" connections, which continuously transfer both shear and moment as loading progresses. Recently, concern has been expressed regarding the adequacy of buildings constructed with this framing scheme if subjected to a moderate or severe earthquake.

Interest has been expressed (37-41), also, in the applicability of semi-rigid beam-column connections for providing a quantifiable degree of energy absorption during seismic loading, whether used in new construction (perhaps to assist a braced frame system after yield) or in retrofitting

older structures built to less stringent earthquake code provisions than those now in force or proposed for the future. Several recent studies have been reported (41-49) which are devoted to examination of the effect of connection flexibility on the static and seismic response of complete structural systems. The analytical predictions of frame behavior are typically based on assumed non-linear mathematical models of the beam-column connections. However, there has been a notable lack of experimental data available to substantiate the appropriateness of the mathematical models used for semi-rigid connections, particularly those utilizing high-strength bolted connection elements.

The objective of the research program reported herein has been to experimentally determine the moment-rotation performance of semi-rigid bolted beam-column connections under static (monotonic) and cyclic loadings. Specifically, the effect of varying the stiffnesses of the various connection elements on the static response of the connections, and on their hysteretic response under cyclic controlled displacement loading, has been studied. From these tests, the significant material and geometric parameters affecting the connection behavior are identified, and used to formulate models of the non-linear connection moment-rotation response.

1.2 Scope of Investigation

The connections tested in this investigation have consisted of top and seat angles bolted to the flanges of the beams and supporting column stub, together with web angles bolted to the beam web and column flange. This type of semi-rigid connection was selected because of the inherent ductility offered by the flexural deformation capabilities of both the flange and web angles in the legs attached to the column.

The top and seat angles were the same for a given test, and the web

angles were centered on the beam; thus symmetrical behavior of the connection was promoted in the full reversal cyclic tests. ASTM A36 steel was used for the members and connection elements; the fasteners were 3/4-inch diameter, ASTM A325 high-strength bolts. A pair of duplicate specimens was tested simultaneously by framing the beams into a centrally-loaded stub column.

A total of 11 members were tested under monotonic loading to obtain static moment-rotation relationships. Four of these test members were framed to W14X38 beam sections and a W12X96 stub column; the remaining seven specimens were bolted to W8X21 beam sections and a W12X58 column stub. For the top and seat (flange) angles, the thickness, length, and gage (in the legs attached to the column flange) were varied, together with beam depth, to effect connections of varying stiffness. Variations in the thickness and length of the web angles were investigated also. The results of these tests were used to quantify the effect of the test variables on the non-linear moment-rotation behavior of the connections, and to establish semi-empirical models of connection response. The data are compared also, to predictions of moment-rotation behavior using finite element models of the connections.

A total of four members were tested under cyclic (quasi-static) loading; two of the specimens included the W14X38 beam sections and two members used the W8X21 sections. For each of the beam sizes, two thicknesses of the top and bottom flange angles were tested. The cyclic tests were conducted using full reversal of controlled displacement to approximate the moment reversals that may be exhibited by beam-column connections during an earthquake. The test procedure consisted of cycling sinusoidally between gradually increasing limits of controlled displacement in a block loading pattern. The hysteretic responses of the connections

were monitored locally using LVDT's mounted between the beam flanges, and compared with moment-rotation curves calculated from overall load-displacment data. Stabilized cyclic hysteresis loops for each displacement amplitude are reported and compared for the test members investigated. For the cyclic studies, testing was discontinued with the appearance of extensive fatigue cracking in the flange angles and corresponding gradual loss of connection load-carrying capability.

1.3 Acknowledgements

The tests reported in this study are from an investigation conducted in the Civil Engineering Department of the University of South Carolina, Columbia, South Carolina. This material is based upon work supported by the National Science Foundation under Grant No. PFR-79-23520. Any opinions, findings, and conclusions or recommendations expressed in this publication are those of the authors and do not necessarily reflect the views of the National Science Foundation.

The investigation was conducted under the supervision of Dr. J. B. Radziminski, Professor, and Dr. J. H. Bradburn, Associate Professor, of the Civil Engineering Department. The testing programs and associated research studies were conducted by W. G. Altman, Jr., A. Azizinamini, and T. Koudelka, Research Assistants in Civil Engineering.

Guidance in the direction of the testing program was provided by an advisory committee comprised of T. C. Carson, Jr., A. K. Courtney, and R. L. Whitaker, practicing structural engineers in South Carolina. Additional advice concerning the scope of the investigation, provided by Dr. J. B. Scalzi of the National Science Foundation and Dr. E. P. Popov of the University of California, Berkeley, is gratefully acknowledged.

The authors wish to express their appreciation to H. Mullinax, G. Dowdey, and B. Ward, laboratory technicians in the College of Engineering, for the fabrication of the beam supports used in the testing program, for help in the machining of the test members, and for the fabrication of instrumentation devices used in data acquisition. Special thanks are extended to Ms. M. Butterworth for the careful typing of this final report.

II. DESCRIPTION OF TEST PROGRAM

2.1 Materials

The material for all of the test specimens, including beam sections, stub columns, and framing angles, was specified to be ASTM A36 steel, supplied by two local fabricators. The mechanical properties obtained from selected coupon specimens for material supplied by each of the fabricators is given in Table 2.1. All of the beam-column connections were made using 3/4-inch diameter, ASTM A325 heavy hex high-strength bolts, and A325 hardened washers. No tests of the mechanical properties of the fasteners were conducted.

2.2 Description of Test Specimens

The specimens consisted of a pair of beam sections attached to a centrally positioned stub column using the particular flange and web angles to be investigated in a given test. The connections contained top and seat angles bolted to the flanges of the beams and supporting stub column, together with double web angles bolted to the beam web and column flange.

Two beam sizes, W8X21 and W14X38, have been used in the testing program. Each of these sections has a flange width to thickness ratio of 6.6, typical of that encountered in building applications. For the W14X38 sections, the overall test beam length was 20 feet, and for the W8X21 sections, 12 feet, so that the span-to-depth ratios were slightly less than 20 in each case. The stub column for the W8X21 beams was a W12X58 section, and a W12X96 column section was used with the W14X38 beams. Heavy column sections were selected to eliminate column panel zone distress as a contributing behavioral factor, thereby confining the moment-rotation interaction to the connection elements. It is noted here that the same stub column sections were used repeatedly throughout the testing program

without exhibiting any evidence of inelastic behavior. The general configurations of typical test members using the 14-inch and 8-inch deep beams are shown in Figures 2.1a, and 2.1b, respectively.

The web angles were centered on the beam web and proportioned initially for shears equal to 1-1/2 times the end reactions the member would experience at its A.I.S.C. allowable uniform load as a simply supported beam with a span equal to the length of the test beam. The lightest web angles used would thus be adequate, also, for shear forces corresponding to the increased loads that would be permitted if end connections had been used that were capable of developing one-half the beam allowable moment at working load.

The top and bottom flange angles were of the same size in a particular test specimen. Because the connections were to experience moment reversals, it was felt that a symmetric arrangement would reduce the parameters influencing the moment-rotation behavior, yet still represent a realistic design configuration. For each of the two beam sizes, two different thicknesses of the top and bottom angles were tested. Initial angle thicknesses were selected approximately equal to the flange thickness of the beam being supported. It was reasoned that these sizes, together with the use of standard gages in the legs of the angles attached to the column flange, would provide the bending flexibility required of semi-rigid connection response. At the same time, the connections would be expected to exhibit sufficient moment capacity (and energy absorption capability) to contribute significantly to the resistance of a structural frame subject to earthquake induced loads.

The details of the connection angles used to frame the W8X21 and W14X38 beams to the stub columns are shown in Figures 2.2 and 2.3, respectively. For the W14X38 beam test, 3/8-inch and 1/2-inch thick top

and seat angles were used; these angles were of 5/16-inch and 3/8-inch thickness for the W8X21 beam tests. For the 14-inch deep beams, the length and thickness of the web angles were varied for the static moment-rotation parameter studies. In addition, the length of flange angle, and the gage and bolt spacing on the leg attached to the column flange were varied in one static test series of W8X21 beam specimens. Dimensions of the various connection elements are presented in the test specimen schedule, Table 2.2.

Bolting of the connection elements was accomplished with an air wrench using the standard turn-of-the-nut method.(36) A325 flat hardened washers were used under the turned elements in all of the connections. The holes were all of standard size, 13/16-inch diameter, for the 3/4-inch diameter bolts.

2.3 Testing Equipment and Test Procedures

A pair of duplicate specimens was tested simultaneously by framing the beams into the centrally loaded stub column using the arrangement shown schematically in Figure 2.4. The beam sections are supported at the ends by roller-type seats located at the beam mid-depth, and designed to allow longitudinal movement so that no direct axial forces would be introduced as the specimen deflects. The height of the beam supports is adjustable to accomodate the mounting of beams of different depth in the structural loading frame; photographs of the supports are shown in Figure 2.5.

Adjustable roller-type guides were used to insure vertical movement of the stub column and, consequently, to prevent torsional displacements at the beam-column interface. The guides are comprised of rollers mounted on channels attached to the top and bottom of the stub column; the rollers ride against the flanges of the actuator supporting columns of the main structural loading frame. Photographs of the roller guides are shown in

Figure 2.6. The rollers were oiled and checked periodically to permit freedom of movement in the vertical direction along the loading frame support columns. Photographs of the complete test set-up, including loading frame, beam supports, and roller guides are shown in Figures 2.7 and 2.8.

A 55 kip, servo-controlled, hydraulically actuated ram was used to apply load to the test members through the stub column, Figure 2.4. Local monitoring of the actuator displacement was accomplished through an X-Y plotter. In addition, the output data from the various measuring devices, described later, were transferred directly to the College of Engineering VAX 11/780 computer system for subsequent retrieval and graphic display; the basic elements of the recording system are illustrated schematically in Figure 2.9.

Using the test arrangement and loading system illustrated in Figure 2.4, the connections were subjected to combined shear and bending moment. For both the static and cyclic tests the controlled input variable was the rate and magnitude of actuator movement and, correspondingly, the displacement of the stub column. Displacement control was imposed to avoid the possibility of instantaneous collapse of the test member should complete separation occur in any of the connecting elements during testing.

2.3.1 Static Tests

For each of the static tests, the beam sections were first mounted in the end supports and then bolted to the stub column, which had been blocked in the loading frame to effect a centered, level specimen. The erection sequence proceeded as follows. For each beam size the actuator load cell was initialized to a load equal in magnitude and opposite in sense to the total weight of the specimen (beams plus stub column) less one-half the

weight of the beams. Having thus established the initial load cell reading, the actuator was next attached to the top of the stub column. The bolts were then loosely inserted in all of the connection elements. Power was supplied to the actuator to maintain the specimen in a level position as the supporting blocks were removed from beneath the stub column. The bolts in the legs of the angles attached to the column flanges were then tightened, followed by tightening of the remaining bolts in the angle-to-beam connections. At this point the load on the specimen caused by fit-up (recorded by the load cell) was removed by adjusting the position of the stub column. Thus, the average static moment at the beam-column interface, resulting from the erection operations, was essentially null. This established the point of origin for the subsequent load-displacement (and moment-rotation) plots; the static moments thereafter calculated from the load-cell output thus excluded the weight of the specimen from the measured moment-rotation response of the connection.

It should be noted that, as a result of member configuration tolerances and slight misalignment of the connection elements, local residual stresses were introduced during the erection operations. All specimens were prepared by area fabricators using standard shop practice, so that the fit-up stresses would be of the order encountered during normal field erection.

For a select number of test specimens (14S1, 14S2, and 8S1) strain gages were mounted on both faces of the leg of the top flange angle attached to the column to determine local strains introduced during the bolting operation, and to monitor the surface conditions as testing progressed. The positions of the strain gages are shown in Figure 2.10. In addition, for all tests, LVDTs were mounted to each flange of the beam sections on either side of the stub column, and seated against the flanges

of the column. The device used to seat the LVDT probe and to accomodate the rotations developed during a test is illustrated in Figure 2.11. The data from a pair of LVDTs mounted on one beam section were used to determine the angle of rotation of the connection as testing progressed. The LVDT data were compared, also, to rotations calculated from the actuator displacement readings.

Besides the direct strain measurements and LVDT displacements, light gage aluminum channel-shaped devices with attached strain gages were used to detect slip between the top and bottom flange angles and the elements to which they were connected. These devices (slip monitors) were intended only to record the presence of major slip, not the magnitude thereof.

After a specimen had been mounted in the loading frame and the displacement- measuring devices attached, the test was undertaken using an actuator displacement rate of 1.0 in./min. for the 14-inch deep beams, and 0.75 in./min. for the 8-inch beams (except for specimen 8S7, for which a rate of 1.0 in./min. was used). The upward (downward for specimen 8S4) movement of the actuator (and stub column) was continuous, with load, displacement, LVDT, strain gage, and slip indicator output each being sampled two times per second. In addition, the actuator load and displacement were recorded locally on an X-Y plotter to allow continuous visual monitoring of the system behavior. A test was concluded when the actuator displacement reached 4 inches for the 20-foot long W14X38 beam specimens, and 3 inches for the 12-foot long W8X21 beams.

2.3.2 Cyclic Tests

The preparation and installation of the specimens in the cyclic tests was the same as that used for the static loading, described above. During mounting of a test member in the loading frame, the initial load setting

was established to exclude the contribution of the weight of the specimen to the static moment at the connection in the manner described above for the static tests. For specimens 14C2, 8C1, and 8C2, strain gages were mounted on the top flange angle using the patterns shown in Figure 2.10. In addition, the same arrangement of LVDTs and slip monitors as in the static tests was employed for measuring joint rotations and determining slip in the flange angles, respectively.

For the cyclic studies, an initial range of actuator displacement of 0.4 inches was selected, approximately 10 percent of the total displacement used in the static tests of the 14-inch beams. The initial displacement amplitude was intended to produce a hysteresis loop representing minimal non-linear response (estimated from the corresponding static moment-rotation curves). In all tests, the full range of controlled displacement was set to provide equal displacement amplitudes about the initial horizontal beam position. Full reversal of displacement was chosen to provide the symmetry required for comparison of test data from beams of different depth, and to approximate the reversals that might be exhibited under extreme conditions during seismic loading.

The first displacement cycle in each test was applied sinusoidally using a frequency of 0.10 Hz. This relatively slow rate of actuator movement was selected to allow visual monitoring of the load-displacement relationship, to insure that the strain and displacement measuring devices were recording properly, and to check the alignment of the lateral support devices. Additional individual cycles were then applied using a frequency of 0.10 Hz or 0.25 Hz until a stable hysteresis loop was established; usually this occurred within a few cycles after the initial cycle had been run. To complete the sequence, ten additional cycles were applied continuously at a frequency of 0.25 Hz, so that a total of 12 to 15

complete cycles were normally imposed at one displacement amplitude. The displacement range was then increased to 0.8 inches and the above procedure repeated; i.e., several individual cycles followed by a continuous run of 10 cycles at 0.25 Hz. Each sequence was followed by an increase of 0.4 inches in the displacement range and the process repeated, resulting in displacement-time histories typified by the block arrangement illustrated in Figure 2.12.

The cyclic tests were terminated when observed fatigue cracking had progressed partially across the faces of the flange angles at the toe of the fillet on the leg bolted to the column flange (see following discussion of test results). This progression of fatigue cracking was usually accompanied by only modest loss of maximum moment at the time a test was discontinued. No test was extended to the point of complete fracture of a connection element.

III. EXPERIMENTAL INVESTIGATION

3.1 Static Tests

3.1.1 Scope of Investigation

Eleven specimens were tested in the static test investigation. The purpose of this phase of the study was twofold: (1) to quantify the static moment- rotation behavior of the semi-rigid beam-column connections; and (2) to identify and measure the effect of various geometric parameters on the connection behavior. The static tests were intended, also, to serve as a frame of reference against which the cyclic hysteresis behavior of the connections could be compared.

The geometric variables that were altered in the parametric study included: the depth of the beam sections (W8X21 and W14X38 sections), the thickness and length of the top and bottom beam flange angles, the gage and spacing of bolts in the leg of the flange angles connected to the column flange, and the thickness and length of the web angles. All bolting was accomplished using 3/4-inch diameter, A325 high-strength bolts tightened by the turn-of-the-nut method. It was recognized that the size of bolt could significantly affect the connection stiffness, by altering the clamping force in the connection, by changing the clear distance between the bolt head (and washer) and the toe of the fillet in the leg of the angle, and by changing the clear distance between the two bolts on the column gage line. However, because of economic constraints, the same stub column sections (one each for the 8-inch and 14-inch beams) were used throughout the testing program; similarly, the same beam sections were used for several tests, to be replaced only if evidence of inelastic deformation was found after a test. Thus, these sections were all drilled to 13/16-inch holes, as described earlier. An attempt was made to simulate one effect of bolt size by changing the gage on the legs of the angles framed to the column

flange.

As discussed subsequently, slip occurred in both legs of the top and bottom angles in one of each of the W14X38 section and W8X21 section tests, demonstrating the inability of the 3/4-inch diameter bolts to maintain sufficient clamping for the stiffer connections through the full range of inelastic response. Consequently, 7/8-inch diameter bolts are to be used with these heavier sections in a future investigation, which is to include both static and cyclic (fatigue) testing.

3.1.2 Test Results

A summary of the test results for the static test investigation is presented in Table 3.1; details of the corresponding specimen geometries are reported in Table 2.2. Table 3.1 includes the initial stiffness of the connections (initial slope of the moment-rotation curve). The slope was measured tangent to the moment-rotation ($M-\phi$) curve at the origin as the derivative of a second degree polynomial fit through the first several data points. Table 3.1 also lists: (1) the slope and intercept moment of a secant line from the origin and intersecting the $M-\phi$ curve at a rotation of $4.0X10^{-3}$ radians; and (2) the slope tangent to the $M-\phi$ curve at $24X10^{-3}$ radians, a rotation achieved in all of the static tests. Although the latter slope offers a measure of the degradation of connection stiffness as the applied moment increases, it should not be interpreted as a constant or final slope for a specific connection. In some tests, the connections continued to "soften" as the moment increased, never actually reaching a constant $M-\phi$ slope at the conclusion of loading. The tangent slope at the rotation of $24X10^{-3}$ radians does, however, allow comparisons to be made among the various connections at a common point, as well as quantifying the degree of connection softening in a particular test. Similarly, the secant

slope offers an additional indication of the early stiffness of the connection. In some respects the secant slope may be more representative than the initial tangent slope, because the latter is highly sensitive to any irregularities in the first few data points from which it was calculated.

The moments reported in Table 3.1 (and the figures to follow) were calculated directly from the actuator load cell readings. To obtain the corresponding ϕ values, initially the displacements measured by the LVDTs mounted to each flange of the beam were converted to relative rotations between the flange of the stub column and the end of the beam. The rotations were also independently calculated using the actuator displacement and the beam span by considering rigid body movement of each beam segment and correcting for elastic curvature from bending of the beam. Because of the high stiffness of the stub column, and the transfer of load in friction between the connecting elements (except for the slip encountered in two tests) the beam did rotate essentially as a rigid body with respect to the column flange, which was maintained in a vertical position by the lateral support system.

A typical comparison of the M-ϕ relationship obtained from LVDT data with the results obtained from the displacement measurements is shown in Figure 3.1. The curves labeled East and West represent the data from individual pairs of LVDTs mounted on the flanges of each of the two beam segments framing into the central stub column. It can be seen from Figure 3.1 that the LVDT data obtained from each of the two connections in the test member were very close, and consistent with the M-ϕ curve calculated using the actuator displacements. Consequently, the data reported in Table 3.1, and plotted in the figures to follow, use rotations calculated from actuator displacements; the results may thus be considered to represent an

"average" of the behavior exhibited by the connections attached to each face of the stub column.

Foil stain gages, 1/8-inch gage length, were mounted initially on a trial specimen adjacent to the toe of the fillet on the leg of the top flange angle mounted on the stub column. These gages peeled from the angles during the operation of bolting the angles to the column, indicating that large strains were introduced at the angle fillet during bolt installation. Subsequently, the strain gages on specimens 14S1, 14S2 and 8S1 were placed at the locations shown in Figure 2.10; the gages mounted approximately mid-way between the angle fillet and the bolt line were positioned at the anticipated inflection point for bending during static loading. Gages were placed at the same position on both faces of the angle to distinguish between the axial and flexural components of strain as loading progressed. It was hoped that this information on local conditions of strain would prove useful both in monitoring the progression of the connection non-linear response, and to aid in establishing appropriate analytical models to predict static behavior.

A typical plot comparing the axial and bending components of surface strain in the angle (calculated from strain gage data) with specimen displacement is shown in Figure 3.2, for specimen 14S2. These data illustrate the increase in both flexural strain and axial strain as the distortion of the vertical leg of the top (tension) flange angle increases. At an actuator displacement of 1.6 inches, the surface strains at gage locations "BF" and "BB" (see Figure 2.10a) on the opposite faces of the angle leg had exceeded two times the nominal yield strain of the material. It should be noted that the plots shown in Figure 3.2 do not include the effects of connection installation which, as noted earlier, were also found to introduce significantly large surface strains, particularly near the toe

of the fillet on the angle.

Although the measurements shown in Figure 3.2 are indicative of the strain patterns expected on the surfaces of the tension flange angle, there was considerable inconsistency in the strain data observed among the three specimens on which gages were mounted. The comparisons served to illustrate the sensitivity of local response to minor variations in angle geometry, installation procedure, etc.. Consequently, the strain data were not used to quantify the moments and axial forces in the angle for purposes of direct comparison with the analytical predictions. Rather, the data were used simply to indicate trends which were useful in helping to describe overall connection response and to suggest possible models for the analytical studies.

For each of the static tests, the beams were observed to rotate, with respect to the stub column, essentially as rigid members by pivoting about a point near the surface of the beam compression flange, as illustrated in Figures 3.3 and 3.4. Photographs of typical deformation patterns observed in the connection flange and web angles are shown in Figures 3.5 and 3.6, respectively. With the exception of specimens 14S2 and 8S2, post-test inspection revealed no apparent inelastic deformation in either the flanges or the web of the beams. Similarly, no distress was evident in the stub columns, because, as discussed previously, intentionally heavy sections were selected to confine the study to the response of the beams and their connection elements.

In the testing of specimen 14S2, major slip first occurred when approximately one-half the final actuator displacement had been reached. After the specimen had been dismantled, the holes in both legs of the tension flange angle and in the beam flange were elongated, as were the holes in the beam web. The plastically deformed steel formed a protruding

lip on the bearing surface of each of the elements exhibiting the elongated holes. Post-test inspection of specimen 8S2 indicated the same pattern of distress in the connection elements as that in specimen 14S2.

At the conclusion of each of the static tests, there was no rupture, nor were there any cracks observed by visual inspection in any of the fasteners or connected elements.

3.1.3 Discussion of Static Test Results

The moment-rotation curves for the tests reported in Table 3.1 are plotted in Figures 3.7 through 3.13. The figures provide comparisons of the initial stiffness and non-linear connection behavior for test members in which individual geometric parameters were altered. General observations with respect to these test results are discussed in the following paragraphs.

From practical design considerations, one of the most apparent means of increasing the initial stiffness and total moment transfer capability in a connection of the type studied herein is to increase the thickness of the angles attached to the top and bottom flanges of the supported beam. This flange angle dimension was, therefore, one of the principal variables investigated in both the static and cyclic test series.

Figure 3.7 presents the moment-rotation curves for two W14X38 beam specimen tests, one (14S1) with flange angles of 3/8-inch thickness, and the other (14S2) with 1/2-inch thick flange angles. Both the initial stiffness and the moment developed at comparable rotations are greater for specimen 14S2. For example, at a rotation of $24X10^{-3}$ radians, specimen 14S2 developed a connection moment of about 950 k-in., or almost 1-1/2 times the 668 k-in. moment of specimen 14S1. The rotation of $24X10^{-3}$ radians has been used for purposes of comparison among the test members in

Table 3.1 and in this discussion because it was a number easily reached in all of the static tests. The rotation corresponds to a deflection of approximately 2-3/4 inches for the 14-inch beam tests, or approximately four times the mid-span deflection a W14X38 beam, 20 feet long, would exhibit as a simply supported member at its AISC allowable uniform load (assuming full lateral support)*. This deflection was considered to be reasonably representative of a severe ductility demand, even under seismic loading conditions.

Specimen 14S2 exhibited major slip in the leg of the tension flange angle bolted to the beam (and in the legs of the web angles attached to the beam web) at a rotation of approximately $12X10^{-3}$ radians, followed by slip in the leg of the flange angle bolted to the column face at approximately $20X10^{-3}$ radians. For the static tests, in which the rate of actuator movement was the controlled input variable, slip as indicated in Figure 3.7 corrresponds to a gradual drop in moment until bearing is achieved in the connected elements. With bearing established, the stiffness of the connection prior to slip is regained, with no anticipated permanent degradation in the capacity of the connection (barring premature bolt shear failure or tear-out in the connected parts). As noted earlier, future tests in a continuing investigation will utilize 7/8-inch diameter bolts in the heavier connections to delay the occurrence of slip during cyclic (fatigue) loading.

For specimens 14S1 and 14S2 (and each of the other specimens

---

* For the 8-inch beam tests, a rotation of $24X10^{-3}$ radians corresponds to a deflection of about 1.6 inches, four times the deflection, at allowable load, of a 12-foot long simply supported beam using the W8X21 sections.

investigated in the static test series), the connections exhibited a moment-rotation response which becomes non-linear relatively early in the loading sequence. This non-linearity is contributed to, in part, by local yielding and eventual plastic hinge formation at each toe of the fillet in the flange angle attached to the tension flange of the beam. Another hinge develops in the vicinity of the bolt line in the leg of the flange angle attached to the column, together with progressive plastic hinging in the outstanding legs of the web angles. It is of interest to note, however, that each of the connections developed a moment greater than two times the capacity that would be predicted by simple plastic hinging mechanisms in the leg of the tension flange angle attached to the column flange and in the legs of the web angles; further analysis of this post-elastic connection response is presented below.

In Figure 3.7, it can be seen that specimens 14S1 and 14S2 were able to develop increasing moments through the full range of rotations imposed during the test. In fact, a nearly constant or slightly decreasing M-ϕ slope was observed during the latter stages of loading for each of the specimens tested in the static test investigation (with the exception of specimen 8S2, discussed later). It is believed that this nearly constant stiffness at large deformations can be attributed in part to material strain hardening, and to the consequences of significant changes in the geometries of the connecting angles. The increasing deflection of the tension flange angle at large connection rotations produces a continuous change in the internal force distribution in the legs of the angle, with axial tension becoming an increasingly larger factor (relative to bending) as the angle progressively "flattens out." A gradual transition from a predominantly flexural to a combined flexural-axial response in the tension flange angle, with the accompanying strain hardening, can thus be expected

to contribute to the ability of the connection to achieve a considerably greater moment capacity than that predicted by a simple plastic-hinge mechanism, as noted above.

In contrast to the influence of flange angle thickness on the moment-rotation behavior of the 14-inch beam specimens, moderate changes in the size of the web angles did not as significantly affect the connection performance. Figures 3.8 and 3.9 show the effect of web angle thickness and length, respectively, on the M-ϕ relationships for W14X38 sections with 3/8-inch thick flange angles. For example, increasing the thickness of the web angle by 50 percent, from 1/4-inch to 3/8-inch (specimens 14S1 and 14S4), produced a corresponding increase in moment, at a rotation of $24X10^{-3}$ radians, of approximately 25 percent, from 668 k-in. to 822 k-in. An apparently lesser influence on post-elastic moment capacity was exhibited by a change in the length of the web angles, as comparison of specimens 14S1 and 14S3, Figure 3.9, indicates. At a rotation of $24X10^{-3}$ radians, specimen 14S3, with web angles having a length of 5-1/2 inches, developed a moment of 652 k-in., some 17 k-in. less than the 668 k-in. moment of specimen 14S1, which had the standard 8-1/2 inch long web angles. It should be noted that specimen 14S3 had the only non-symmetrical connection in the test series, with the legs of the web angles attached to the beam and column stub each using two bolts placed in the upper two holes of the standard detail, Figure 2.3. In this location, with the web angles closer to the beam tension flange, they would be expected to contribute differently to the moment transfer capability of the connection than if they had been positioned at mid-depth, closer to the pivot point of the connection. The arrangement used is of practical importance, however, in that it represents a normal positioning of web angles designed for shear transfer in beams using simple (flexible) framing.

The influence of flange angle thickness on moment-rotation behavior was examined also for the W8X21 beam specimens, the results of which are shown in Figures 3.10a and 3.10b. Figure 3.10a presents a comparison of the M-ϕ curves for specimen 8S1, with a flange angle thickness of 5/16-inch, and specimen 8S2, with a 3/8-inch thick flange angle. The gage in the legs of the flange angles attached to the stub column was 2 inches, and the angle length was 6 inches in both of these specimens. Although comparison of the initial portion of the moment-rotation relationships indicated a considerably stiffer connection for specimen 8S2 compared to that of 8S1 ($123.4X10^3$ k-in./radian vs. $66.7X10^3$ k-in./radian), and correspondingly greater moment transfer capability, specimen 8S2 exhibited major slip in the connection elements at a rotation of approximately $16X10^{-3}$ radians. Unlike specimen 14S2, in which slip also occurred during static loading, specimen 8S2 did not regain nor approach the stiffness it had maintained prior to slip. The stiffness continued to degrade with continued loading, the slope of the M-ϕ curve reducing to only $1.5X10^3$ k-in./radian at a rotation of $24X10^{-3}$ radians. As there were no cracks or other geometric irregularities observed in the connection elements of specimen 8S2, either during testing or upon post-test visual inspection, no explanation is offered for the singular behavior of this specimen. As with the stiffer connections in the 14-inch deep beams, it is expected that slip in specimen 8S2 would have been delayed or obviated had larger bolts been used in the connection elements.

In Figure 3.10b, the moment-rotation curves for specimens 8S6 (5/16-inch flange angle thickness) and 8S7 (3/8-inch angle thickness) are compared. In these specimens, the gage in the legs of the flange angles attached to the column was 2-1/2 inches, and the angle length was 6-inches. As with the 14-inch deep beam tests, both the initial stiffness and the

moments developed at common rotations were greater for the W8X21 beam connection having the heavier flange angles. For example, the 1/16-inch increase in flange angle thickness of specimen 8S7 over that of specimen 8S6 effected a greater than 50 percent increase in moment (381 k-in. vs. 244 k-in.) at a connection rotation of $24X10^{-3}$ radians. As no slip occurred in either of these two tests, the comparative behavior of the two specimens, shown in Figure 3.10b, may be considered representative of similar connections framing the 8-inch deep beams. Note again the early non-linearity of the M-ϕ curve, followed by a continuing increase in moment transfer capability, with only gradual decrease in stiffness, toward the latter stages of loading. Further, as with the W14X38 beam tests, the W8X21 beam connections examined in this study easily achieved moments in excess of twice the capacity that would be predicted by a simple plastic hinging mechanism in the tension flange angle and in the web angles.

The effect of varying the gage in the leg of the flange angle attached to the column flange was examined in the W8X21 beam test series. With an angle thickness of 3/8-inch, gages of 2, 2-1/2, and 4-1/2 inches were used in specimens 8S2, 8S7, and 8S4, respectively. To accomodate the 4-1/2 inch gage in specimen 8S4, a 6X6X3/8 angle was used in place of the smaller 6X3-1/2X3/8 and 6X4X3/8 angles used in the other two specimens. Specimens 8S1 and 8S6, with flange angles of 5/16-inch thickness, had gages of 2 inches and 2-1/2 inches, respectively. Complete details of the dimensions for these specimens are presented in Table 2.2.

The static test results for these five specimens are summarized in Table 3.1. For the three members having 3/8-inch thick flange angles, the moment-rotation curves are plotted in Figure 3.11a; the curves for the two specimens with flange angles of 5/16-inch thickness are compared in Figure 3.11b. Although the intent of these tests specifically was to quantify the

effect of the flange angle gage on the stiffness of the connection, the results also may be considered indicative, qualitatively, of the effect of varying the bolt diameter on the initial connection stiffness. Increasing the bolt diameter would be expected to have a similar effect on initial connection stiffness as decreasing the flange angle gage, as the clear span for bending in the angle would be decreased in both cases. The analogy is not a complete one, of course, because differences in initial clamping force, distribution of stress in the angle betweeen bolts, and post-elastic prying action would accompany changes in bolt size, and thereby affect the complete moment-rotation behavior of the connections.

As expected, changes in flange angle gage had a pronounced effect on both the initial slope of the M-ϕ curve, and on the moment capacity of the connection at large displacements. For example, with the 3/8-inch thick flange angles, the initial connection stiffness decreased from $123.4X10^{3}$ k-in./radian to $15.3X10^{3}$ k-in./radian as the angle gage was changed from 2 inches to 4-1/2 inches (specimens 8S2 and 8S4). Specimen 8S7, with a gage of 2-1/2 inches, exhibited an initial M-ϕ slope of 48.0 k-in./radian, intermediate in stiffness between those of the other two members. At a rotation of $24X10^{-3}$ radians, specimen 8S7 achieved a moment of approximately 380 k-in., more than twice the 165 k-in. moment of specimen 8S4 at that rotation. It should be noted again, that specimen 8S2 sustained slip at about $16X10^{-3}$ radians, after which its moment-rotation curve reduced to a slope of only $1.5X10^{3}$ k-in./radian at a rotation of $24X10^{-3}$ radians. This behavior is not considered indicative of the performance expected of the connection had slip not occurred; consequently, comparison of specimen 8S2 with the other two members at large displacements is not appropriate.

The two connections with 5/16-inch thick flange angles exhibited the

same relative response as those with 3/8-inch angles; i.e., decreasing the gage resulted in an increase in initial connection stiffness and subsequent moment capacity at large displacements. For specimen 8S1 (2-inch gage), the initial slope of the M-ϕ curve was $66.7X10^3$ k-in./radian, almost double the $39.5X10^3$ k-in./radian slope for specimen 8S6 with a 2-1/2 inch gage. Similarly, at a connection rotation of $24X10^{-3}$ radians, specimen 8S1 developed a moment of 329 k-in., significantly higher than the 244 k-in. moment in specimen 8S6.

For the W8X21 beam sections, the effect of changing the length of the flange angle was examined. As indicated in Table 2.2, with all other connection dimensions remaining the same, a flange angle length of 6 inches was used for specimen 8S1, and a length of 8 inches used for specimen 8S3. The one-third increase in flange angle length resulted in a corresponding increase of about one-third in the initial connection stiffness ($104.7X10^3$ k-in./radian vs. $66.7X10^3$ k-in./radian), and the development of higher moments at large displacements (422 k-in. vs. 329 k-in. at a rotation of $24X10^{-3}$ radians). The complete moment rotation curves for specimens 8S1 and 8S3 are plotted in Figure 3.12.

Finally, in Figure 3.13, a comparison is made between a W14X38 section specimen (14S1) and a W8X21 specimen (8S5) in which the dimensions of all of the connection elements were the same except for the length of the web angle (8-1/2 inches for 14S1, and 5-1/2 inches for 8S5). As seen from the M-ϕ curves of Figure 3.13 and the data recorded in Table 3.1, the initial slope of the moment-rotation curve is increased significantly, from $76.7X10^3$ k-in./radian to $195.0X10^3$ k-in./radian, for the W14X38 specimen in comparison to the W8X21 member. Similarly, the moment developed at $24X10^{-3}$ radians was 668 k-in. for specimen 14S1, about double the 337 k-in. moment of specimen 8S5. The increase in initial connection stiffness and

moment development capability are to be expected, as the deeper beam section provides, at comparable rotations, a larger displacement of the tension flange angle (and larger force in the angle) together with a larger moment arm from the position of the tension flange angle to the pivot point of the connection in the vicinity of the compression flange.

3.1.4 Summary of Static Test Results

In summary of the static test results, it has been found that the geometric parameters that most significantly affect the static moment-rotation performance of the semi-rigid connections investigated were: the depth of the beam section to which the connection elements were framed; the thickness of the flange angles; and the gage in the leg of the flange angles attached to the column flange. (As noted earlier, although not considered in this study, changes in bolt diameter would be expected to affect connection response, at least initially, in a manner similar to altering the flange angle gage; i.e., an increase in bolt diameter would decrease the effective span for bending of the angle, as would a decrease in angle gage). Variations in the length of the flange angles, and in the length and thickness of the web angles, had a less pronounced effect on connection response than the parameters listed above.

Several analytical models have been proposed to establish the initial stiffness of semi-rigid connections of the type considered in the study. Comparisons of the predicted stiffnesses with the experimental data from this static test investigation are presented in Section 4.1. Further, using the results of the parametric study, a semi-empirical analytical model has been developed to generate complete non-linear moment-rotation curves for the connections; the results of this phase of the study are reported also in Section 4.1.

3.2 Cylic Tests

3.2.1 Scope of Investigation

The purpose of this phase of the investigation was threefold: (1) to quantify the cyclic moment-rotation behavior of the semi-rigid beam-column connections; (2) to determine the energy absorption capabilities under complete reversal of moment; and (3) to qualitatively describe the characteristics of the hysteresis loops obtained.

Four specimens, 14C1, 14C2, 8C1, and 8C2 were tested under cyclic loading. Two of the specimens used the W14X38 beam sections; the other two used the W8X21 sections. For each of the beam depths, specimens having two different flange angle thicknesses were tested. These four specimens were identical to four of the static specimens, 14S1,14S2,8S1, and 8S2, respectively. Consequently, the two variables investigated in the cyclic test series were the depth of the beam section and the thickness of the flange angles.

The intent of the cyclic tests was to examine the connection response to moment reversals, not the behavior of a complete subassemblage under seismic loading. Consequently, the rate of loading in the cyclic tests was "quasi-static", and was not intended to suggest that the loading would be the direct result of actual earthquake induced ground motions.

3.2.2 Test Results

A summary of the cyclic test results is presented in Tables 3.2 through 3.5; details of the test specimens are reported in Table 2.2.

Tables 3.2 through 3.5 include the actuator displacement amplitude, the number of cycles at each amplitude and test frequency, and the cumulative number of test cycles. For each displacement amplitude, the range of rotation (peak-to-peak) and the range of moment is given for the

hysteresis loops. The area enclosed by a single hysteresis loop is given as well as the cumulative loop area.

As discussed previously, all of the cyclic test specimens were subjected to complete displacement reversal to facilitate comparison of the hystersis loops generated for beams of different depth. The initial displacement amplitude was 0.2 inches, which produced a nearly linear moment-rotation curve. The initial loading consisted of a single cycle, applied at a frequency of 0.10 Hz, to allow visual monitoring of the specimen behavior. Additional individual cycles (usually two) were applied using the same frequency of 0.10 Hz, followed by two or three cycles at 0.25 Hz (specimens 14C1 and 14C2 only), until a relatively stable load-displacment hysteresis loop was established. Ten additional cycles were then applied continuously at a frequency of 0.25 Hz. The displacement amplitude was next increased by 0.2 inches to 0.4 inches, and the above procedure repeated. Each sequence was followed by an increase of 0.2 inches in the displacement amplitude and the process repeated. The cyclic tests were terminated when observed fatigue cracking had progressed partially across the faces of the flange angles. At that time, none of the cracks in the angles had propagated completely through the angle thickness. No test was extended to the point of complete rupture of a connection element. No slip was observed during the cyclic tests.

Figure 3.14 shows front and rear views of a top flange angle from specimen 14C1 after the test was stopped. It can be seen that cracking had progressed over most of the width at the toe of the fillet on the leg bolted to the column flange. This crack pattern is typical of those observed in both of the 14-inch deep beam test specimens; for the 8-inch beam specimens, cracking initiated at the toe of the fillet on the leg bolted to the beam flange.

After disassembly of test specimen 14C1, it was discovered that significant cracking had progressed in the vicinity of the bolt hole under the washer. Although the formation of fatigue cracks had an observable effect on the load-displacement hysteresis loops, the decrease in maximum load was usually a small percentage of the maximum load for the stabilized loops at the time the tests were discontinued. The permanent distortions shown in the flange and web angles of specimen 14C1, Figure 3.15, give an indication of the large deformations experienced by the connection angles during the cyclic tests.

As mentioned previously, the specimens were intended to simulate, within reason, actual connections in situ. During the erection procedure, it would be natural to seat the beam on the bottom flange angle for support, thereby aligning the bottom angle as required at the expense of the top angle. As a consequence, the top angle would be subjected to the greater initial strains resulting from any lack of fit during the bolting procedure. This same erection sequence was followed in the the test program, and is believed to explain the tendency of the top angle to form the first cracks in most of the cyclic tests. Also, as seen in Figures 3.16 through 3.19, the hysteresis loops tend to exhibit signs of stiffness degradation first in the negative moment region, corresponding to tension in the top flange angle.

3.2.2.1 Specimen 14C1

The cyclic moment-rotation hysteretic loops of specimen 14C1, Figure 3.16, show a consistent performance under complete moment reversal. An increase in displacement amplitude resulted in a corresponding increase in the range of moment and area of the hysteresis loop. Subsequent cycles at the same amplitude generated nearly the same range of moment as the first

cycle. As the connection response stabilized, a slight softening was noted corresponding to an increase in the range of rotation and a decrease in the area of the loop. The moment range of the final stabilized hysteresis loop was usually within 5 per cent of the initial value. At larger displacement amplitudes, the negative moment is seen, in Figure 3.16, to remain nearly constant as the displacement amplitude was increased. This suggests the presence of some irreversible damage (cracking) in the tension angle that corresponds to the negative moment quadrant of Figure 3.16; however, no cracking was observed visually at this time. It is significant that the loops were able to stabilze even though the stiffness of some of the connecting elements appears to have been compromised. The hysteresis loops are generally distinguished by a smooth curve, except at the ends, which exhibit a pinched appearance corresponding to an appreciable change in connection stiffness. This change in stiffness will be discussed in detail later.

No degradation of the overall connection stiffness attributed to impending failure was noted until the last block of 10 cycles at the conclusion of the test. In the last 6 cycles, at a displacement amplitude of 2.0 inches, the load-displacement plots indicated a gradually decreasing stiffness, unlike the previous loops, which had stabilized by this time. Examination of the specimen during this latter stage of loading revealed the presence of the fatigue cracking described in Section 3.2.2. The locations of the cracks correspond to the locations where the tensile strains resulting from bending and axial force are additive. The test was then stopped before complete separation of the flange angle occurred.

3.2.2.2 Specimen 14C2

Specimen 14C2 was identical to specimen 14C1 in all details except for

the larger flange angle thickness of 1/2 inch. As expected, a larger range of moment was achieved, for corresponding ranges of rotation, than that of specimen 14C1, as shown in Figure 3.17.

The cyclic moment-rotation behavior of this specimen was similar to that of specimen 14C1. The stabilized range of moment for the block of ten continuous cycles at a given actuator displacement amplitude was very close to the range established on the initial cycle at the same amplitude.

During loading at a displacement range of 1.8 inches, a small crack was discovered in one of the bottom flange angles at the root of the radius of the leg attached to the column flange. It is interesting to note that, even with a visible crack, the loops remained stable.

The displacement amplitude was further increased to 2.0 inches and four single cycles applied. The moments achieved during this loading were about the same as at the previous amplitude, and the corresponding hysteresis loops were stable. The test was discontinued when propagation of the cracks was evident at the toe of the fillet in the line of both rows of bolts of the flange angle, (i.e., when cracks were observed progressing along the toe of the fillet, and positioned approximately between the bolt in the column flange leg and the first bolt in the beam flange leg of the angle).

3.2.2.3 Specimen 8C1

Specimen 8C1 had the thinner flange angles of the two connections with 8-inch deep beams. The moment-rotation behavior of specimen 8C1 was noticably different from the behavior of specimens 14C1 and 14C2, which can be seen by comparing Figures 3.16, 3.17, and 3.18.

The hysteresis loops for specimen 8C1 did not exhibit the stability encountered in the 14 inch specimens. At each increase in displacement

amplitude, the connection exhibited a continual, though minor, softening for each additional cycle; however, the loops were similar in appearance. In addition, for larger displacement amplitudes, the moment-rotation plots are inconsistent with regard to the maximum moments achieved at each amplitude. A decrease appears in the negative moment region of the loop, suggesting the presence of a crack in the corresponding tension flange angle not detected by visual examination.

Failure occurred by the abrupt, nearly simultaneous propagation of cracks almost completely across the width of both top flange angles, along the root of the radius on the leg bolted to the beam flange. The observed crack had not extended to the sheared edge on one side, indicating that the crack (or cracks) had originated at some interior point along the width of the angle (see discussion of specimen 8C2 results). Post-test examination of specimen 8C1 showed that the angle had undergone severe bending at the location of the crack, where the angle was in bearing at the end of the beam flange. Testing was discontinued before complete rupture occurred in any of the flange angles.

3.2.2.4 Specimen 8C2

This specimen had thicker flange angles than specimen 8C1, but was otherwise identical; hence larger ranges of moment were generated for comparable ranges of rotation. Note the lack of pinching in the hysteresis loops of specimen 8C2, Figure 3.19, compared to the behavior of specimen 8C1, Figure 3.18. Like specimen 8C1, the hysteresis loops of 8C2 exhibited a slight softening with progressive cycles at a constant displacement amplitude. This is attributed to changing connection stiffness, the cause of which is uncertain. It is possible that the initation of cracks in the connection angles during the latter stages of loading may be one reason.

The sensitivity of the overall connection behavior to the stiffness of the connection elements will be examined later.

Toward the end of the test, cracks appeared in specimen 8C2 along the toe of the fillet on the leg of a top flange angle bolted to the beam flange, similar in location to the crack observed in specimen 8C1. Two cracks formed, each located in the most highly strained areas of the flange angle, between the bolt in the column flange leg and the first corresponding bolt in the beam flange leg. It is probable that the combination of severe bending caused by the angle in bearing on the beam flange and the tension forces in the line of the column and beam bolts precipitated the initiation of cracking at these locations. It is likely that failure of the angle would have been similar to the abrupt extension of the cracks across the entire width of the angle as in specimen 8C1, had the test been continued.

3.2.3 Discussion of Moment-Rotation Hysteresis Loops

The shape of the hysteretic loops of specimens 14C1, 14C2, 8C1 and 8C2 can be described in terms of the changes in the geometry of the connection as the moment is reversed. Consider one half of a typical loop, shown as a solid line in Figure 3.20. Point 1 in Figure 3.20 corresponds to one extreme of the actuator movement (Point 1 in Figure 3.21, actuator displacement vs. time). The portion of the moment-rotation curve that is generated as the actuator moves from Point 1 to Point 3 can be divided into three regions based on the configuration of the connection; these regions are labeled I, II, and III in Figure 3.20.

The initial loading of the connection in a cycle, culminating in the attainment of maximum negative moment, causes the connection to assume the configuration shown in Figure 3.22a. In this configuration the beam is

pivoting about a point near BFA, the current compression angle. The remaining connection angles are pulled away from the column flange, generating the tension forces which establish the corresponding resisting moment at the beam-column interface. With the bottom angle in full bearing on the column flange, the stiffness of the connection is now at a relative maximum. The completion of this initial loading is indicated as Point 1 in Figure 3.20.

Reversal of the direction of actuator movement, with the specimen in the configuration shown in Figure 3.22a, effects a period of essentially elastic unloading at a slope comparable to the initial slope of a statically loaded connection. This is identified as Region I in Figure 3.20.

Region II is a transition stage. During this time, the geometry of the connection is undergoing significant change. The compression force in BFA, which bears on the column face in Region I, decreases and eventually converts to a tension force as the moment is reversed; hence, the angle moves away from the column face (see Figure 3.22b).

The force in the top flange angle, TFA, changes from tension to compression in Region II, causing the angle to move toward the column face. As a result, the center of rotation of the connection moves (reflecting the redistribution of forces taking place) and eventually maintains a position near the top of the beam. During the time when both flange angles are temporarily bent away from the column face, the connection stiffness is at a minimum. The stiffness of Region II is not a constant for all loading histories. The initiation of yield in the flange angles is affected by the residual stresses present. The response of the connection in Region II is analogous to a rigid beam on an elastic-plastic foundation, where the foundation is represented by springs with changing stiffnesses. The

relative stiffnesses of the springs depend on the magnitude of the connection rotation at the previous reversal of moment. As a result of this behavior, it is hypothesized that unloading from the central range of Region II will not be at a slope equal to that of Region I. Rather, the slope will lie between the limits established from the Region I response and the Region II slope immediately preceding unloading. This has not been experimentally verified in the present investigation but will be tested in a future study. The end of Region II is reached when angle TFA has folded back upon the column face in compression. The behavior of the connection in Region II occurs only in cyclic loading, and hence cannot be compared to a monotonic static test.

Region III can be considered geometrically the reverse of the configuration existing in Region I. As shown in Figure 3.22c, the compression angle in bearing against the column face is now TFA, whereas flange angle BFA and the web angles are now pried in tension from the column. The center of rotation is again stationary, located near the top flange of the beam. The stiffness of the connection is comparable to a statically loaded connection at large rotations. The change in stiffness as the configuration changes from that of Figure 3.22b to the one in Figure 3.22c can be determined by noting the difference in the slope of the moment-rotation curve. The magnitude of this change depends on the connection details, as discussed below.*

Comparing the change in slope between Regions II and III of specimens

---

* The same type of "pinching" behavior has been observed, also, by other investigators (50) in tests of similar connections framed to smaller beam sections.

14C1 and 14C2 (Figures 3.16 and 3.17, respectively), it can be seen that the change is more pronounced in specimen 14C1. This difference can be attributed to the thicker flange angles of specimen 14C2, the web angles being identical for the two specimens. Assuming the angles behave as beams, an analogy may be drawn between a span-to-depth ratio for a beam and the ratio of the gage length to the thickness of the angle, g/t, for the leg of the flange angle mounted to the column flange. For specimen 14C1, g/t is 6.7 and, for specimen 14C2, g/t is 5.0, indicating a stiffer beam in bending for the flange angles of specimen 14C2. During the transition phase of Region II the stiffer flange angles of specimen 14C2 offer more resistance to movement than the flange angles of specimen 14C1. Thus, when the compression flange angle goes into bearing, the change in stiffness is greater in specimen 14C1 than the corresponding change in stiffness of specimen 14C2. Comparing the moment-rotation curves of specimens 8C1 and 8C2, Figures 3.18 and 3.19, the same arguments apply. The change in slope from Region II to Region III is more pronounced in specimen 8C1, with a g/t ratio of 6.4, than for specimen 8C2, with g/t of 5.3.

The contribution of the flange angle stiffness to the overall connection stiffness warrants further examination. Consider specimens 14C1 and 8C2, each with a flange angle thickness of 3/8 inch. The resisting moment of the connection can be calculated by summing the contributions of each connecting angle to the total moment. In Region III, the moment arm is approximately equal to the depth of the beam, 14 inches for specimen 14C1, and 8 inches for specimen 8C2. With the center of rotation fixed, increasing rotation results in an increase in displacement of the flange angle proportional to the depth of the beam, and a corresponding increase in the force in the angle. In this situation, specimen 14C1 would be expected to have a signifigantly higher stiffness, due to both the larger

moment arm and the larger angle displacement. Thus, in Region III, the effect of the depth of the beam contributes in two distinct ways to the overall connection stiffness.

The connection stiffness in Region II is largely dependent upon the flexural stiffness of the individual elements, since neither flange angle is in bearing. The forces in the top and bottom angles should be approximately equal and much less than the compression force possible in bearing. The difference in stiffness of the two specimens, 14C1 and 8C2, in Region II is not as great as in Region III, the influence of the depth of the beam being felt primarily in its contribution through the moment arm. As a result, the Region II stiffness of the 8-inch deep beam is a higher percentage of its Region III stiffness than that of the 14 inch beam, suggesting a more pronounced change in moment-rotation behavior (pinching) for the 14 inch beam going from Region II to Region III. Comparison of the moment-rotation curves for the four cyclic tests shows that the change in slope from Region II to Region III is indeed more pronounced for the 14-inch beams than for the 8-inch deep beams. In fact, the change in slope for specimen 8C2 is hardly noticeable.

Assuming that the stiffness in Region II is predominately due to the stiffness of the flange angles, represented by t/g, and that the Region III stiffness is influenced predominately by the depth of the beam, d, for a given specimen, the ratio of the two stiffnesses can be represented by the parameter d/(t/g). For the four cyclic test specimens, this ratio is 93.3, 70, 51.2 and 42.7 for specimens 14C1, 14C2, 8C1 and 8C2, respectively. These values show a trend which corresponds to the degree of pinching observed in the hysteretic moment-rotation loops. Specimen 8C2, with the least degree of pinching observed has the lowest value of the ratio d/(t/g), 42.7. The other specimens show an increase in the degree of

pinching as the parameter d/(t/g) increases, with specimen 14C1 showing the most pronounced pinching and having the highest value, 93.3.

3.2.4 Connection Hysteretic Energy Capacity

The "average" hysteresis loop area at each displacement amplitude, and the total hysteretic energy accumulated at the termination of testing, is presented in Tables 3.2 through 3.5 for the four cyclic tests. The results indicate that, with the exception of the initial cycle following an increase in displacement amplitude, the hysteretic energy absorbed per cycle remained reasonably constant at each amplitude for the four specimens. Further, the ductile behavior of the connections is demonstrated by the increase in hysteresis loop area with each succeeding increase in displacement amplitude (and connection rotation) through the full range of testing, even with pinching evident at the larger amplitudes.

The total hysteretic energy accumulated in each of the connections framed to the W14X38 sections was approximately the same, 520 k-in. for specimen 14C1 and 527 k-in. for specimen 14C2. It may be noted, also, that the displacement-time history was about the same for the two tests, with specimen 14C1 subjected to 149 total cycles and a final displacement amplitude of 2.0 inches, while specimen 14C2 achieved 130 cycles and the same 2.0 inch final displacement amplitude before testing was terminated.

The accumulated hysteretic energy of each of the two specimens framed to the W8X21 sections was also quite similar. For specimen 8C1, with 5/16-inch thick flange angles, the cumulative area of the hysteresis loops was 195 k-in.; specimen 8C2, with 3/8-inch flange angles, achieved a cumulative hysteresis loop area of 243 k-in. For both specimens, the displacement-time histories consisted of cycling to a maximum displacement amplitude of 1.4 inches, and the total number of cycles sustained was about

the same, 78 cycles for specimen 8C1 and 76 cycles for 8C2.

As a consequence of the general stability of the connections at large rotations, and of the ductility of the connection elements, it is reasonable that the energy absorption capacities of like connections would increase directly with the depth of the beam sections to which they are framed. This is evident by comparing the data for specimens 14C1 and 8C2, both of which contained the 3/8-inch thick flange angles. For specimen 14C1, the total accumulated hysteresis loop area was 520 k-in., more than double the 243 k-in. achieved by specimen 8C2. Because of the limited number of tests conducted to date, however, no quantified conclusions are drawn with regard to the effect of varying connection geometries on the hysteretic energy response of specimens of the same depth, nor for specimens subjected to loading histories different from the block-type increasing displacements used in the current program. In a subsequent investigation, constant amplitude cyclic tests are to be conducted with similar connections, to obtain benchmark fatigue data, and to obtain additional measurements of energy absorption capacity for comparison with the results of this study. The goal of the future program will be to consider the applicability of various fatigue damage models to the cyclic behavior of the connections, and, if possible, to relate hysteretic energy accumulation to fatigue life.

IV. ANALYTICAL INVESTIGATION

The analytical investigation of this project was conducted with the objective of establishing procedures capable of describing the behavior of semi-rigid beam-to-column connections, yet retain sufficient simplicity to be used as a design tool. Because of the complex behavior of the subject connections, obtaining a simple analytical procedure with both accurate prediction capability and simple design applicability was not feasible. Several analytical models are presented which develop a logical progression from simple linear elastic models of the connection to more complicated models which account for both geometric and material nonlinear behavior.

The analytical investigation considered separately the static and cyclic behavior with the hypothesis that a clear understanding of static behavior is prerequisite to the understanding of cyclic performance.

4.1 Static Tests

4.1.1 Models of Beam-Column Connections

4.1.1.1 Beam Models for Initial Stiffness

In an attempt to predict the inital stiffness of semi-rigid beam-column connections, a model was developed under the assumptions that material behavior is linearly elastic, that displacements are small, and that the angles connecting the beam to the column could be represented by beam behavior. The precedent for such models has been established in earlier investigations (47,51).

The assumed behavior for this model, Model I, is presented in Figure 4.1a,* where

$\Delta = \phi d$

Δ = horizontal displacement of heel of flange angle

ϕ = rotation of beam at the connection

For Model I, it is assumed that the vertical leg of the flange angle can be represented by a single beam with cross-sectional area, t x L, and assumed beam length, λ, as shown in Figures 4.1a and 4.2a, where

M_{AB} = moment at end A of beam AB

M_{BA} = moment at end B of beam AB

F = shear force in beam (nominal bolt force)

It is assumed that the outstanding legs of the web angles may be represented by three separate beams, as shown in Figures 4.1b and 4.2b, where

λ_c = assumed beam length

P_c = beam width, $L_c/3$

Δ_i = $d_i \phi (i = 1, 2, 3)$, displacement of heel of web angle for beam i

---

* See, also, nomenclature and corresponding Figure A1.

d_i = distance from assumed center of rotation to beam i

$d_1 = d/2 + L_c/3$

$d_2 = d/2$

$d_3 = d/2 - L_c/3$

F_i = shear force in beam i

$(M_{CD})_i$ = moment at end C of beam i

$(M_{DC})_i$ = moment of end D of beam i

The beam and all angle legs attached to the beam are assumed to rotate as a rigid body about the heel of the compression flange angle. The validity of this assumption has been confirmed by test results to be reasonable.

Considering equilibrium of the beam shown in Figure 4.2a and using the Slope Deflection equations, it can be shown that

$$F = (M_{AB} + M_{BA})/\lambda$$

$$M_{AB} = \frac{ELt^3}{6\lambda}\left[1 + \frac{3d}{\lambda}\right]\phi \qquad (4.2)$$

$$M_{BA} = \frac{ELt^3}{6\lambda}\left[2 + \frac{3d}{\lambda}\right]\phi$$

Similarly, considering the beams of Figure 4.2b, the respective shear and moment are found to be

$$F_i = (M_{CD} + M_{DC})_i/\lambda_c$$

$$(M_{CD})_i = (M_{DC})_i = \frac{EL_c t_c^3}{6\lambda_c^2} \Delta_i \qquad (4.3)$$

Neglecting the bending moment in the compression flange angle at the assumed center of rotation, the total resisting moment for the connection can be computed as the sum of the contributions of all beams used to represent the flange angle and the web angles. Therefore, the total resisting moment of the connection is, approximately

$$M = F(d + g) - M_{AB} + 2F_1 d_1 + 2F_2 d_2 + 2F_3 d_3 \qquad (4.4)$$

Since Equation 4.4 is a linear function of the beam rotation, ϕ, this equation may be used to evaluate the initial slope of the actual moment-rotation curve for the connection; i.e., the initial rotational stiffness. Evaluation of Equation 4.4 for comparison with selected test data showed the equation to be very sensitive to the parameter λ, and, in general, overestimates the actual initial stiffness. It is difficult to establish the value of λ since it is affected by prying action at end A of the beam and deformation at end B (Figure 4.2a) that is not accounted for in the analysis. Values of λ chosen for comparison purposes were varied between a maximum $\lambda_{max} = g$ to a minimum value $\lambda_{min} = g-k-d_w/2$.

In order to improve the results predicted by Model I, refinements were introduced, resulting in Model II. The refinements consisted of introducing shear deformations into the beam behavior and further refinement of the representation of the flange and web angles as beams. The refined model of the flange angle is shown in Figure 4.3 and assumes that the angle can be represented by a combination of "stiff" and "flexible" beams. The contribution of the flange angle to the total resisting moment of the connection is then found to be

$$M_f = \left\{ \frac{6EI_1}{b^2(1+r_1)}\left[\frac{2D}{b} + 1\right] + \frac{6EI_2 D}{B^3(1+r_2)}\left[1 - \frac{2-r_2}{4+r_2}\right](D + B)\right\} \phi \qquad (4.5)$$

where

$$r_1 = \frac{12EI_1}{A_{S1}Gb^2} \qquad r_2 = \frac{12EI_2}{A_{S2}GB^2}$$

$$A_{S1} = 2/3\ tm_1 \qquad A_{S2} = 2/3tm_2$$

$$I_1 = m_1 t^3/12 \qquad I_2 = m_2 t^3/12$$

$$m_1 = (\text{no. of bolts}) \times d_w \qquad m_2 = L - m_1$$

The refined model of the web angle is shown in Figure 4.4, also assuming the angle to be the sum of stiff and flexible beams. Based on this definition, the contribution of the web angles to the total resisting moment of the connection is found to be

$$M_c = M_c(\text{stiff}) + M_c(\text{flexible}) \qquad (4.6)$$

$$M_c(\text{stiff}) = \frac{24EI_3}{b_c^3(1+r_3)}\left[d_1^2 + d_2^2 + d_3^2\right]\phi$$

$$M_c(\text{flexible}) = \frac{12EI_4}{B_c^3(1+r_4)}\left[1 - \frac{2-r_4}{4+r_4}\right]\left[(d_1+e)^2 + (d_3-e)^2\right]\phi +$$

$$\frac{12EI_5}{B_c^3(1+r_5)}\left[1 - \frac{2-r_5}{4+r_5}\right]\left[(d_2+f)^2 + (d_2-f)^2\right]\phi$$

where

$$r_i = \frac{12EI_i}{GA_{Si}\lambda_i^2}, \quad I_i = \frac{1}{2}p_i t_c^3, \quad A_{Si} = \frac{2}{3}p_i t_c, \quad i = 3, 4, 5$$

$$p_3 = d_w \qquad \lambda_3 = b_c$$

$$p_4 = \frac{1}{2}(L_c - d_w - 2p_c) \qquad \lambda_4 = B_c$$

$$p_5 = p_c - d_w \qquad \lambda_5 = B_c$$

$$e = (d_w + p_4)/2$$

$$f = p_c/2$$

4.1.1.2 Modified Beam Models for Complete Moment-Rotation Prediction

In an attempt predict the complete moment versus rotation relationship for the beam-to-column connection, Model I was modified by introducing inelastic material behavior into the beam definition of both the flange and web angles. This will be referred to as Model III; the specific nature of the modifications is shown in Figure 4.5, where

j = percentage of the beam depth that remains elastic

σ_y = stress at initial yield

ε_y = strain at initial yield

E_{sth} = slope of stress-strain curve beyond initial yield

y = distance from neutral axis

Based on these assumptions, the resisting moment on the beam cross section may be calculated as

$$M_b = [j^2\varepsilon_y(E-E_{sth})+\varepsilon E_{sth}]S + (\sigma_y-\varepsilon_y E_{sth})(1-j^2)Z \qquad (4.7)$$

where

S = elastic section modulus, $Lt^2/6$

Z = plastic section modulus, $Lt^2/4$

In order to obtain a usable solution for Model III, it was necessary to introduce the approximation that the beam stiffness does not vary over the length of the beam, permitting the integration of the governing beam equation:

$$EI_{eff}\ \frac{d^2v}{dx^2} = M_b$$

For a fixed-fixed beam subject to relative end translation, Δ, this integration produces

$$\frac{M_b}{EI_{eff}} = \Delta(6 - \frac{12x}{\lambda})/\lambda^2 \qquad (4.8)$$

where

x = distance from end of beam
λ = length of beam
M_b = moment in beam representing angle, at x
I_{eff} = effective moment of inertia of beam
v = lateral beam displacement

Assuming a linear variation of strain across the beam depth, the familiar relationship

$$\varepsilon = - \frac{d^2v}{dx^2} y \qquad (4.9)$$

is obtained, and the stress in the elastic core of the beam may be computed from Hooke's Law and Equation 4.9 as

$$\sigma = E\varepsilon = - \frac{Ed^2v}{dx^2} y \qquad (4.10)$$

Combining Equations 4.8 and 4.10, letting $\sigma = \sigma_y = M_b y/I_{eff}$ at $y = \pm jt/2$, and rearranging

$$j = \left| \frac{\sigma_y}{Et} \frac{\lambda^2}{\Delta(3 - \frac{6x}{\lambda})} \right| \leq 1 \qquad (4.11)$$

Equations 4.7 and 4.11 are used to compute the internal resisting moment at any point along the beam and, in particular, at the ends of the beam. Once the end moments are known the shear force in the beam is determined from Equation 4.2. Both the flange angle and web angle beams

were assumed to behave according to the preceding development. Points on the moment-rotation curve were then established using Equation 4.4.

4.1.1.3 Two Dimensional Finite Element Model

This model, Model IV, is similar to Model III with the exception that the beam behavior of Model III is replaced with two dimensional plane stress behavior. The plane stress behavior was obtained for specific examples, such as shown in Figure 4.6, by employing a finite element analysis. In Figure 4.6, u and v represent the horizontal and vertical displacement field variables, and γ is a dimension arbitrarily chosen to be one inch for purposes of analysis. The finite element analysis was performed using the general purpose ANSYS (52) computer program and the constant stress triangular element to model the angle cross-section. The material model assumed was the bilinear, strain hardening type of Model III, shown in Figure 4-5d, and was applied according to the kinematic hardening technique employed by ANSYS (53). Load was applied by imposing a uniform horizontal displacement along Section A-A, Figure 4.6, and a nonlinear analysis was achieved as follows. First a linear analysis was performed to determine the point of maximum stress and the load level necessary to cause yielding at this point. Small increments of displacement were then added and subsequent nonlinear analyses performed at the new load level. Values of horizontal force, F, were determined for each value of total horizontal displacement, thus establishing the force versus displacement, Δ, relationship at Section A-A. A typical plot of F vs. Δ is shown in Figure 4.7, and indicates that the curve can be replaced by a bi-linear relationship with little error.

The web angles for Model IV were assumed to be represented by three segments, as in Model III, and a force deformation curve established for

each segment similar to that described above for the flange angle.

Angle displacement, Δ, is assumed to be related to joint rotation, ϕ, as indicated by Equations 4.1 and 4.3, and the connection resisting moment computed using the equation

$$M = Fd + 2F_1d_1 + 2F_2d_2 + 2F_3d_3 \qquad (4.12)$$

where d_i is defined as in Models I and III. The moment versus rotation curve for the connection is now established as follows: specify ϕ, calculate Δ and Δ_i from geometry, obtain F and F_i from established curves, and compute the moment from Equation 4.12.

4.1.1.4 Dual Spring Model

In order to investigate the effects of large displacements and axial tension in the vertical leg of the flange angle on the moment-rotation relationship, Model V was developed. Model V utilizes the force-deformation relationships developed for Model IV to represent the beam behavior of the angle, and adds to this behavior the axial stiffness of the angle. Model V is shown in Figure 4.8, where

K_b = bi-linear beam stiffness of vertical leg of the flange angle

A = cross section area = t x L

g = length of axial member

The material model for the axial element was assumed to be of the bi-linear strain hardening type shown in Figure 4.5d. This model was analyzed assuming the displacement, Δ, to be finite when compared to the length, g; thus both material and geometric nonlinearity are included in

this model.

4.1.1.5 Three Dimensional Finite Element Model

In order to investigate the validity of the concept of treating connecting angles in a connection as a combination of beams, a three dimensional, finite element model, Model VI, was developed. The complete connection of specimen 14S2, Figure 2.3, including all connecting angles and the beam, was modeled with nonlinear triangular and quadrilateral shell elements and gap elements. These elements are STIF63, STIF48, STIF52, and STIF12 in the computer program ANSYS.

The finite element model consisted of a total of 125 nodes and 203 elements (see Appendix B, Figures B1-B3), and utilized the plane of symmetry about the midplane of the beam web (line A-A, Figure 4.9). All nodes in the plane of symmetry were restrained against translation perpendicular to the symmetry plane and against rotation about both orthogonal axes contained in the plane.

The beam web was modeled with quadrilateral shell elements, and the beam flanges were modeled with triangular shell elements. Triangular elements were required to model the flange in order to eliminate fictitious node forces associated with out-of-plane warping in quadrilateral elements. A seven-inch length of beam was modeled to allow attachment of the connecting angles.

The flange angles were modeled with triangular elements, with the vertical leg of the angle restrained against translation but not against rotation in the vicinity of the bolt. Nodes along the bolt line not in the region encompassed by the compression zone of the washer were not restrained. Nodes along line B-B, shown in Figure 4.9, were restrained against rotation about line B-B and against translation in the direction

perpendicular to line B-B (z-direction) in order to effect some degree of restraint intermediate between fixed and pinned about the bolt line. The horizontal leg of the flange angle was discontinued at the second bolt line from the column face and was attached to the beam flange at the interface between the angle and the flange. Attachment was accomplished by assigning the same nodes to elements in the flange and elements in the angle. The short section of the angle between the column face and the end of the beam was not attached.

Web angles were modeled with triangular shell elements and attached to the beam web along the bolt line by defining elements of the beam web and elements of the web angle along the line by the same node number. Compression forces transmitted between the web angle and beam web were represented by gap elements connecting nodes of one region to nodes of the other. Gap elements were also used to connect the web angle to the column face in regions where separation could occur.

The material model assumed for Model VI was the bilinear strain hardening type defined in Figure 4.5d.

Loading of the model was accomplished by applying a couple to the beam in the form of a tension force in the top flange and a compression force in the bottom flange. Shearing forces were not considered. To achieve a nonlinear analysis, the couple was applied in small increments with iteration being performed at each load level. Beam rotation at each load level was determined by considering the horizontal displacement of the ends of the top and bottom flanges of the beam.

4.1.1.6 Empirical Model

An empirical model, Model VII, was developed to predict the moment-rotation behavior of the beam-to-column connections; it is based on

the original work by Sommer (34). In this model, it is assumed that the relationship between moment, M, and rotation, ϕ, can be expressed in the form

$$\phi = C_1(KM) + C_2(KM)^3 + C_3(KM)^5 \qquad (4.13)$$

where

C_i = coefficients to be determined

$K = P_1^{\alpha_1} P_2^{\alpha_2} - - - P_n^{\alpha_n}$

P_i = parameters affecting relationship between M and ϕ.

α_i = exponents to be determined.

The technique for determining α_i is as follows. The relationship between M and ϕ is obtained from experiment for two values of the parameter, P_i, while holding all other parameters constant, as indicated by Figure 4.10. For some arbitrary rotation, ϕ_o, Equation 4.13 may be used to obtain the relationship

$$M_1 P_{i1}^{\alpha_i} = M_2 P_{i2}^{\alpha_i}$$

from which α_i may be determined as

$$\alpha_i = \frac{\log(M_2/M_1)}{\log(P_{i1}/P_{i2})} \qquad (4.14)$$

Because the value of α_i calculated from Equation 4.14 is dependent on the choice for ϕ_o, the average value of α_i must be determined by considering values of ϕ_o over the applicable range of the equation. Once the average

values for all the ϕ_o are known, the coefficients C_i may be determined through a statistical analysis applied to known test data.

Sommer assumed that the relative values of all other parameters did not affect the determination of α_i in the previously described technique, permitting the use of the linear least-squares method for determining the C_i. A more attractive approach would be to determine both α_i and C_i statistically; however, a nonlinear approach is required. If a nonlinear least-squares technique is employed, the problem of determining the correct solution from an infinite number of local optimum solutions is encountered.

In this investigation Sommer's method was used to obtain initial values for α_i and C_i for use in a subsequent nonlinear least-squares analysis. Using this technique, the ability to predict the experimental M-ϕ curves was improved in comparison to the Sommer method.

Five parameters, P_i, were chosen for consideration in this investigation:

$$P_1 = t$$

$$P_2 = d$$

$$P_3 = t_c$$

$$P_4 = L$$

$$P_5 = b + t/2$$

The parameter L_c was not included because the test data (tests 14S1 and 14S3) indicated that its effect was small. Application of Model VII indicates that good correlation with test data performance may be expected for a range of .6 to .75 for the ratio L_c/d. This choice of parameters for

the test data of the current investigation resulted in values for the quantities α_i and C_i which are presented Section 4.1.2.2.

4.1.2 Prediction of Moment-Rotation Behavior

4.1.2.1 Initial Stiffness

The initial stiffness of the moment-rotation curve predicted by Model I was always larger than that determined from test results, even when the beam lengths were assumed to be maximum. The maximum beam lengths were taken to be $(\lambda)_{max} = g$ and $(\lambda_c)_{max} = g_c$ for the flange angle and the web angle, respectively. That Model I predicts too large an initial stiffness is attributed to the fact that the model assumes uniform behavior across the length, L, of the angle. Model II was developed in order to overcome this inadequacy.

Table 4.1 presents a comparison between Model II and test results for the initial slope of the moment-rotation curve. The test results presented in this table are taken from Table 3.1. Results are presented for Model II for both inclusion and exclusion of shear stiffness. The comparison indicates that Model II does, in general, predict reasonable values for the initial stiffness for the connections of this investigation. Table 4.1 also indicates that the effect of shear in Model II is relatively small but significant as a parameter, and predicts a lower initial stiffness for the connection.

A deficiency in Model II is that the stiff beam portion of the angle is assumed to be a function of the washer diameter, d_w, only. As a refinement to the model, the effective width of the stiff beam zone could be considered a function also of the length, L, of the angle, and the spacing, p, of the bolts in the angle.

4.1.2.2 Post-Elastic Behavior

The analysis procedure, described in Section 4.1.1.2 as Model III, was applied to test specimen 14S2 which had one-half inch thick flange angles and one-quarter inch thick web angles. The analysis was performed by first evaluating Equations 4.2, 4.7 and 4.11 to obtain a relationship between the shear, F, in the beam and the displacement, Δ , for the given angle dimensions (see Figure 4.11). Equation 4.11 was evaluated for values of x corresponding to the end points of the beam. The relationship between F and Δ is shown in Figure 4.11 for several combinations of beam dimensions. In order to establish the moment-rotation, M-ϕ , relationship for the connection, the individual F-Δ relationships for the beams representing the angles must be related to M and ϕ. M is related to the F's by Equation 4.4 and ϕ is related to the Δ's as described in Section 4.1.1.1. The M-ϕ relationship from Model III for specimen 14S2 is shown in Figure 4.12, together with the experimentally determined relationship.

As can be seen in Figure 4.12, Model III underestimates the strength of the connection by approximately fifty percent. This inadequacy in Model III might be attributed to various individual factors or a combination of these factors. Such factors include: inadequacy of flexure alone to model the angle, inappropriate selection of the length of the beam, inaccurate material model, and geometrically nonlinear behavior.

In order to investigate the ability of flexural behavior to represent the angle legs, as in Models I through III, Model IV (two-dimensional finite element model) was also used to analyze connection 14S2. The force-displacement relationship is shown in Figure 4.11 and the moment-rotation relationship is shown in Figure 4.12. It should be noted that the results from Model III indicated that the contribution of the web angles to the total moment resisting capacity of the connections considered

herein was small and could reasonably be neglected. The contribution of the web angles was thus neglected in Model IV because its effect was again considered to be relatively small, as in Model III, and in light of the effort required to include it.

Although Model IV does represent an increase in strength prediction of the connection over Model III, the increase is not so large as to rule out bending alone of the angle leg as a valid model. Also, the source of the larger moment carrying capacity of the connection was left unanswered by Model IV.

As indicated earlier, Model V was developed to investigate the geometrically nonlinear behavior of the subject connections. Results were obtained using Model V for connection 14S2 for comparison with other models. The bilinear beam stiffness, K_b , was determined using the curve shown in Figure 4.11 for Model IV; K_b was found to be 2300 k/in. for the initial slope and 33.33 k/in. for the second slope. Axial stiffness for Model V was modeled assuming the cross-sectional area to be L x t and the length, λ , taken to be equal to g, 2.5 inches. The material model for the axial stiffness was assumed to be linearly elastic, perfectly plastic with an initial modulus, E = 29000 ksi.

The analysis with Model V was achieved through the ANSYS (52) program for four different assumptions with respect to material properties and connection displacements. Condition A assumed linearly elastic behavior for all material, using the initial slope, and small displacement theory. Condition B assumed nonlinear material behavior and small displacement theory. Condition C assumed nonlinear material behavior and large displacement theory without stress stiffening. Condition D assumed nonlinear material behavior and large displacement theory with stress stiffening. Eliminating the obviously unrealistic Condition A, the results

shown in Figure 4.13 indicate that Condition D predicts the greatest strength for the angle.

Condition D was selected to represent the behavior of both the flange angles and the web angles in a subsequent analysis of the entire connection in order to establish the moment-rotation relationship for the connection. Since the analysis of the connection required the use of the computer (ANSYS), it was necessary to create an overall model of the connection. This overall model is shown in Figure 4.14; it simulates the same type connection behavior assumed for Models I through IV. However, this model does permit the location of the center of rotation of the connection to vary. GAP* elements were used at the top and bottom flanges to allow the behavior of the model to determine the center of rotation.

Results of the analysis using Condition D of Model V indicated that the center of rotation is near the bottom flange of the beam; therefore, the results from Model V are comparable to Models I through IV. Results were obtained both including web angles and excluding web angles, and are shown in Figure 4.15.

Figure 4.15 indicates that Model V, with Condition D assumptions, is in general capable of predicting the M- ϕ relationship much better than Models I through IV, and that the primary effect of the web angles is to "smooth out" the curve. The results from this model are questionable however, because the analysis indicates the existence of a very large tension force in the vertical leg of the flange angle. It is difficult to conceive of a mechanism in the actual connection capable of developing such

---

* An element which models compression with an infinite stiffness and tension with zero stiffness (see Ref. 52).

large tensile forces. In addition, it is the opinion of the authors that this analysis procedure produces a model that is too stiff.

The objective of Model VI was to model and analyze as accurately as possible the beam-to-column connection for comparison with the simpler models. The results of the analysis using Model VI applied to connection 14S2, along with test results for the same connection, are shown in Figure 4.16. Comparison of the results shows that Model VI predicts well the actual behavior for this connection for the range of results given. Results are not shown for larger values of ϕ because of the enormous amount of computer time required to produce a single point on the curve. A significant finding of this model, for the range of results available, is that the very large axial forces in the vertical leg of the flange angle predicted by Model V are unrealistic.

Model VII was completed by using test data to determine the unknown quantities in the model. Test data from tests 14S1, 14S2, 14S4, 8S1, 8S3, 8S5, and 8S6 was used to determine the α_i and C_i for Model VII. A direct application of Sommer's method, as described in Section 4.1.1.6, resulted in the values

$$\alpha_1 = -1.22$$

$$\alpha_2 = -1.37$$

$$\alpha_3 = -.387$$

$$\alpha_4 = -1.148$$

$$\alpha_5 = 1.141$$

$$C_1 = -.2245865$$

$C_2 = .00301236$

$C_3 = - .000002071785$

These values for α_i and C_i were then used as initial values for the nonlinear, least-squares analysis technique, which resulted in the values

$\alpha_1 = - 1.12808769$

$\alpha_2 = - 1.2870455$

$\alpha_3 = - .41454097$

$\alpha_4 = - .69412158$

$\alpha_5 = 1.34994572$

$C_1 = .02232429$

$C_2 = .00001850728$

$C_3 = .000000003188976$

Equation 4.13 was used, with these values of α_i and C_i, to predict the moment-rotation curves for connections having the same geometries as those of specimens 14S1, 14S2, 14S4, 8S1, 8S2, 8S3, 8S5, 8S6, and 8S7; the results are compared in Figures 4.17a - 4.17i with the test data for those specimens. This comparison between Model VII and the test data shows that Model VII produces satisfactory predictions of moment-rotation behavior for the range of geometric parameters under consideration.

Comparisons were not made between Model VII and test specimens 14S3 and 8S4. The 4-1/2-inch gage in the vertical leg of the flange angle of 8S4 was considered to be unrealistically large for practical applications;

thus, the data from this test were not included in determining the α_i and C_i terms for Model VII, nor were the data used to test the efficacy of the model.

As noted earlier, the test data indicated that moderate changes in the length of the web angle, L_c, did not appreciably affect the moment-rotation behavior of the connections. Thus, for simplicity, L_c was not included as one of the parameters in the expression for K; rather a limitation was imposed on the range of the ratio L_c/d for which the empirically determined Model VII was considered valid (see Section 4.1.1.6). For Specimen 14S3, the L_c/d ratio was 0.39, less than the 0.6 minimum considered applicable to the model, and the data from the specimen were not included in the α_i and C_i determinations.

4.2. Cyclic Tests

4.2.1. Spring-Rigid Region Model for Cyclic M-ϕ Curve

The purpose of this model is to understand the important factors which dictate the behavior of the flange and web angle type semi-rigid connection under investigation in this study. As will be discussed subsequently, a tri-linear curve model, appropriately modified, would be used in the analysis of a structure.

The model of the connection, referred to as the spring-rigid region model, consists of two separate phases, similar to Model V discussed in Section 4.1. First, the constituent angles are analyzed individually to determine their force-displacement relations. Second, the complete connection is modeled, replacing the angle with springs which have the force-displacement characteristics of the actual angles. The beam is modeled as a rigid region (infinitely stiff relative to the springs). Gap elements are used at the locations of the flange angle springs to simulate

bearing or separation.

The flange and web angles are simulated by an axial element representing the bending stiffness of the angle. The membrane force in the angle will not be considered, because of the unrealistically large forces generated, as discussed in Section 4.1.2.2.

Analysis of the flange angles in Section 4.1 assumed two dimensional behavior, which is obviously unrealistic. The restraints of the angle on the column leg are localized around the bolts rather than fixed along the bolt line. Prediction of the M-ϕ behavior from a two dimensional analysis of the angle was initially too stiff and, with the formation of a hinge, lacked sufficient strength to generate the large moments found in the test results.

A three-dimensional analysis of the angles with solid elements should alleviate both of the problems encountered with the two dimensional beam model. The 3-D model will be somewhat more flexible, with a more realistic displaced shape of the angle possible, hence decreasing the initial stiffness. The spread of plastic regions should also be more realistic than a single plastic hinge, resulting in a smoother transition from elastic to plastic response.

Hardening of the material in the regions of large strain, around the column bolt and at the toe of the fillet, should proceed at a faster rate because of the inclusion of shear in the solid element. The increase in the rate of hardening and the more realistic restraints should increase the strength of the angle with respect to its force-displacement curve.

Large displacement effects are not considered in the 3-D analysis of the angle. The membrane tension forces will not be considered explicitly because it is believed the restraint necessary to generate the membrane tension force does not exist in the angle to beam flange connection.

Static tests show the initial unloading portion of the curve to have the same slope as the initial portion of the loading curve, suggesting that the change in configuration does not significantly affect the force-displacement behavior of the flange angles. Large strains must be considered, however.

The contribution of the web angles to the overall connection behavior is small compared to that of the flange angles. Consequently, the web angles do not warrant as extensive an analysis as the flange angles.

Knowing the force-displacement properties of the connecting angles, the analysis of the complete connection is straightforward. The connection model is similar to Figure 4.14, with the exception of the "axial" elements. The type of analysis is non-linear material and small displacement. The changing status of the gap elements will require reformulation of the stiffness matrix upon change in loading direction and during the transition period. This allows the center of rotation to adjust and to enable this model to predict the pinching effect, discussed in Section 3.2.3.

Analysis of the connection as a spring-rigid region is currently under investigation.

4.2.2. Tri-Linear Model for Cyclic M-ϕ Curve

In previous investigations of the behavior of connections, empirical models capable of predicting cyclic moment-rotation behavior have been devised. In one such study (42), the static moment-rotation curve is tri-linearized by defining an initial slope k_1, an elastic limit moment, M_{el}, a secondary slope, k_2, a yield moment, M_y, and a final slope, k_3. The tri-linear moment-rotation curve is then used as a skeleton curve in the modeling of cyclic behavior.

To predict cyclic behavior with the tri-linear model, a constant strength envelope is assumed. Also, upon unloading, the connection is assumed to behave elastically for a moment range equal to $2M_{el}$. After reaching the limit of the elastic moment range, the response continues at a slope of k_2 until intersection with the constant strength envelope, whereupon the slope changes to k_3 (see Figure 4.18).

A serious drawback of this tri-linear model, when applied to the type of connection considered in this investigation, is the inability to predict the pinching observed in the test results, as illustrated in Figure 4.19. This deficiency is attributed to the use of the static M-ϕ curve as the skeleton curve. Upon entering Region II, the connection behaves in a mode not present in static loading, as described in Section 3.2.3.

A simple modification would be to ignore the k_2 stiffness and simply connect the elastic limit, Point A, to the extreme point predicted by the tri-linear model, Point B, Figure 4.19. This modification predicts the Region II slope rather well. This suggests replacing the skeleton curve with a cyclic moment-rotation curve after the initial loading. Unfortunately, the stiffness in Region II is not a constant, as discussed in Section 3.2.3 (see Figures 3.16 through 3.19). Modifications to the tri-linear curve model are currently under investigation.

V. SUMMARY AND CONCLUSIONS

5.1 Static Tests

A total of 11 members were tested under monotonic loading to generate static moment-rotation relationships for the test connections. The connections consisted of top and seat angles bolted to the flanges of beam sections and a supporting stub column, together with double web angles bolted to the beam web and column flange. Four of the test connections were framed to W14X38 beams; the remaining seven specimens were framed to W8X21 sections. For the top and seat flange angles, the thickness, length, and gage (in the leg attached to the column flange) were varied, together with the beam depth, to effect connections of varying stiffness. The thickness and length of the web angles were varied also.

In all of the static test specimens, the connections exhibited a moment- rotation response that became non-linear relatively early in the loading sequence. This is attributed, primarily, to local yielding and eventual plastic hinge formation at each toe of the fillet in the angle attached to the tension flange of the beam. Another hinge developed in the vicinity of the bolt line in the leg of the flange angle attached to the column, together with progressive plastic hinging in the outstanding legs of the web angles.

With the exception of specimens 8S2 and 14S2, all of the test members and their connections were able to develop continually increasing moments through the full range of rotations imposed during the tests. (The maximum rotations corresponded to deflections exceeding four times the deflection, at allowable load, of simply supported beams having the same section and span as those in the test program.) During the latter period of loading, a nearly constant or only very gradually decreasing positive slope of the moment-rotation curve was exhibited by each of the specimens (except 8S2).

This nearly constant stiffness at large deformations has been attributed to material strain hardening, and to the consequences of progressive changes in the geometries of the connecting angles. The increasing deflection of the tension flange angle at large connection rotations produces a continuous change in the internal force distribution in the legs of the angle, with axial tension becoming an increasing factor as the angle progressively "flattens out." The gradual transition from a predominately flexural response to a combined flexural-axial response, with the accompanying strain hardening, can thus account for the ability of the connections to achieve considerably greater moment capacities, by a factor of at least two, than those predicted by a simple flexural plastic hinge mechanism.

Specimens 8S2 and 14S2 exhibited slip in the connection angles during the course of testing; these were the stiffer connections for each beam size, thereby developing the larger moments (and, correspondingly, larger bolt shear forces) in each test group. In a subsequent investigation, 7/8-inch diameter bolts will be used in the heavier connections in place of the 3/4-inch bolts used exclusively in this investigation, to obviate or delay the occurrence of slip during testing.

The static tests have shown that the geometric parameters that most significantly affect the initial stiffness and static moment-rotation performance of the connections investigated are: the depth of the beam section to which the connections are framed; the thickness of the flange angles; and the gage in the leg of the flange angles attached to the column. Although not considered in this study, an increase in bolt diameter would be expected to affect connection response, at least initially, in a manner similar to the effect of decreasing the angle gage. Variations in the length of the flange angles, and the length and thickness

of the web angles, had a less pronounced effect on connection response than the other parameters.

Several analytical models are proposed to predict the initial stiffness and complete moment-rotation relationship for semi-rigid connections of the type considered in this study. These include: segmental "beam" models (representing the legs of the flange and web angles attached to the column), a dual spring representation of the flexural and axial stiffness of the connection elements, and two- and three-dimensional finite element models of the flange and web angles. In additional, a direct empirical model was considered, with the requisite parametric constants being generated from a statistical analysis of the test data.

The ability of the analytical models to predict the initial slope and complete moment-rotation curve for the test connections varied in direct relation to the complexity of the model, with the sophisticated (and most computationally time-consuming) three-dimensional finite element model offering the best correlation with the experimental results. However, the empirical model, with further refinements to be gained from additional test data, offers the greatest immediate promise as a practical means of describing the non-linear static response of the semi-rigid connections.

5.2 Cyclic Tests

Four specimens, with geometries comparable to those of the static test series, were tested under cyclic (quasi-static) loading. Two of the specimens were framed to the W14X38 beam sections, the other two framed to the W8X21 beams. For each of the beam sizes, two thicknesses of the top and seat flange angles were tested. The tests were conducted using full reversal of controlled displacement to generate data indicative of the

displacement extremes to which the connections could be subjected under seismic loading. The test procedure consisted of cycling sinusoidally between progressively increasing limits of displacement, while monitoring the range in moment and local displacements (rotations) developed during each cycle. The displacement-time histories followed a sequential block loading pattern, with a total of 12-15 cycles applied in each block before the amplitude was increased. The stabilized cyclic hysteresis loops at each displacement amplitude are reported for the four test members.

Stable hysteresis loops were established, for the 14 inch test specimens, within a few cycles after an increase amplitude was imposed relative to the preceding displacement under the block-type loading pattern. For the 8-inch deep connections, a continual, though small, softening (loss of moment) was noted for each progressive cycle at a constant displacement amplitude; however, the hysteresis loops were otherwise similar in appearance.

For each of the four test specimens, the moment-rotation behavior was characterized by loops of continually decreasing slope for relatively small displacements in the non-linear range. In contrast, the hysteresis loops exhibited a "pinching" effect at larger amplitudes, the degree of pinching being more pronounced in the W14X38 beam connections than in the W8X21 members. This increase in connection stiffness observed toward the tip of each hysteretic loop may be attributed, in large measure, to the changing geometry of the connection during each half cycle of loading. As rotation progresses, following a reversal in the direction of the moment at the connection, there is a period when both flange angles are drawn away from the column. With the connection in this configuration, the slope of the moment-rotation curve decreases as rotation proceeds. Eventually, the vertical leg of compression flange angle folds back into full bearing on

the column flange, with the connection exhibiting a concurrent increase in relative stiffness (pinching of the $M-\phi$ curve).

Each of the cyclic tests culminated in the formation and subsequent propagation of fatigue cracks at the toe of the fillet in one or more of the beam flange angles. The tests were terminated when cracking had progressed at least partially across the face of the angle at the fillet; no tests were extended to the point of rupture of a connection element. The connections maintained ductile behavior during the full extent of the cyclic tests, and exhibited only modest loss of maximum moment from the time fatigue cracking was noticed to the termination of the test. No slip was observed during the cyclic tests, nor was there any local buckling of the connection elements.

The block-type cyclic tests have demonstrated the general stability of the semi-rigid connections under large amplitude displacements, and enabled quantification of the cyclic energy absorption capacities of these connections. The tests have shown, also, that unless general frame instability intervenes under multiple excursions of lateral displacement typical of seismic loading, the effectiveness of connections of the type studied herein may be limited by low cycle fatigue of the connection elements. Additional data are needed with which to assess the accumulation of fatigue damage in these connections; this is to be addressed in a subsequent investigation.

REFERENCES

1. Popov, E. P., and Pinkney, R. B., "Cyclic Yield Reversal in Steel Building Connections," Journal of the Structural Division, ASCE, Vol. 95, No. ST3, Proc. Paper 6441, March 1969.

2. Naka, T., Kato, B., Watabe, M., and Nakao, M., "Research on the Behavior of Steel Beam-to-Column Connections on Earthquake Engineering, Vol. II, Santiago, Chile, January 1969.

3. Popov, E. P., and Pinkney, R. B., "Reliability of Steel Beam-to-Column Connections under Cyclic Loading," Proc. of the Fourth World Conference on Earthquake Engineering, Vol. II, Santiago, Chile, January 1969.

4. Bertero, V. V., "Seismic Behavior of Steel Beam-to-Column Connection Subassemblages," Proc. of the Fourth World Conference on Earthquake Engineering, Vol. II, Santiago, Chile, January 1969.

5. Naka, T., Kato, B., Watabe, M., Tanaka, A., and Sasaki, T., "Research on the Behavior of Steel Beam-to-Column Connections Subjected to Lateral Force," Report No. 3, Trans. of the Architectural Inst. of Japan, Vol. 103, October 1964.

6. Roeder, C. W., and Popov, E. P., "Eccentically Braced Steel Frames for Earthquakes," Journal of the Structural Division, ASCE, Vol. 104, No. ST3, Proc. Paper 13619, March 1978.

7. Johnston, B. G., and Deits, G. R., "Tests of Miscellaneous Welded Building Connections," Welding Journal, January 1942.

8. Beedle, L. S., and Christopher, R., "Tests of Steel Moment Connections," Engineering Journal, AISC, Vol. 1, No. 3, October 1964.

9. Popov, E. P., and Stephen, R. M., "Cyclic Loading of Full-Sized Steel Connections," Bulletin No. 21, AISI, February 1972.

10. Rathbun, J. C., "Elastic Properties of Riveted Connections," Transactions, ASCE, Vol. 101, 1936.

11. "Second Report of the Steel Structures Research Committee," Great Britain, Dept. Sci. Ind. Res., London, 1934.

12. Galambos, T. V., "Deformation and Energy Absorption Capacity of Steel Structures in the Inelastic Range," Bulletin No. 8, AISI, March 1968.

13. Hanson, R. D., "Characteristics of Steel Members and Connections," Proc. of the U.S. Nat. Conference on Earthquake Engineering, EERI, Ann Arbor, Michigan, June 1975.

14. Hanson, R. D., "Comparison of Static and Dynamic Hysteresis Curves," Journal of the Engr. Mech. Div., ASCE, Vol. 92, No. EM5, Proc. Paper 4949, October 1966.

15. Krishnamurthy, N., Juang, H.-T., and Jeffrey, "Analytical M-θ Curves for End-Plate Connections., Journal of the Structural Division, ASCE, Vol. 105, No. ST1, Proc. Paper 14294, January 1979.

16. Douty, R. T., and McGuire, W., "High Strength Bolted Moment Connections," Journal of the Structural Division, ASCE, Vol. 91, No. ST2, Proc. Paper 4298, April 1965.

17. Popov, E. P., and Bertero, V. V., "Cyclic Loading of Steel Beams and Connections," Journal of the Structural Division, ASCE, Vol. 99, No. ST6, Proc. Paper 9790, June 1973.

18. Carpenter, L. D., and Ly, L.-W., "Reversed and Repeated Load Tests of Full-Scale Steel Frames," Bulletin No. 24, AISI, April 1973.

19. Parfitt, J., Jr., and Chen, W. F., "Tests of Welded Steel Beam-to-Column Moment Connections, "Journal of the Structural Division, ASCE, Vol. 102, No. ST1, Proc. Paper 11854, January 1976.

20. Degenkolb, H.J., "Design of Earthquake Resistant Structures - Steel Frame Structures," in Earthquake Engineering, R. L. Wiegel, ed., Prentice-Hall, Inc., Englewood Cliffs, N. J., 1970.

21. Grundy, P., Thomas, I. R., and Bennetts, D., "Beam-to-Column Moment Connections," Journal of the Structural Division, ASCE, Vol. 106, No. ST1, Proc. Paper 15108, January 1980.

22. Rentschler, G. P., Chen, W. F., and Driscoll, G. C., "Tests of Beam-to-Column Web Moment Connections," Journal of the Structural Division, ASCE, Vol. 106, No. ST5, Proc. Paper 15386, May 1980.

23. Kato, B., "Beam-to-Column Connection Research in Japan," Journal of the Structural Division, ASCE, Vol. 108, No. ST2, Proc. Paper 16852, February 1982.

24. Krawinkler, H. and Popov, E. P., "Seismic Behavior of Moment Connections and Joints," Journal of the Structural Division, ASCE, Vol. 108, No. ST2, Proc. Paper 16865, February 1982.

25. Rentschler, G. P., Chen, W. F., and Driscoll, G. C., "Beam-to-Column Web Connection Details," Journal of the Structural Division, ASCE, Vol. 108, No. ST2, Proc. Paper 16880, February 1982.

26. Witteveen, J., Startk, J. W. B., Bijlaard, F. S. K., and Zoetemeijer, P., "Welded and Bolted Beam-to-Column Connections," Journal of the Structural Division, ASCE, Vol. 108, No. ST2, Proc. Paper 16873, February 1982.

27. Krishnamurthy, N. "A Fresh Look at Bolted End-Plate Behavior and Design," Engineering Journal, AISC, Vol. 15, No.2, 1978.

28. Krawinkler, H., "Shear in Beam-Column Joints in Seismic Design of Steel Frames, Engineering Journal, AISC, Vol. 15, No. 3, 1978.

29. Popov, E. P., Bertero, V. V., and Chandramouli, S., "Hysteretic Behavior of Steel Columns," Report No. EERC 75-11, University of California, Berkeley, California, September 1975.

30. Bertero, V. V., Krawinkler, H. and Popov, E. P., "Further Studies on Seismic Behavior of Steel Beam-Column Subassemblies," Report No. EERC 73-27, University of California, Berkeley, California, December 1973.

31. Krawinkler, H., Bertero, V. V., and Popov, E. P., "Inelastic Behavior of Steel Beam-to-Column Subassemblies," Report No. EERC 71-7, University of California, Berkeley, California, October 1971.

32. Lewitt, C. W., Chesson, E., and Munse, W. H., "Restraint Characteristics of Flexible Riveted and Bolted Beam-to-Column Connections," Bulletin No. 500, University of Illinois, College of Engineering, Engr. Exp. Station, January 1969.

33. Kennedy, D. J. L., "Moment-Rotation Characteristics of Shear Connections," Engineering Journal, AISC, Vol. 6, No. 4, October 1969.

34. Sommer, W. H., "Behavior of Welded Header Plate Connections," Master's Thesis, University of Toronto, Toronto, Ontario, 1969.

35. Yura, J. A., Birkemoe, P. C., and Ricles, J. M., "Beam Web Shear Connections, an Experimental Study," Journal of the Structural Division, ASCE, Vol. 108, Proc. Paper 16848, February 1982.

36. Specification for the Design, Fabrication and Erection of Structural Steel for Buildings, American Institute of Steel Construction, New York, 1969.

37. "Summary of Earthquake Conference," University of California, Berkeley, California, April 13-14, 1977.

38. Hanson, R. D., "Repair, Strengthening and Rehabilitation of Buildings - Recommendations for Needed Research," University of Michigan, Department of Civil Engineering, UMEE 77R4, October 1977.

39. Donovan, N. C., "Report on a Study of Needs in Earthquake Engineering Research," Vol. 12, No. 1, Newsletter, Earthquake Engineering Research Institute, Berkeley, California, January 1978.

40. Monograph on Planning and Design of Tall Buildings, Vol. SB, American Society of Civil Engineers, 1979.

41. Ackroyd, M. H., and Gerstle, K. H., "Behavior of Type 2 Steel Frames," Paper No. 8, Preprint 80-179, ASCE Convention, April 1980.

42. Moncarz, P. D., and Gerstle, K. H., "Steel Frame with Nonlinear Connections," Journal of Structural Division, ASCE, Vol. 107, No. ST8, Proc. Paper 16440, August 1981.

43. Frye, M. H., and Morris, G. A., "Analysis of Flexibly Connected Steel Frames," Can. J. Civil Engineering, Vol. 2, 1975.

44. Lathrop, R. P., Onderdonk, A. B., and Coel, J., "End Plate Connections in Plastically Designed Structures," Engineering Journal, AISC, Vol. 1, No. 1, January 1964.

45. Disque, R. O., "Wind Connection with Simple Framing," Engineering Journal, AISC, Vol. 1, No. 3, July 1964.

46. Abolitz, A. L., and Warner, M. E., "Bending Under Seated Connections," Engineerng Journal, AISC, Vol. 2, No. 1, January 1965.

47. Lothers, J. E., Advanced Design in Structural Steel, Prentice-Hall, Inc., Englewood Cliffs, NJ. 1960.

48. Monforton, G.R., and Wu, T. S., "Matrix Analysis of Semi-Rigidly Connected Frames," Journal of Structural Division, ASCE, Vol. 89, No. ST6, Proc. Paper 3713, December 1963.

49. Ronstad, K. M., and Sabramanian, C. V., "Analysis of Frames with Partial Connectin Rigidity," Journal of Structural Division, ASCE, Vol. 96, No. ST11, Proc. Paper 7664, November 1970.

50. Marley, M. H., "Analysis and Tests of Flexibly-Connected Steel Frames," Report to AISI under project No. 199, Dept. of Civil, Environmental, and Architectural Engineering, University of Colorado, Boulder, Colorado, March 1982.

51. Gaylord, E. H., and Gaylord, C. N., Design of Steel Structures, McGraw-Hill Book Company, NY, 1972.

52. Desalvo, G. J. and Swanson, J. A., ANSYS Engineering Analysis System User's Manual (Revision 3), Swanson Analysis Systems, Inc., July 1979.

53. Kohnke, P. C., ANSYS Engineering Analysis System Theoretical Manual, Swanson Analysis Systems, Inc., November 1977.

APPENDIX A

NOMENCLATURE

Symbol

A = cross-sectional area of flange angle, t X L

B = $B' - t/2$

B' = overall length of leg of flange angle adjacent to column face

B_c = $B'_c - t_c/2$

B'_c = overall length of leg of web angle adjacent to column face

C_i = coefficients in empirical equation of static M-ϕ curve, Model VII

D = $d + t/2$

E = Modulus of Elasticity of steel, 29000 ksi

E_{sth} = assumed Modulus of Elasticity in strain hardening region

F = shear force in beam representative of angle leg

G = shear modulus of steel

K = $P_1^{\alpha_1} P_2^{\alpha_2} \text{ --- } P_n^{\alpha_n}$

K_b = bending stiffness including strain hardening region

L = overall length of flange angle

L_c = overall length of web angle

M = resisting moment transferred from beam to column through connection

M_b = moment in beam representing connection angle, Model III

M_c = moment contribution of web angles

M_{el} = moment in connection at elastic limit

M_f = moment contribution of flange angle

M_y = yield moment of connection

P_i = parameters affecting relationship between M and ϕ in Model VII

NOMENCLATURE (Con'd)

Symbol

S = elastic section modulus

Z = plastic section modulus

a = $g - k$

b = $g - d_b/2 - t/2$

b_c = $g_c - d_b/2 - t_c/2$

d = depth of beam

d_b = diameter of bolt

d_h = diameter of bolt hole

d_w = diameter of washer

g = gage in flange angle; from heel of angle to center of bolt hole in leg adjacent to column face

g_c = gage in web angle; from heel of angle to center of bolt hole in leg adjacent to column face

k = distance from heel of angle to toe of fillet, flange angle

k_c = distance from heel of angle to toe of fillet, web angle

P = pitch, center-to-center spacing of bolts in leg of flange angle adjacent to column face

P_c = pitch, center-to-center spacing of bolts in each leg of web angle

t = thickness of flange angle

t_c = thickness of web angle

α_i = exponents in empirical equation of static M-ϕ curve, Model VII

γ = length of flange angle used in finite element analysis

Δ = displacement of heel of flange angle

ε_y = strain at initial yielding in connection angles

NOMENCLATURE (Con'd)

Symbol

λ = length of beam representative of flange angle leg adjacent to column face

λ_c = length of beam representative of web angle leg adjacent to column face

σ_y = stress at initial yielding in connection angles

ϕ = rotation of end of beam with respect to column face

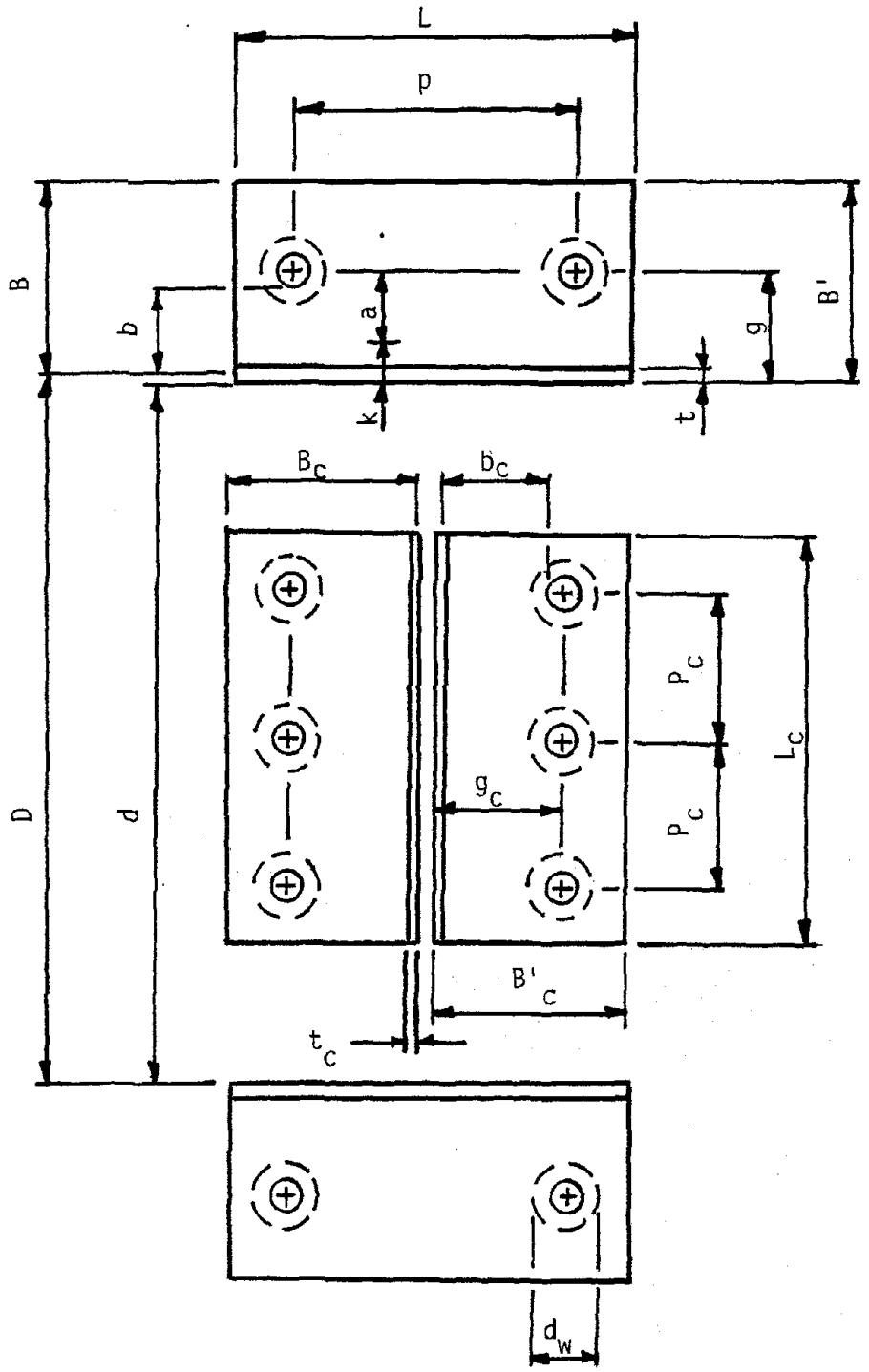

FIG. A1 NOMENCLATURE FOR CONNECTION ELEMENTS

APPENDIX B

THREE DIMENSIONAL

FINITE ELEMENT MODEL

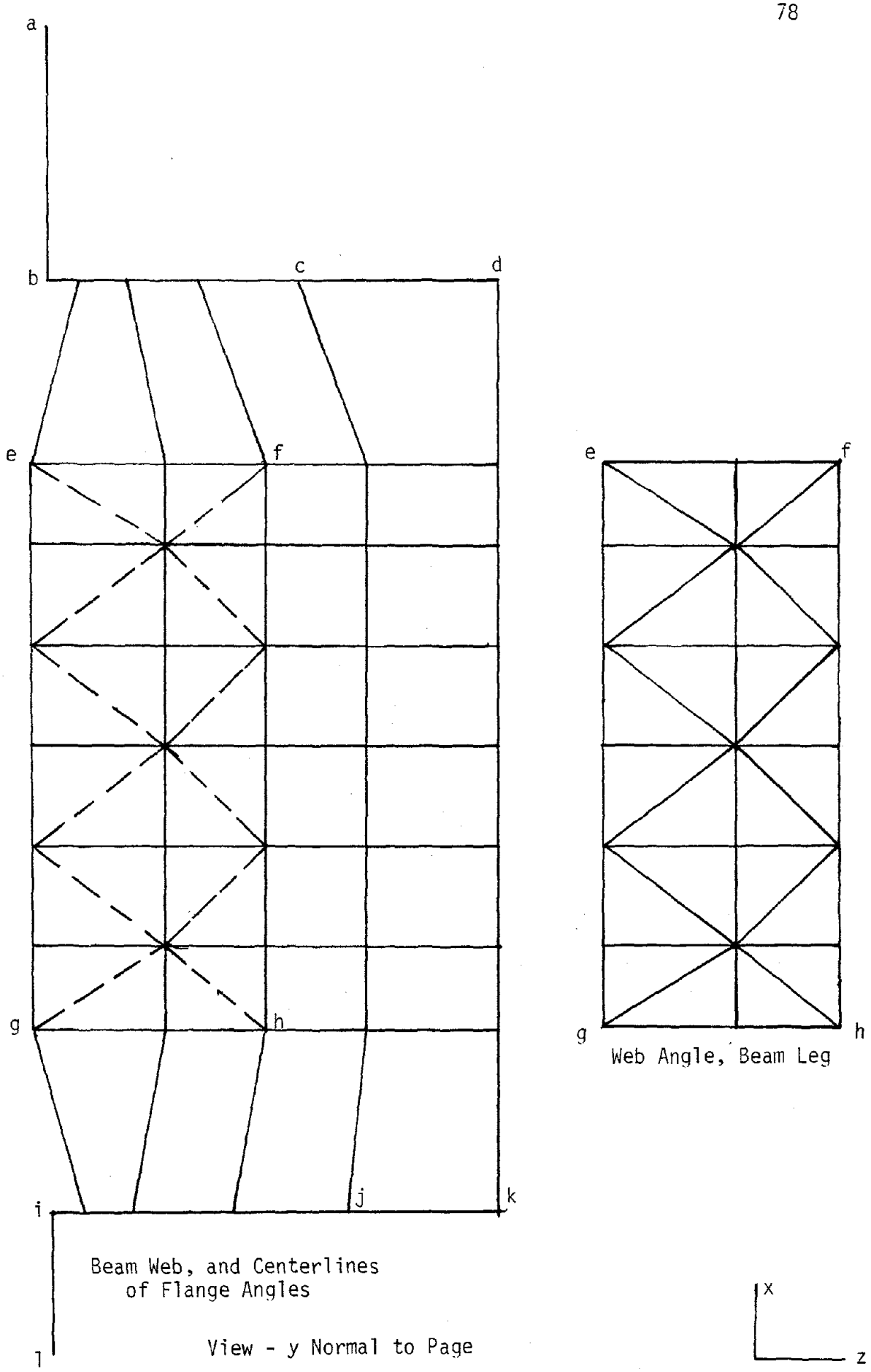

FIG. B1 MODEL VI FINITE ELEMENT MESH — BEAM ELEVATION

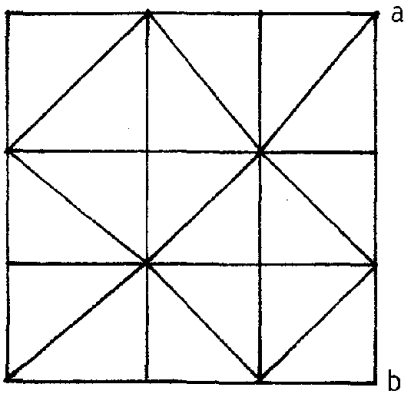

Top Flange Angle,
Column Leg

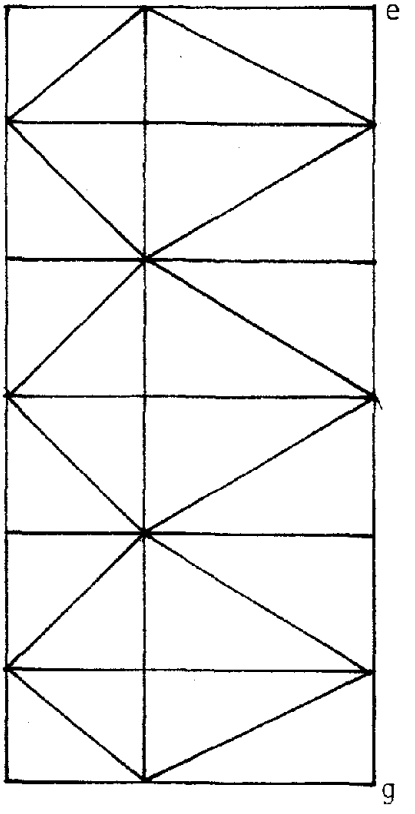

Web Angle,
Column Leg

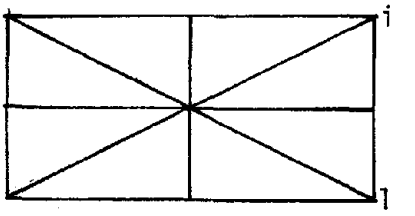

Bottom Flange Angle,
Column Leg

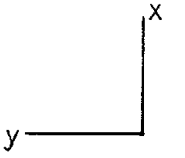

View - z Normal to Page

FIG. B2 MODEL VI FINITE ELEMENT MESH — COLUMN ELEVATION

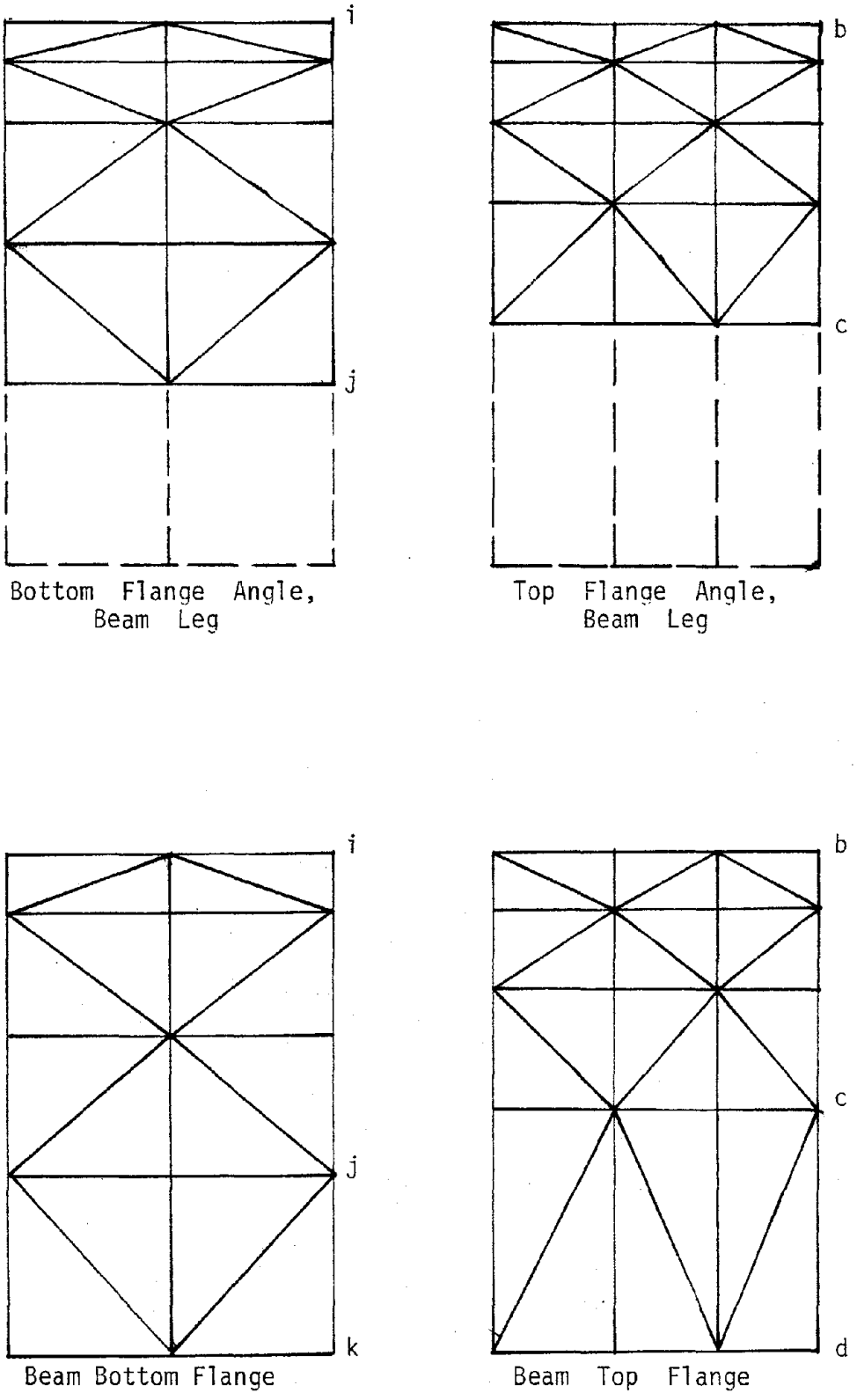

FIG. B3 MODEL VI FINITE ELEMENT MESH — TOP VIEW

TABLE 2.1

MECHANICAL PROPERTIES OF TEST MATERIAL

Steel Designation	Mechanical Properties		
	Yield Stress (ksi)	Ultimate Strength (ksi)	Elongation in 2-inch Gage Length (percent)
ASTM A36	42.8	69.9	23.8
	42.9	67.9	22.9
	39.3	68.0	32.5
	37.6	67.9	31.9
	53*	80*	--

*Flange angle material, specimen 14S2

TABLE 2.2

SCHEDULE OF TEST SPECIMENS

Specimen No.	Type of Test	Beam Selection	Top and Bottom Flange Angles*				Web Angles*	
			Angle	Length, "L" (inches)	Gage in Leg on Column Flange, "g" (inches)	Bolt Spacing in Leg on Col.Flange, "p" (inches)	Angle	Length, "L_c" (inches)
14S1	Static	W14X38	L6X4X3/8	8	2½	5½	2L4X3½X¼	8½
14S2	Static	W14X38	L6X4X½	8	2½	5½	2L4X3½X¼	8½
14S3	Static	W14X38	L6X4X3/8	8	2½	5½	2L4X3½X¼	5½†
14S4	Static	W14X38	L6X4X3/8	8	2½	5½	2L4X3½X3/8	8½
8S1	Static	W8X21	L6X3½X5/16	6	2	3½	2L4X3½X¼	5½
8S2	Static	W8X21	L6X3½X3/8	6	2	3½	2L4X3½X¼	5½
8S3	Static	W8X21	L6X3½X5/16	8	2	3½	2L4X3½X¼	5½
8S4	Static	W8X21	L6X6X3/8	6	4½	3½	2L4X3½X¼	5½
8S5	Static	W8X21	L6X4X3/8	8	2½	5½	2L4X3½X¼	5½
8S6	Static	W8X21	L6X4X5/16	6	2½	3½	2L4X3½X¼	5½
8S7	Static	W8X21	L6X4X3/8	6	2½	3½	2L4X3½X¼	5½
14C1	Cyclic	W14X38	L6X4X3/8	8	2½	5½	2L4X3½X¼	8½
14C2	Cyclic	W14X38	L6X4X½	8	2½	5½	2L4X3½X¼	8½
8C1	Cyclic	W8X21	L6X4X5/16	6	2	3½	2L4X3½X¼	5½
8C2	Cyclic	W8X21	L6X4X3/8	6	2	3½	2L4X3½X¼	5½

*See Nomenclature, Appendix A.

†Two bolts at 3-inch spacing, mounted in top two holes on stub column, Fig. 2.3.

TABLE 3.1

SUMMARY OF STATIC TEST RESULTS

Specimen Number	Initial Slope of M-ϕ Curve (k-in./radian)	Slope of Secant Line to M-ϕ Curve at $4.0X10^{-3}$radians (k-in./radian)	Moment at $4.0X10^{-3}$radians (k-in.)	Slope of M-ϕ Curve at $24X10^{-3}$radians (k-in./radian)	Moment at $24X10^{-3}$radians (k-in.)	Remarks
14S1	$195.0X10^{+3}$	$108.7X10^{+3}$	435	$5.8X10^{+3}$	668	
14S2	295.0	151.8	607	12.6	(947)	Major slip at $12X10^{-3}$ & $20X10^{-3}$ radians
14S3	115.9	88.8	355	7.2	652	
14S4	221.9	124.0	496	8.3	822	
8S1	66.7	44.3	177	4.1	329	
8S2	123.4	69.0	276	1.5	(384)	Major slip at $16X10^{-3}$ radians
8S3	104.7	64.3	257	4.0	422	
8S4	15.3	14.4	57.5	2.2	165	
8S5	76.7	47.9	191.5	2.7	337	
8S6	39.5	30.0	120	3.2	244	
8S7	48.0	40.8	163	3.2	381	

TABLE 3.2

SUMMARY OF CYCLIC TEST RESULTS - SPECIMEN 14C1

Actuator Displacement Amplitude (inches)	Frequency (Hz)	Number of Cycles	Range of Rotation (radians X 1000)	Range of Moment (kip-inches)	Area of a Single Hysteresis Loop* (kip-inches)	Cumulative Area of Hysteresis Loops (kip-inches)	Cumulative Number of Cycles	Remarks
0.2	.05	4	-	-	-	-	4	No Data
	.1	1	2.20	435.8	0	0	5	
		1	2.08	441.5	0	0	6	
	.5	1	2.10	428.5	0	0	7	
		10	2.34	439.2	0	0	17	
0.4	.1	1	4.75	745.0	.296	.296	18	
		1	4.87	738.5	.123	.419	19	
		1	4.89	741.5	.111	.530	20	
	.25	1	4.91	742.5	.069	.599	21	
		1	4.77	737.1	.064	.663	22	
		10	5.04	751.7	.069	1.353	32	
0.6	.1	1	7.84	931.3	.734	2.087	33	
		1	7.77	934.9	.419	2.506	34	
		1	7.85	933.2	.320	2.826	35	
	.25	1	7.78	924.9	.283	3.109	36	
		1	7.88	922.0	.279	3.388	37	
		10	8.08	932.2	.282	6.208	47	
0.8	.1	1	11.10	1068	1.608	7.816	48	
		1	10.99	1046	.998	8.814	49	
		1	10.86	1031	.824	9.638	50	
	.25	1	10.95	1032	.812	10.450	51	
		1	11.03	1034	.831	11.281	52	
		10	11.23	1042	.829	19.571	62	
1.0	.1	1	14.44	1142	2.45	22.021	63	
		1	14.32	1105	1.912	23.933	64	
		1	14.37	1102	1.875	25.808	65	
	.25	1	14.49	1095	1.818	27.626	66	
		1	14.28	1094	1.83	29.456	67	
		10	14.70	1109	1.78	47.256	77	

*For multiple cycles, the area of one loop is computed as the average of the first and last loop areas.

Continued -

TABLE 3.2 (continued)

SUMMARY OF CYCLIC TEST RESULTS - SPECIMEN 14C1

Actuator Displacement Amplitude (inches)	Frequency (Hz)	Number of Cycles	Range of Rotation (radians X 1000)	Range of Moment (kip-inches)	Area of a Single Hysteresis Loop* (kip-inches)	Cumulative Area of Hysteresis Loops (kip-inches)	Cumulative Number of Cycles	Remarks
1.2	.1	1	17.73	1185	3.747	51.003	78	
		1	17.64	1146	3.372	54.38	79	
		1	17.78	1142	3.39	57.77	80	
	.25	1	17.67	1139	3.278	61.04	81	
		1	17.70	1140	3.241	64.28	82	
		10	17.94	1140	3.193	96.21	92	
1.4	.1	1	21.12	1207	5.480	101.69	93	
		1	21.17	1183	5.230	106.9	94	
		1	21.36	1173	5.232	112.2	95	
	.25	1	21.22	1171	5.09	117.2	96	
		1	21.18	1169	5.033	122.3	97	
		10	21.73	1170	4.98	172.1	107	
1.6	.1	1	24.51	1276	7.092	179.2	108	
		1	24.65	1250	6.704	185.9	109	
		1	24.68	1238	6.577	192.5	110	
		1	24.83	1230	6.594	199.0	111	
	.25	1	24.52	1217	6.58	205.6	112	
		1	24.60	1219	6.537	212.2	113	
		10	25.11	1217	6.507	277.2	123	
1.8	.1	1	28.30	1261	9.0	286.2	124	
		1	28.42	1232	8.912	295.1	125	
		1	28.31	1213	8.734	303.9	126	
	.25	1	28.17	1213	8.615	312.5	127	
		1	28.22	1203	8.60	321.1	128	
		10	28.55	1206	8.415	405.2	138	
2.0	.1	1	31.81	1257	11.0	416.2	139	
		1	31.76	1225	10.87	427.1	140	
		1	32.17	1220	10.775	437.9	141	
	.25	1	----	----	----	----	----	half cycle
		1	31.85	1193	10.55	448.4	142	
		1	31.90	1198	10.474	458.9	143	
		6	32.46	1197	10.26	520.5	149	cracks detected-6th cycle

*For multiple cycles, the area of one loop is computed as the average of the first and last loop areas.

TABLE 3.3

SUMMARY OF CYCLIC TEST RESULTS - SPECIMEN 14C2

Actuator Displacement Amplitude (inches)	Frequency (Hz)	Number of Cycles	Range of Rotation (radians X 1000)	Range of Moment (kip-inches)	Area of a Single Hysteresis Loop* (kip-inches)	Cumulative Area of Hysteresis Loops (kip-inches)	Cumulative Number of Cycles	Remarks
0.2	.1	1	2.16	472.3	0		1	
	.25	1	2.12	478.1	0		2	
		1	2.09	474.2	0		3	
		10	2.37	488.7	0	0	13	
.4	.1	1	4.47	850.7	.238	.238	14	
	.25	1	4.45	831.1	.152	.390	15	
		1	4.54	857.0	.135	.525	16	
		10	4.43	**	.211**	2.635	26	
.6	.1	1	7.07	1132	.725	3.360	27	Inverted cycle***
	.25	1	7.0	1143	.404	3.764	28	Inverted cycle
		1	7.1	1139	.310	4.074	29	Inverted cycle
		10	7.31	1154	.304	7.114	39	
.8	.1	1	10.12	1357	1.469	8.583	40	
		1	9.95	1345	.878	9.461	41	Inverted cycle
		1	9.87	1345	1.038	10.499	42	Inverted cycle
	.25	1	10.08	1334	.748	11.247	43	
		1	9.82	1331	.928	12.175	44	
		10	10.09	1332	.919	21.365	54	
1.0	.1	1	13.12	1490	2.809	24.174	55	
	.25	1	12.98	1477	2.437	26.611	56	
		1	13.26	1466	2.262	28.873	57	
		10	13.43	1465	2.197	50.843	67	
1.2	.1	1	16.28	1571	4.563	55.406	68	
	.25	1	16.31	1548	4.237	59.643	69	
		1	16.18	1541	4.101	63.744	70	
		10	16.70	1536	4.012	103.86	80	

*For multiple cycles, the area of one loop is computed as the average of the first and last loop areas.
**Questionable data.
***Load cycle inverted from normal sine wave, Fig. 3.21.

Continued -

TABLE 3.3 (continued)

SUMMARY OF CYCLIC TEST RESULTS - SPECIMEN 14C2

Actuator Displacement Amplitude (inches)	Frequency (Hz)	Number of Cycles	Range of Rotation (radians X 1000)	Range of Moment (kip-inches)	Area of a Single Hysteresis Loop* (kip-inches)	Cumulative Area of Hysteresis Loops (kip-inches)	Cumulative Number of Cycles	Remarks
1.4	.1	1	19.79	1637	6.837	110.70	81	
	.25	1	19.96	1608	6.481	117.18	82	
		1	19.80	1590	6.389	123.57	83	
0.5	.1	1	6.92	660.4	.451	124.02	84	Inspection for cracks
0.5		1	6.83	662	.234	124.26	85	
1.4	.1	1	19.80	1579	6.206	130.46	86	
		1	19.89	1577	6.428	136.89	87	
		1	20.15	1560	4.595	141.49	88	Inverted cycle**
		1	19.95	1559	6.363	147.85	89	Inverted cycle
	.25	10	20.21	1562	6.24	210.25	99	Inverted cycle
1.6	.1	1	23.39	1653	7.933	218.18	100	
		1	23.52	1622	9.069	227.25	101	
	.25	1	23.44	1615	8.79	236.04	102	
		1	23.30	1613	8.749	244.79	103	
		10	23.78	1606	8.559	330.38	113	
1.8	.1	1	26.78	1670	11.487	341.87	114	
	.25	1	26.86	1647	11.296	353.16	115	
		1	27.05	1636	11.113	364.28	116	
		10	27.20	1633	10.777	472.05	126	Crack detected
2.0	.1	1	30.48	1687	14.032	486.08	127	
		1	30.37	1659	13.871	499.95	128	
		1	30.54	1643	13.722	513.67	129	
		1	30.60	1623	13.529	527.20	130	

*For multiple cycles, the area of one loop is computed as the average of the first and last loop areas.
**Load cycle inverted from normal sine wave, Fig. 3.21.

TABLE 3.4

SUMMARY OF CYCLIC TEST RESULTS - SPECIMEN 8C1

Actuator Displacement Amplitude (inches)	Frequency (Hz)	Number of Cycles	Range of Rotation (radians X 1000)	Range of Moment * (kip-inches)	Area of a Single Hysteresis Loop** (kip-inches)	Cumulative Area of Hysteresis Loops (kip-inches)	Cumulative Number of Cycles	Remarks
0.2	.1	1	4.33	231.2	.045	.045	1	
	.25	10	4.27	233.8	.037	.415	11	
.4	.1	1	9.11	399.7	.370	.785	12	
		1	8.96	394.9	.247	1.032	13	
	.25	10	9.54	422.2	.162	2.652	23	
.6	.1	1	13.81	495.9	1.089	3.741	24	
		1	13.98	488.4	.871	4.612	25	
		1	14.11	485.3	.821	5.433	26	
	.25	10	14.50	484.0	.774	13.173	36	
.8	.1	1	20.22	538.6	2.303	15.476	37	
		1	19.80	523.5	2.299	17.775	38	
		1	19.98	500.2	2.342	20.117	39	
		1	20.18	495.9	2.417	22.534	40	
	.25	10	20.5	490.1	2.361	46.144	50	
1.0	.1	1	26.03	511.6	4.188	50.332	51	
		1	26.36	516.2	4.222	54.554	52	
		1	26.23	490.8	4.154	58.708	53	
		1	27.20	490.9	4.431	63.139	54	
	.25	10	28.00	499.7	4.283	105.969	64	
1.2	.1	1	32.35	521.3	6.130	112.10	65	
		1	32.71	513.9	6.320	118.42	66	
	.25	5	32.82	505.7	6.118	149.01	71	
		5	32.55	480.5	6.004	179.03	76	
1.4	.1	1	38.94	498.2	7.923	186.95	77	
		1	39.05	478.6	7.626	194.58	78	
		—	—	—	—	—	—	Half cycle, abrupt crack formation

*Extreme values reported.

**For multiple cycles, the area of one loop is computed as the average of the first and last loop areas.

TABLE 3.5

SUMMARY OF CYCLIC TEST RESULTS - SPECIMEN 8C2

Actuator Displacement Amplitude (inches)	Frequency (Hz)	Number of Cycles	Range of Rotation (radians X 1000)	Range of Moment* (kip-inches)	Area of a Single Hysteresis Loop** (kip-inches)	Cumulative Area of Hysteresis Loops (kip-inches)	Cumulative Number of Cycles	Remarks
0.2	.1	1	4.13	252.2	.062	.062	1	
	.25	10	4.39	268.9	.317	3.232	11	
.4	.1	1	8.39	439.3	.454	3.686	12	
		1	8.05	454.0	.307	3.993	13	
	.25	10	8.49	453.8	.254	6.533	23	
.6	.1	1	13.43	564.3	1.438	7.971	24	
		1	13.29	556.0	1.272	9.243	25	
	.25	10	13.85	554.5	1.265	21.89	35	
.8	.1	1	19.00	605.2	3.112	25.01	36	
		1	19.12	601.5	3.039	28.04	37	
		1	18.80	589.6	2.886	30.93	38	
	.25	10	19.89	592.9	2.903	59.96	48	
1.0	.1	1	25.02	616.0	5.202	65.16	49	
		1	25.32	619.4	5.22	70.38	50	
	.25	10	25.75	611.1	4.956	119.9	60	
1.2	.1	1	30.78	635.0	7.265	127.2	61	
		1	31.12	637.1	7.303	134.5	62	
	.25	10	32.17	650.2	7.063	205.1	72	Cracks detected-btm. angle
1.4	.1	1	37.29	663.7	9.704	214.8	73	
		1	36.89	659.1	9.647	224.5	74	
	.25	2	37.21	653.2	9.449	243.4	76	Cracks detected-top angles

*Extreme values reported

**For multiple cycles, the area of one loop is computed as the average of the first and last loop areas.

TABLE 4.1

COMPARISON OF INITIAL CONNECTION STIFFNESS
PREDICTED BY MODEL II WITH TEST RESULTS

SPECIMEN	INITIAL SLOPE (k-in./radian)		
	TEST	MODEL II	
		INCLUDING SHEAR	EXCLUDING SHEAR
14S1	195000	152871	172020
14S2	295000	328695	409842
14S3	115900	150442	169461
14S4	221900	212206	240919
8S1	66700	62134	72279
8S2	123400	103170	128971
8S3	104700	63300	73455
8S4	15300	12513	13032
8S5	76700	52850	59673
8S6	39500	31748	34547
8S7	48000	51429	58238

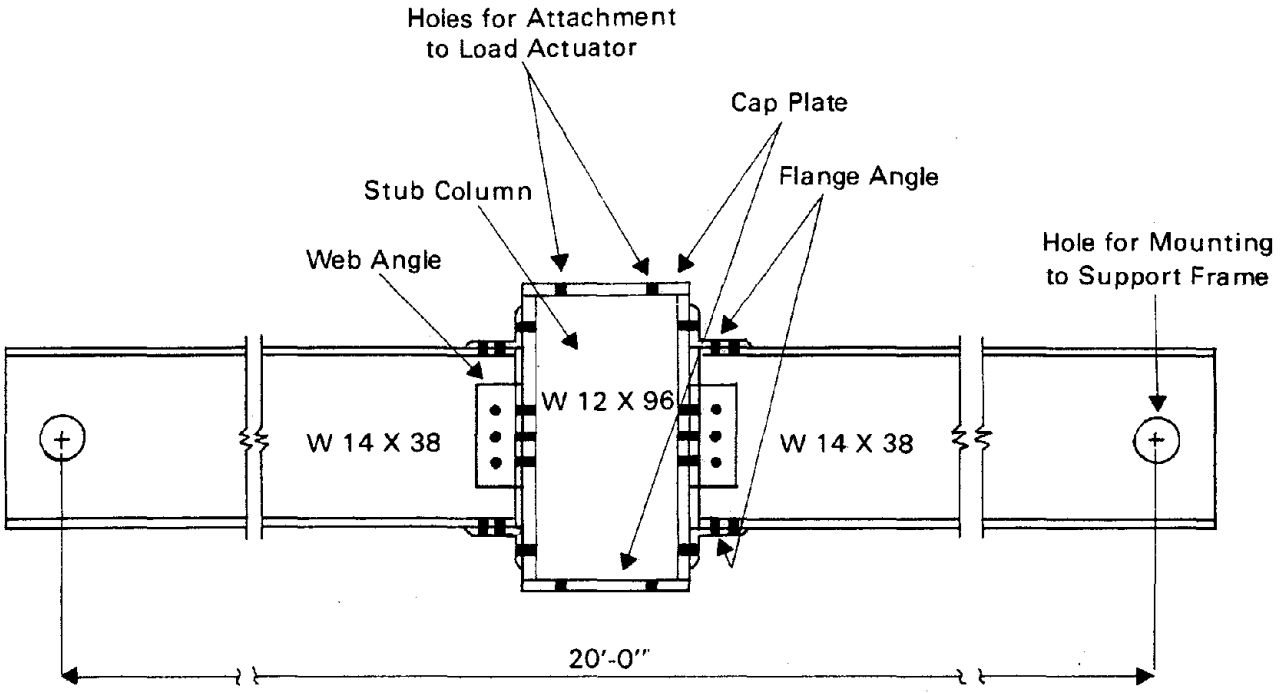

a. W 14 X 38 BEAM TEST SPECIMEN

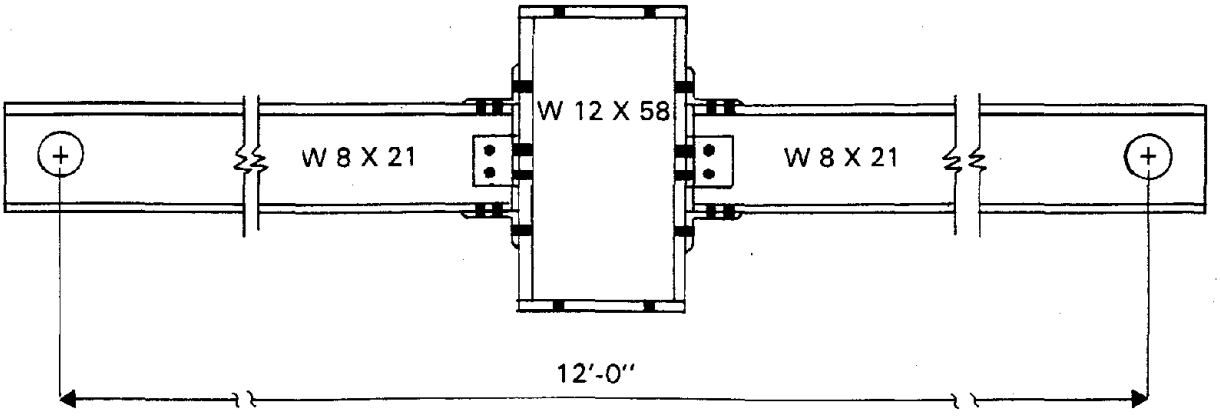

b. W 8 X 21 BEAM TEST SPECIMEN

FIG. 2.1 GENERAL CONFIGURATIONS OF TEST SPECIMENS

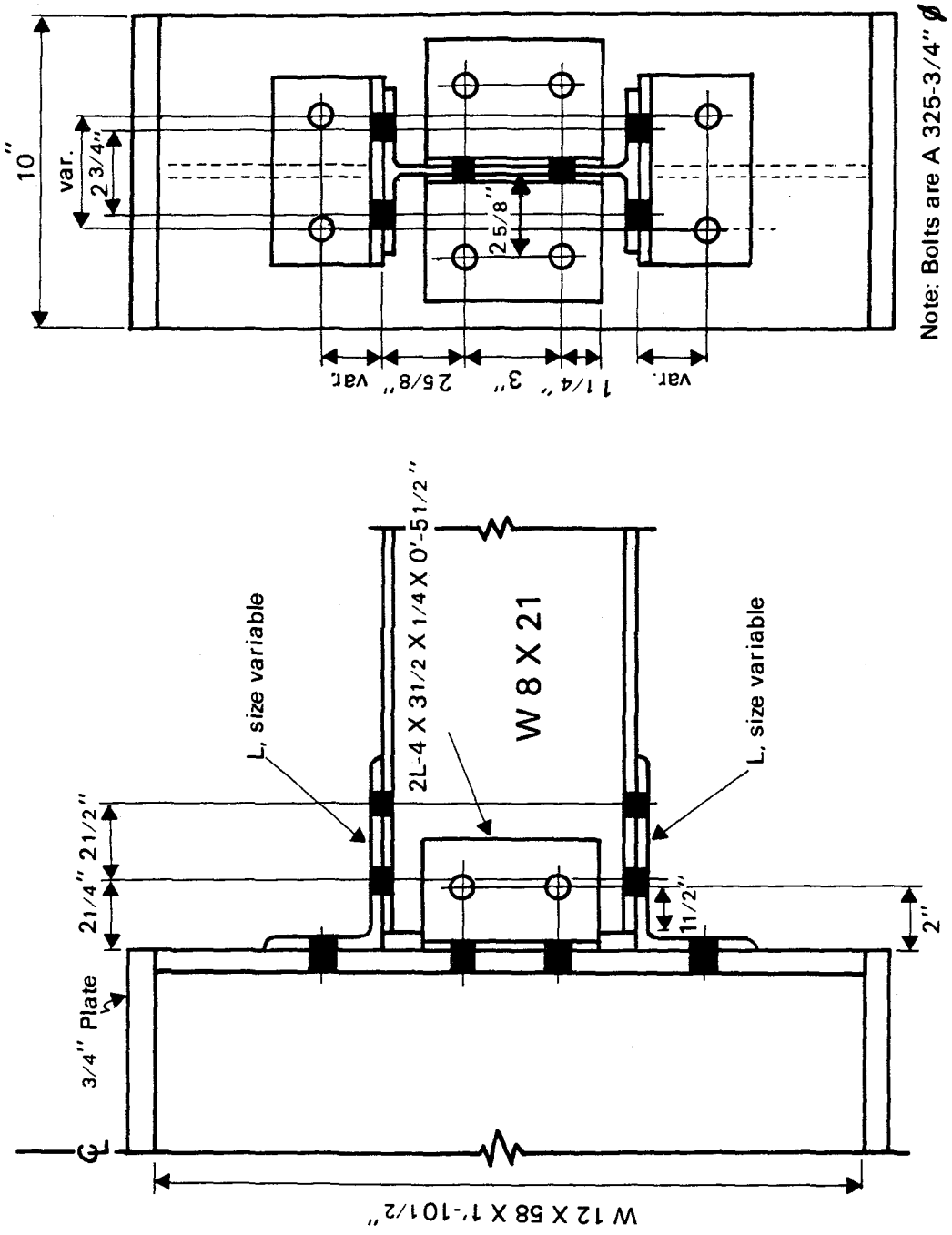

FIG. 2.2 DETAILS OF CONNECTION FOR W 8 X 21 BEAM

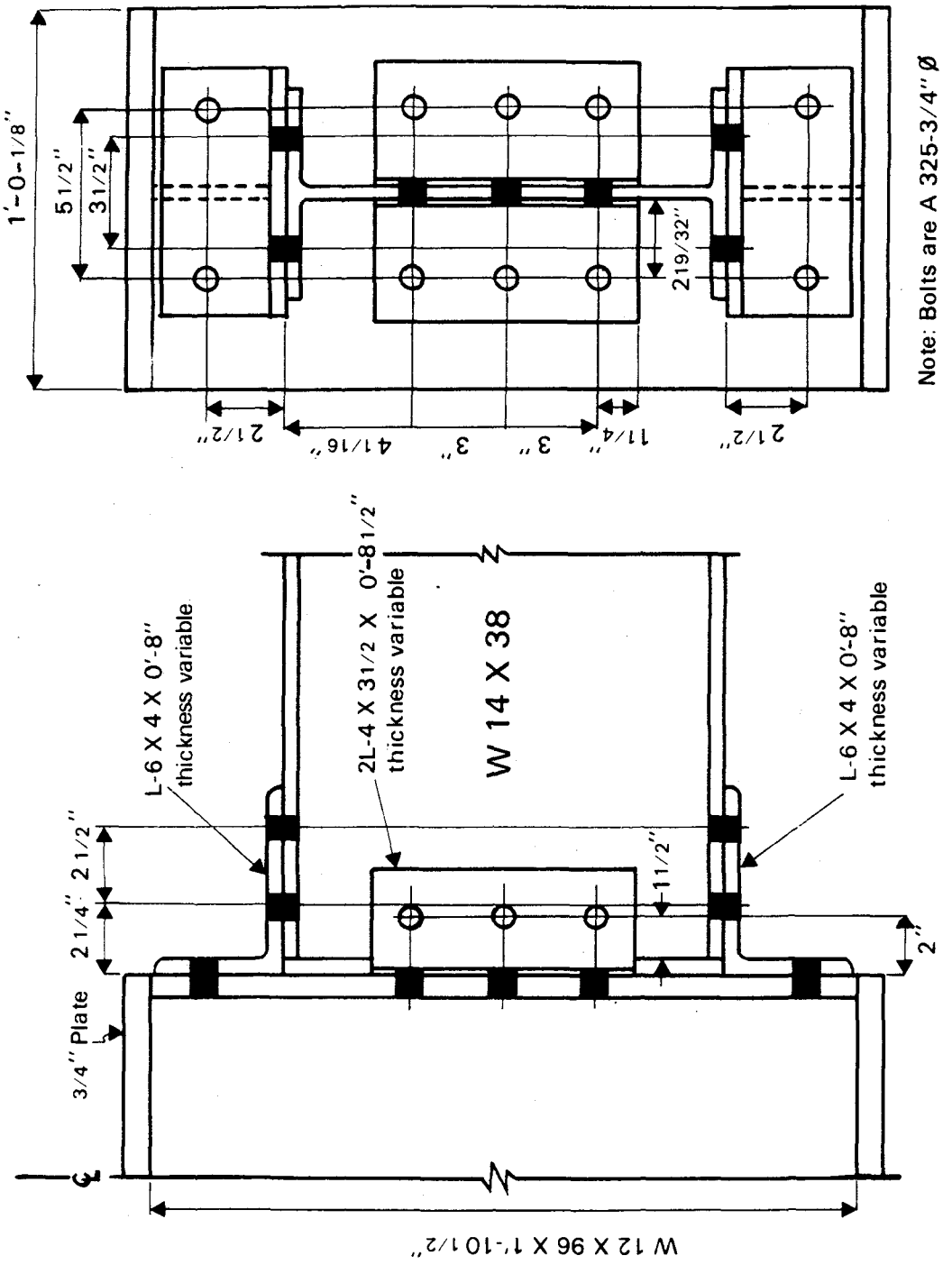

FIG. 2.3 DETAILS OF CONNECTION FOR W 14 X 38 BEAM

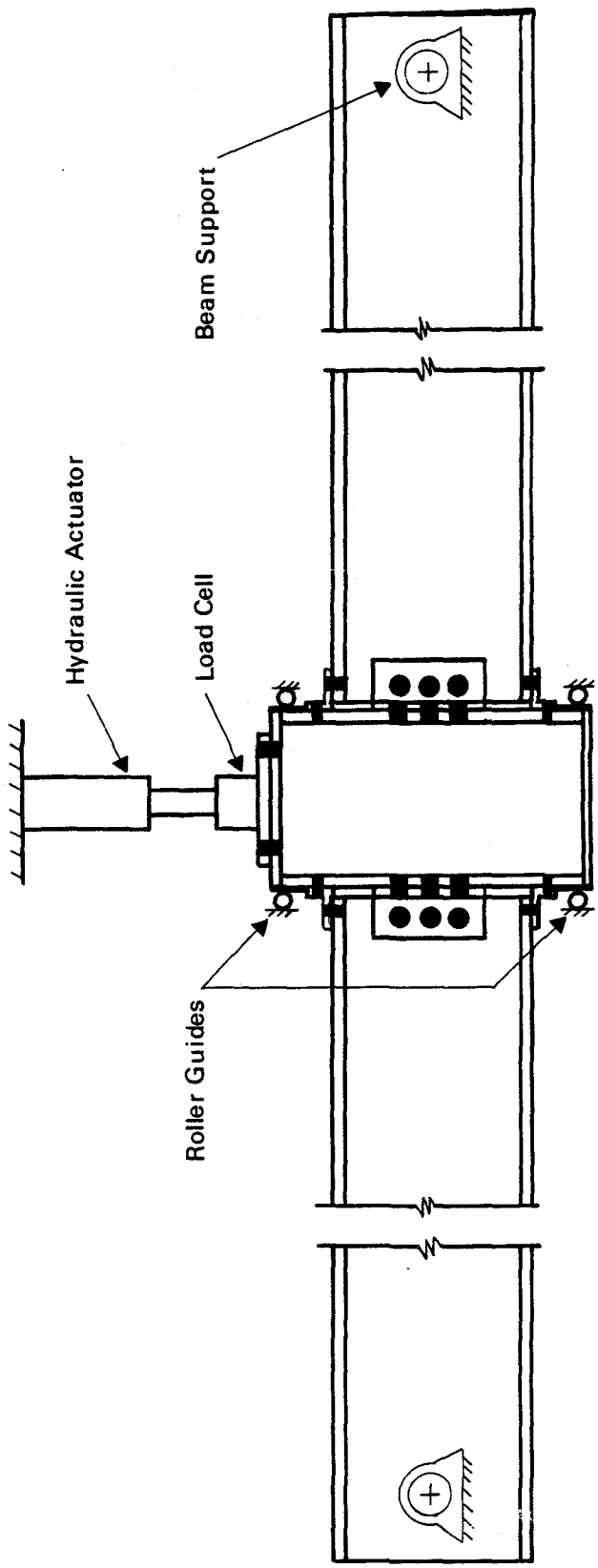

FIG. 2.4 SCHEMATIC OF LOADING SYSTEM FOR TEST BEAMS

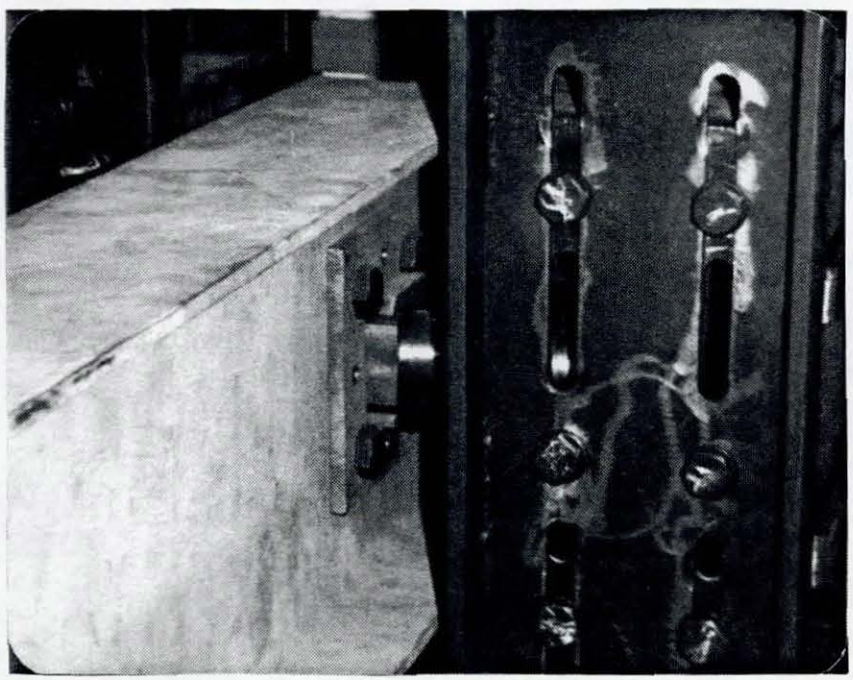

FIG. 2.5 BEAM SUPPORTS FOR TEST SPECIMENS

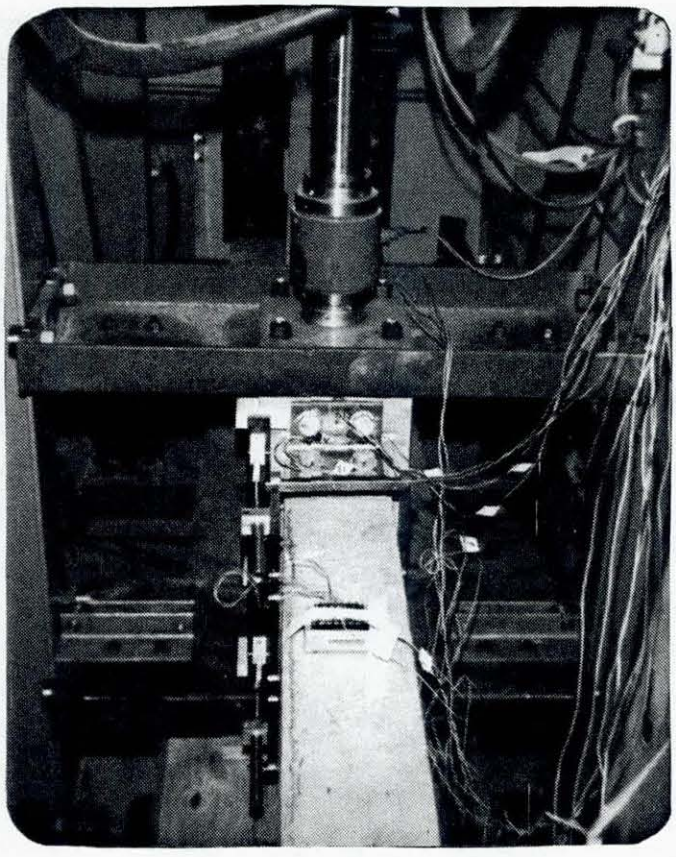

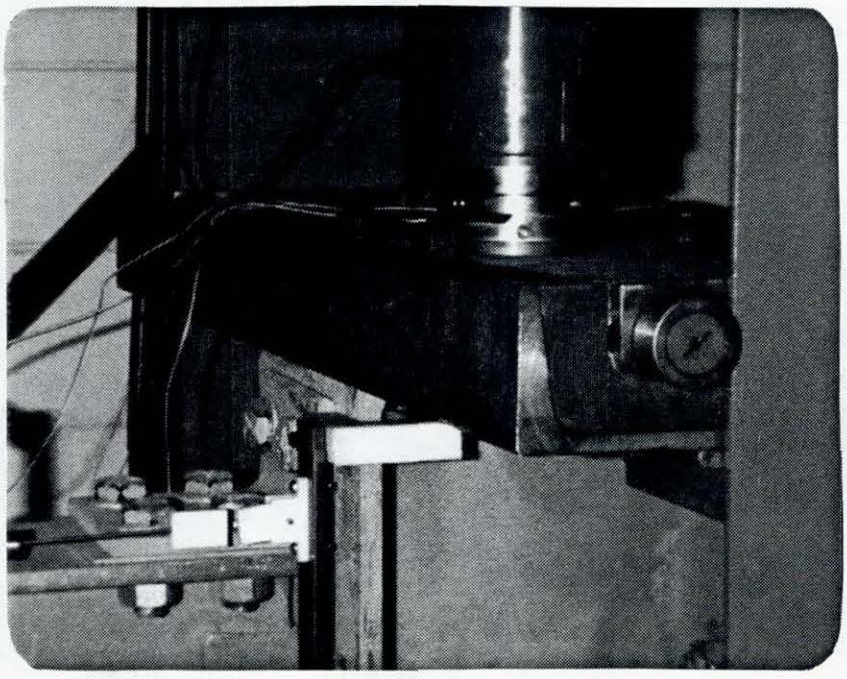

FIG. 2.6 LATERAL SUPPORT SYSTEM FOR TEST SPECIMENS

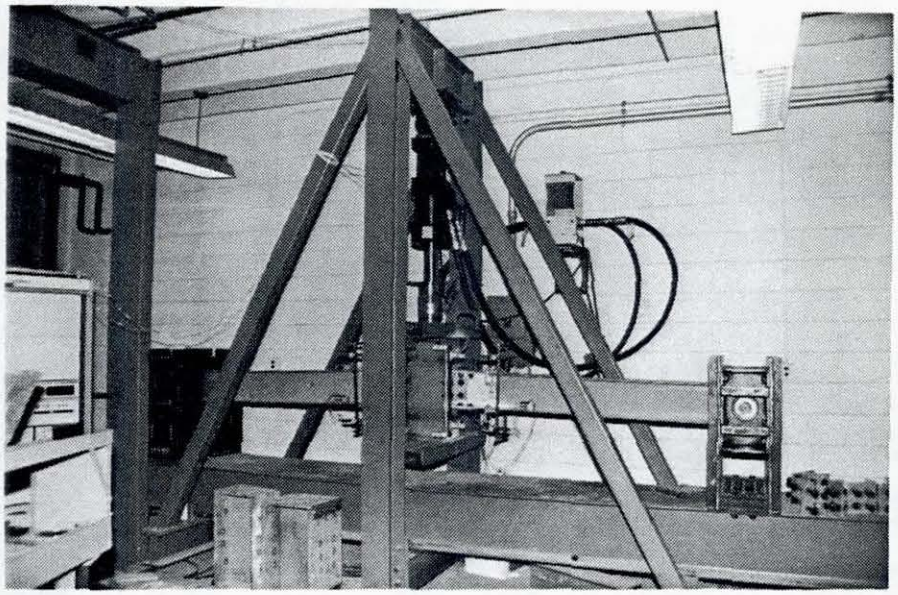

FIG. 2.7 LOADING FRAME AND TEST SET-UP

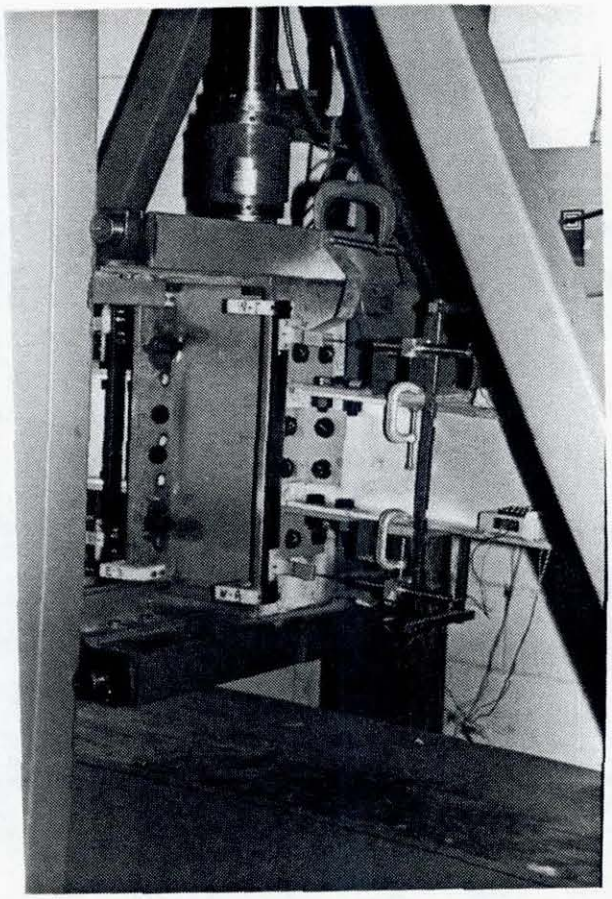

FIG. 2.8 CLOSE-UP OF TEST CONNECTION

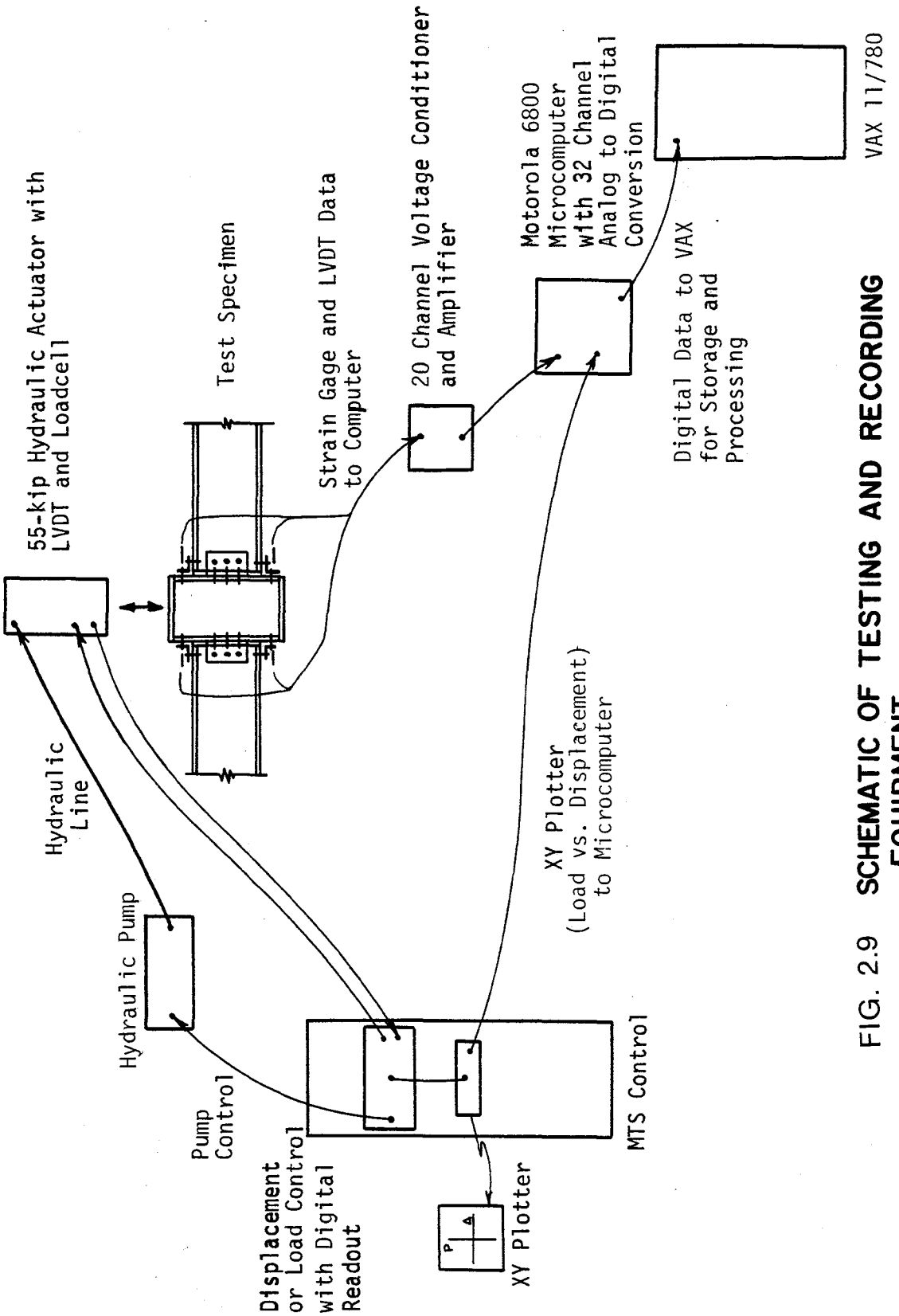

FIG. 2.9 **SCHEMATIC OF TESTING AND RECORDING EQUIPMENT**

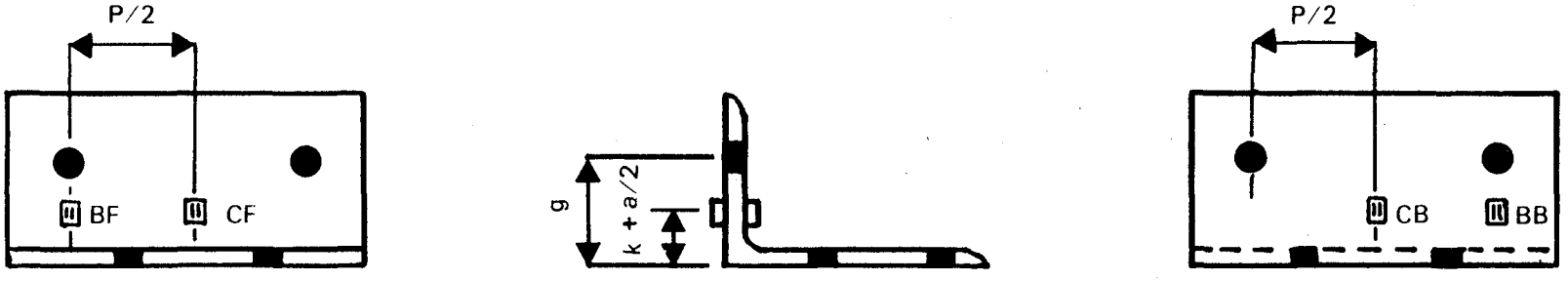

a. TYPICAL POSITIONS OF STRAIN GAGES FOR W 14 X 38 BEAMS

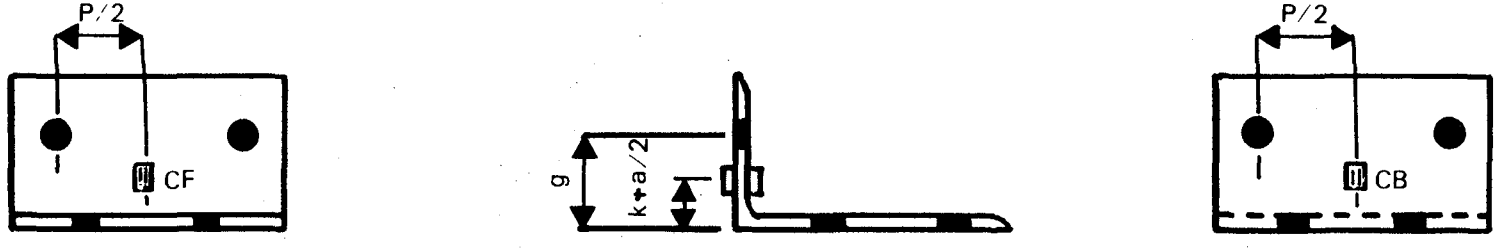

b. TYPICAL POSITIONS OF STAIN GAGES FOR W 8 X 21 BEAMS

FIG. 2.10 LOCATION OF STRAIN GAGES ON TENSION FLANGE ANGLES

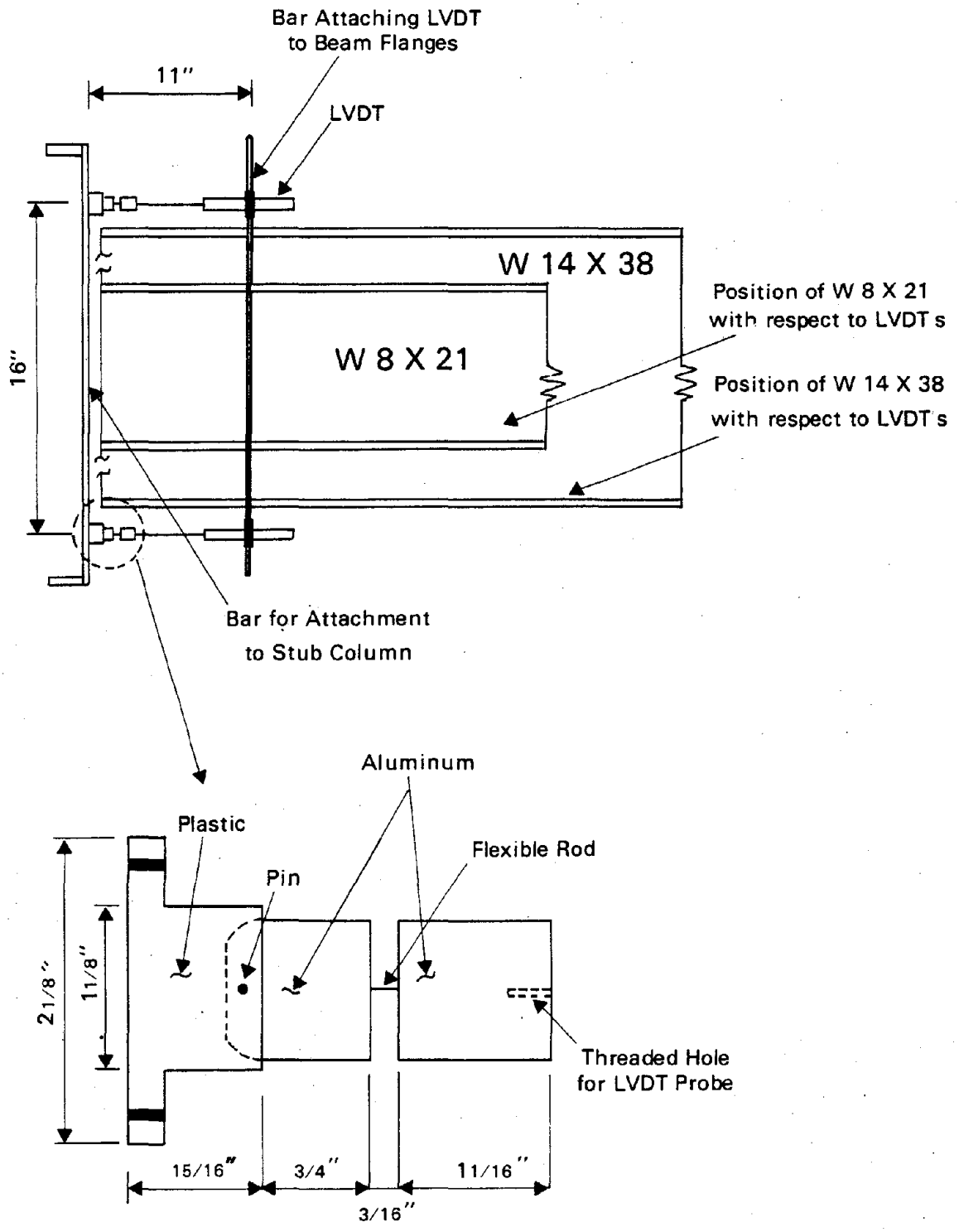

FIG. 2.11 LVDT MOUNTING APPARATUS

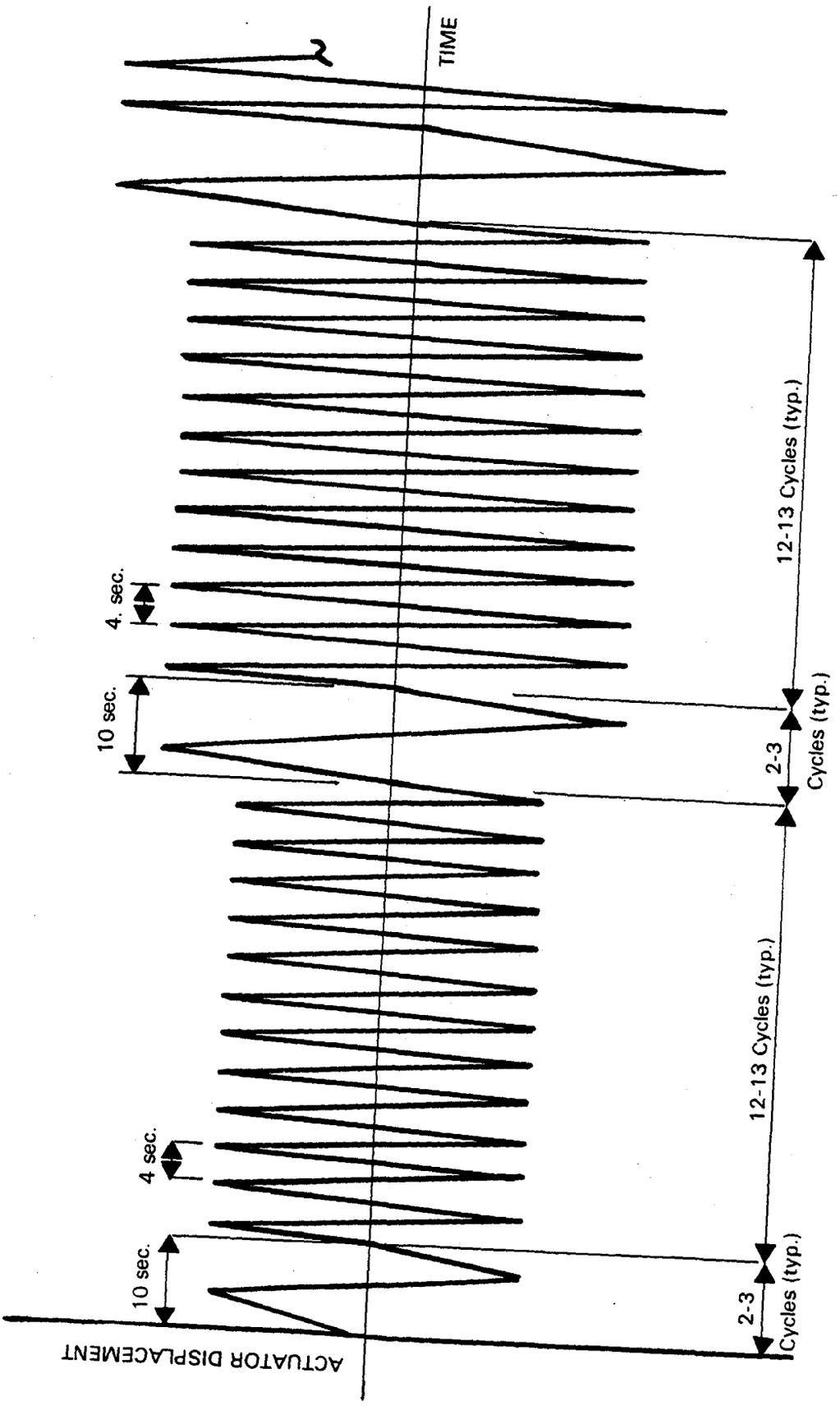

FIG. 2.12 TYPICAL TIME-DISPLACEMENT HISTORY FOR CYCLIC TESTS

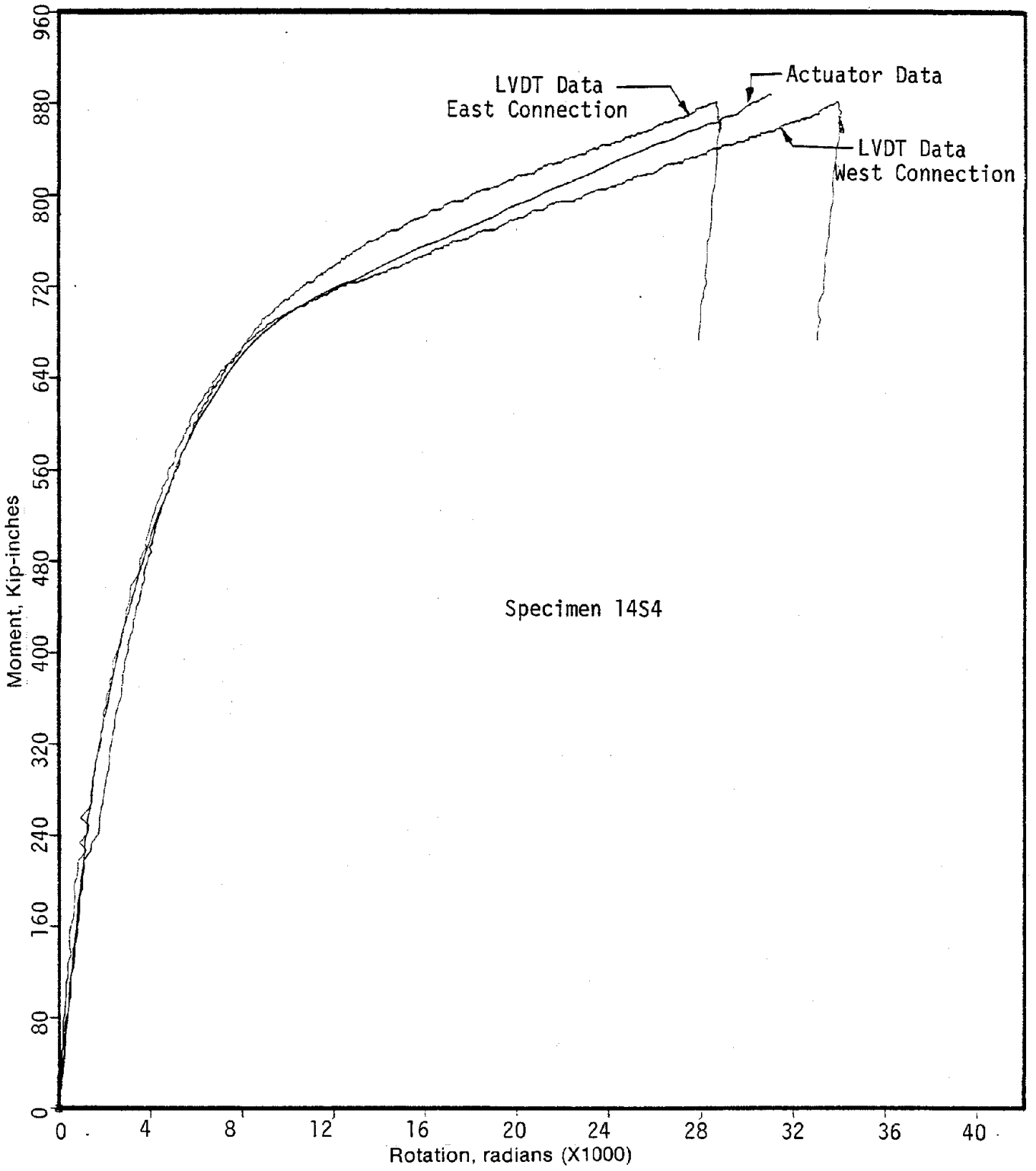

FIG. 3.1 COMPARISON OF MOMENT-ROTATION CURVES OBTAINED FROM LVDT MEASUREMENTS WITH CURVE OBTAINED FROM ACTUATOR DISPLACEMENTS

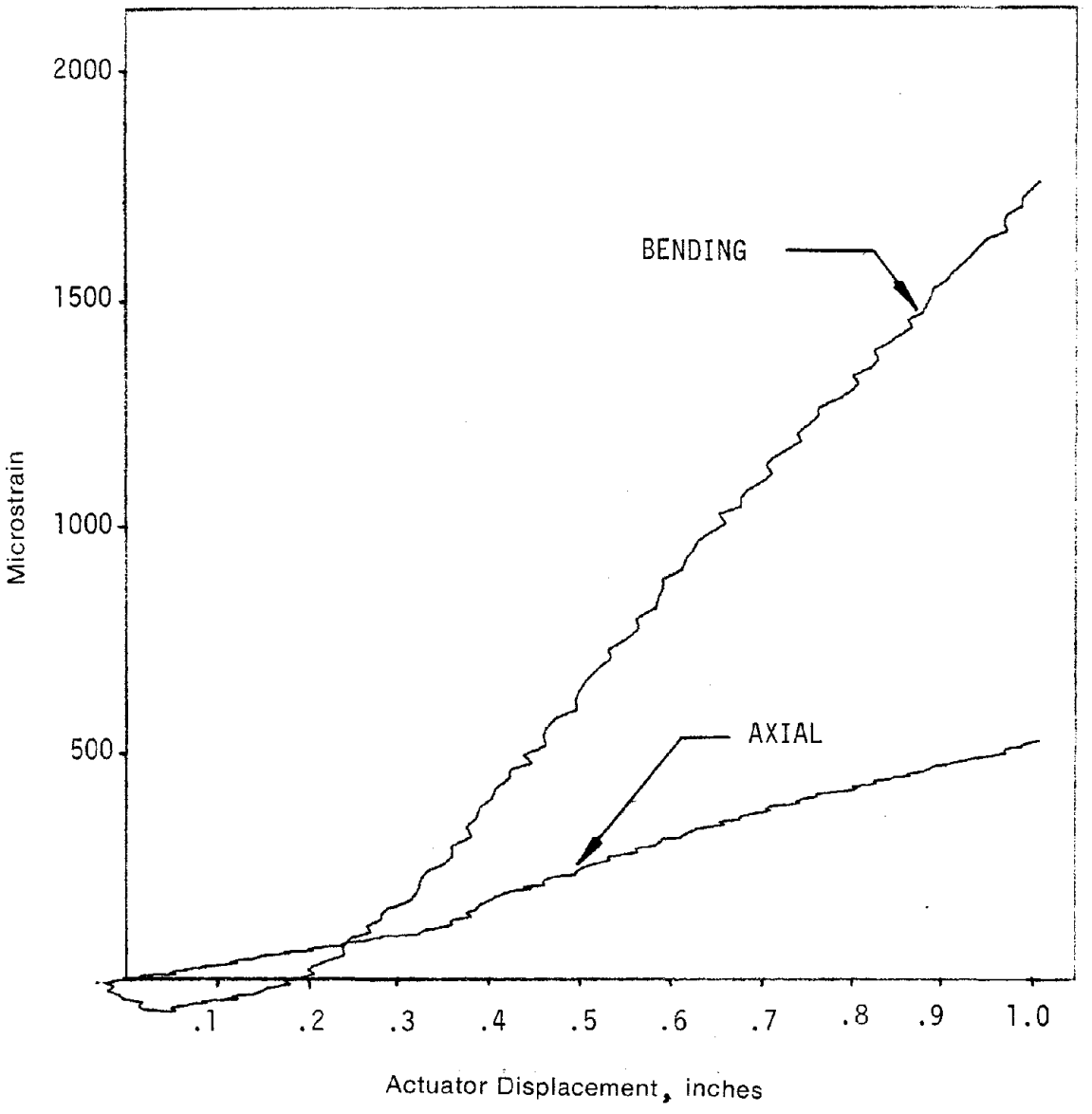

FIG. 3.2 DATA FROM STRAIN GAGE RECORDINGS — SPECIMEN 14S2

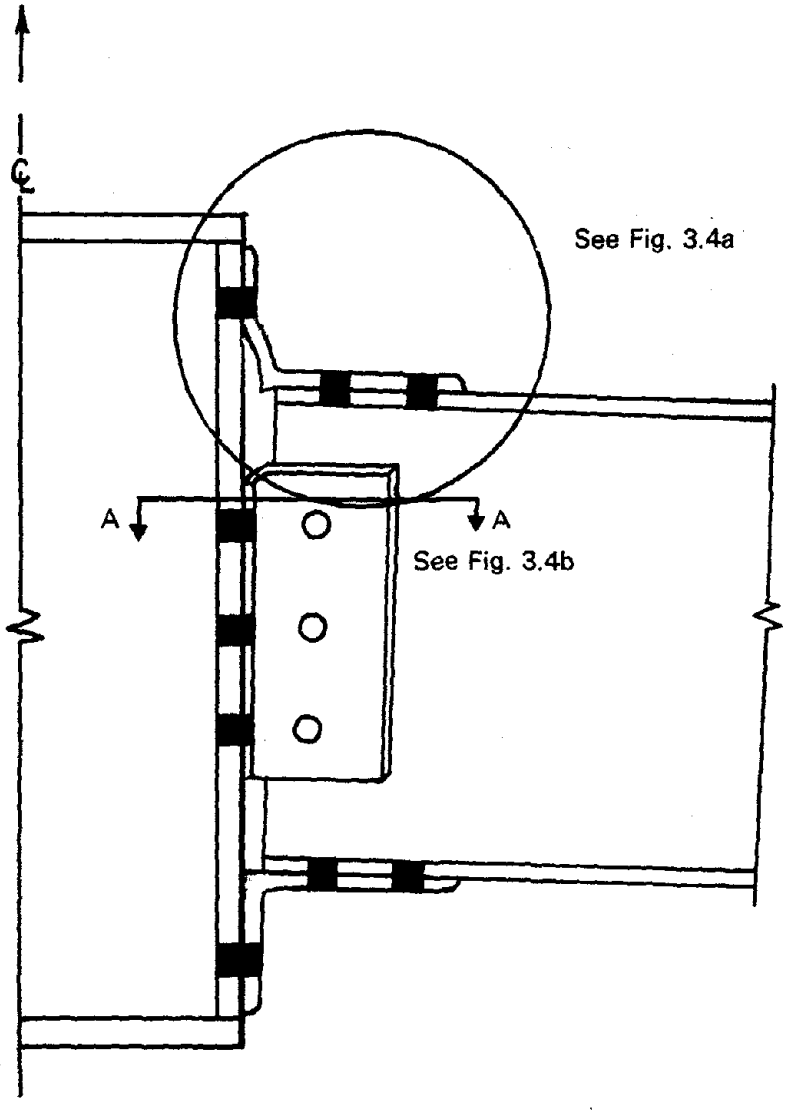

FIG. 3.3 ROTATION OF BEAM RELATIVE TO STUB COLUMN- STATIC LOADING

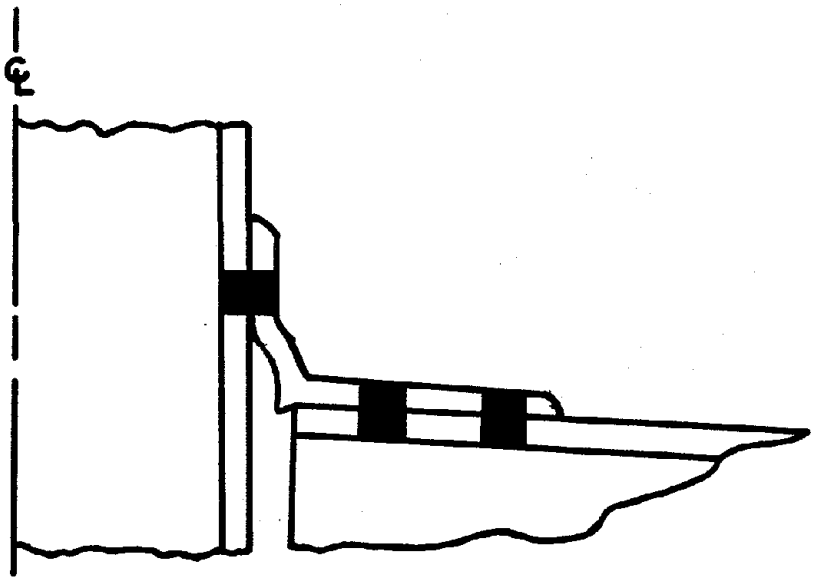

a. DETAILS OF FLANGE ANGLE DEFORMATION

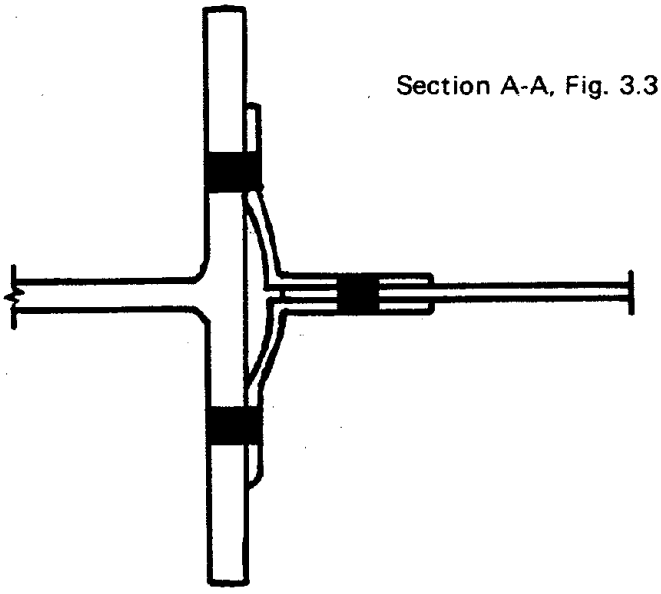

b. DETAILS OF WEB ANGLE DEFORMATION

FIG. 3.4 DEFORMATION PATTERNS IN BEAM-COLUMN CONNECTION ELEMENTS

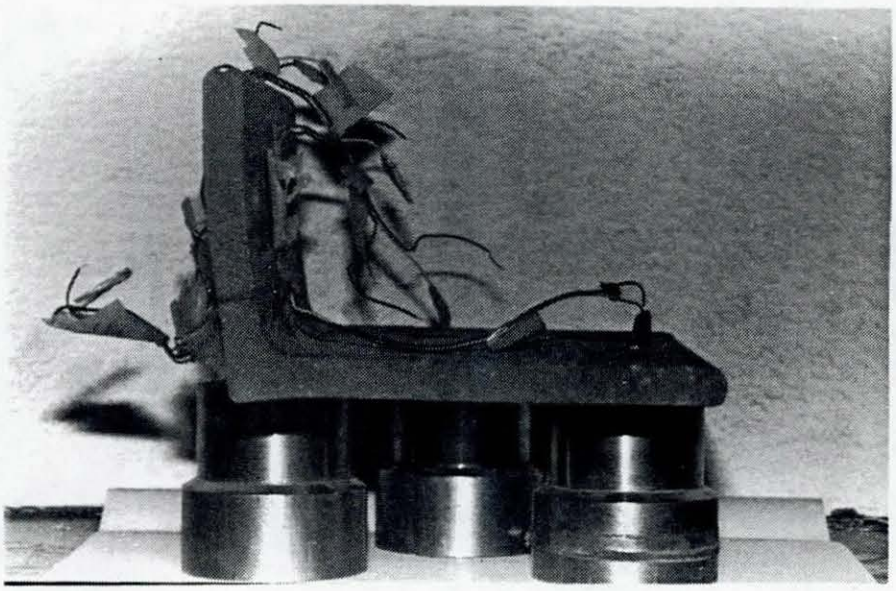

FIG. 3.5 FLANGE ANGLE FROM SPECIMEN 14S2 AFTER TEST

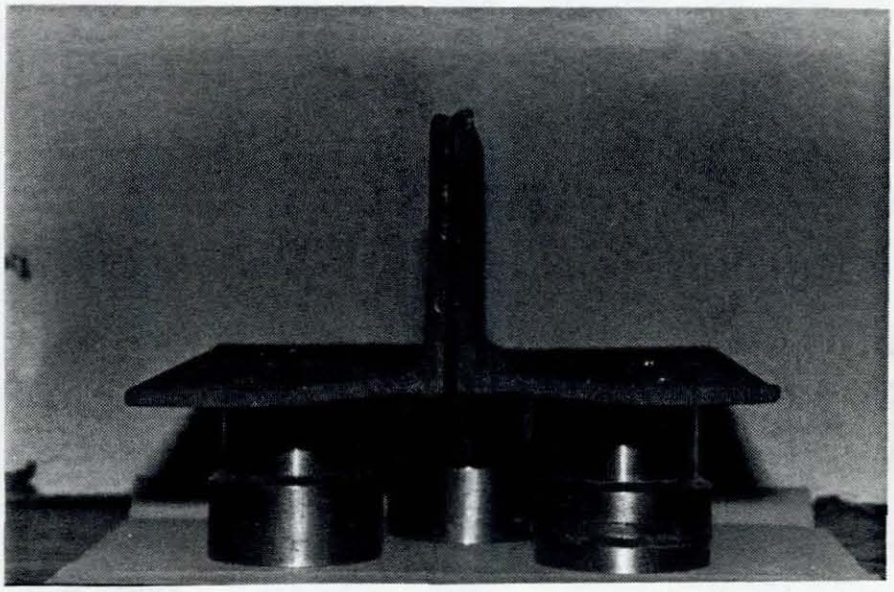

FIG. 3.6 WEB ANGLES FROM SPECIMEN 14S2 AFTER TEST

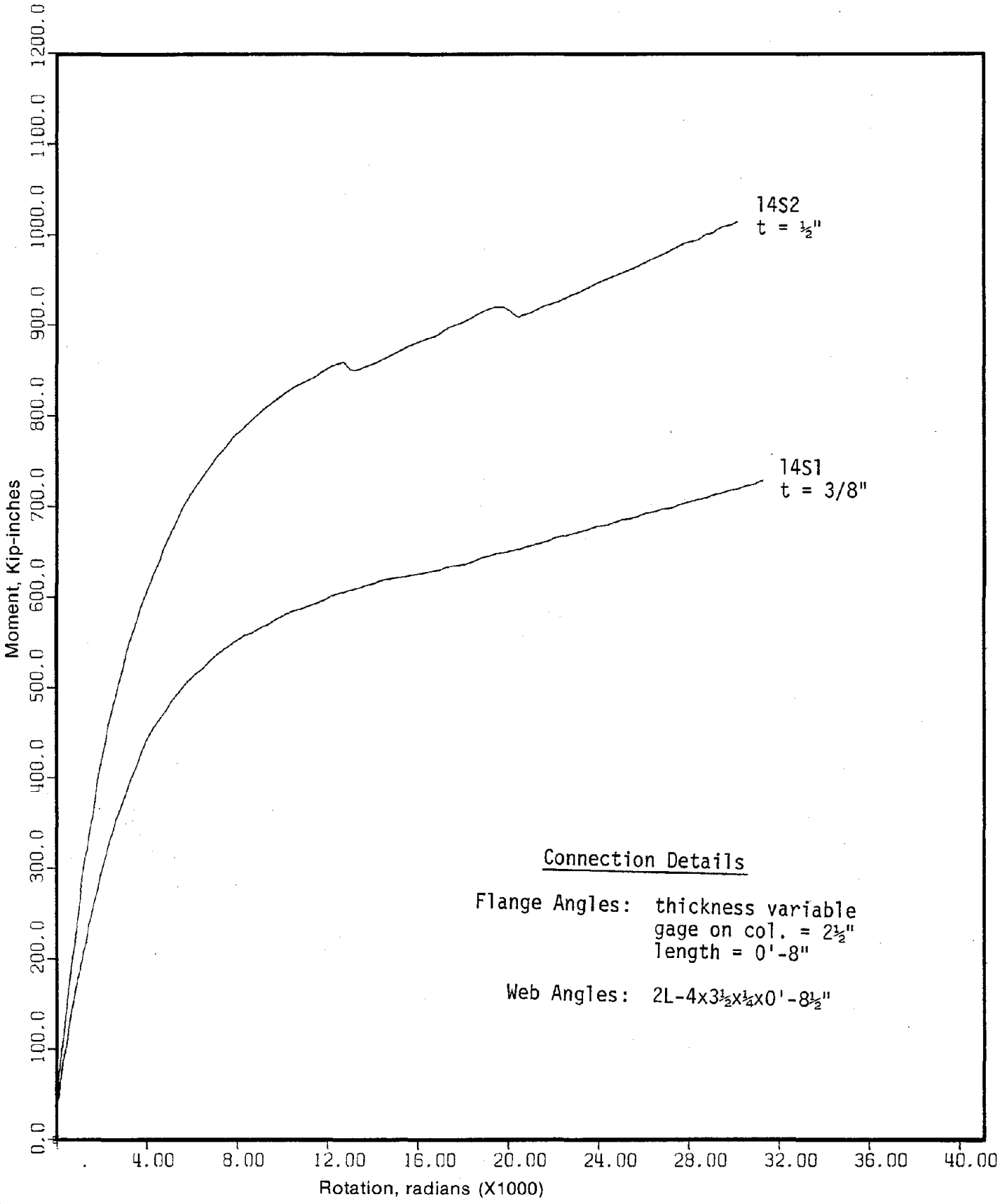

FIG. 3.7 EFFECT OF FLANGE ANGLE THICKNESS ON STATIC MOMENT-ROTATION BEHAVIOR — W14X38 BEAM CONNECTION

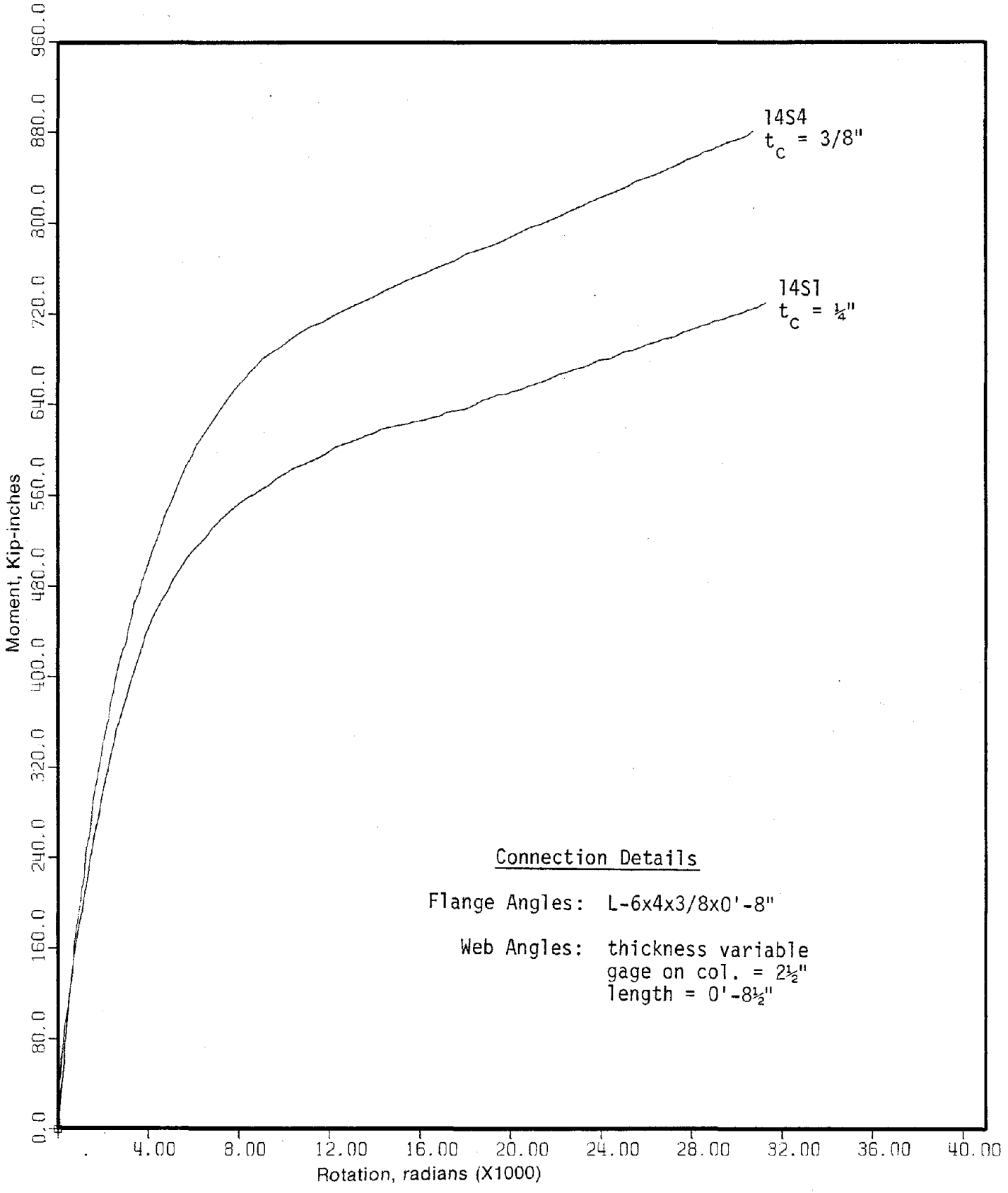

FIG. 3.8 EFFECT OF WEB ANGLE THICKNESS ON STATIC MOMENT-ROTATION BEHAVIOR — W14X38 BEAM CONNECTION

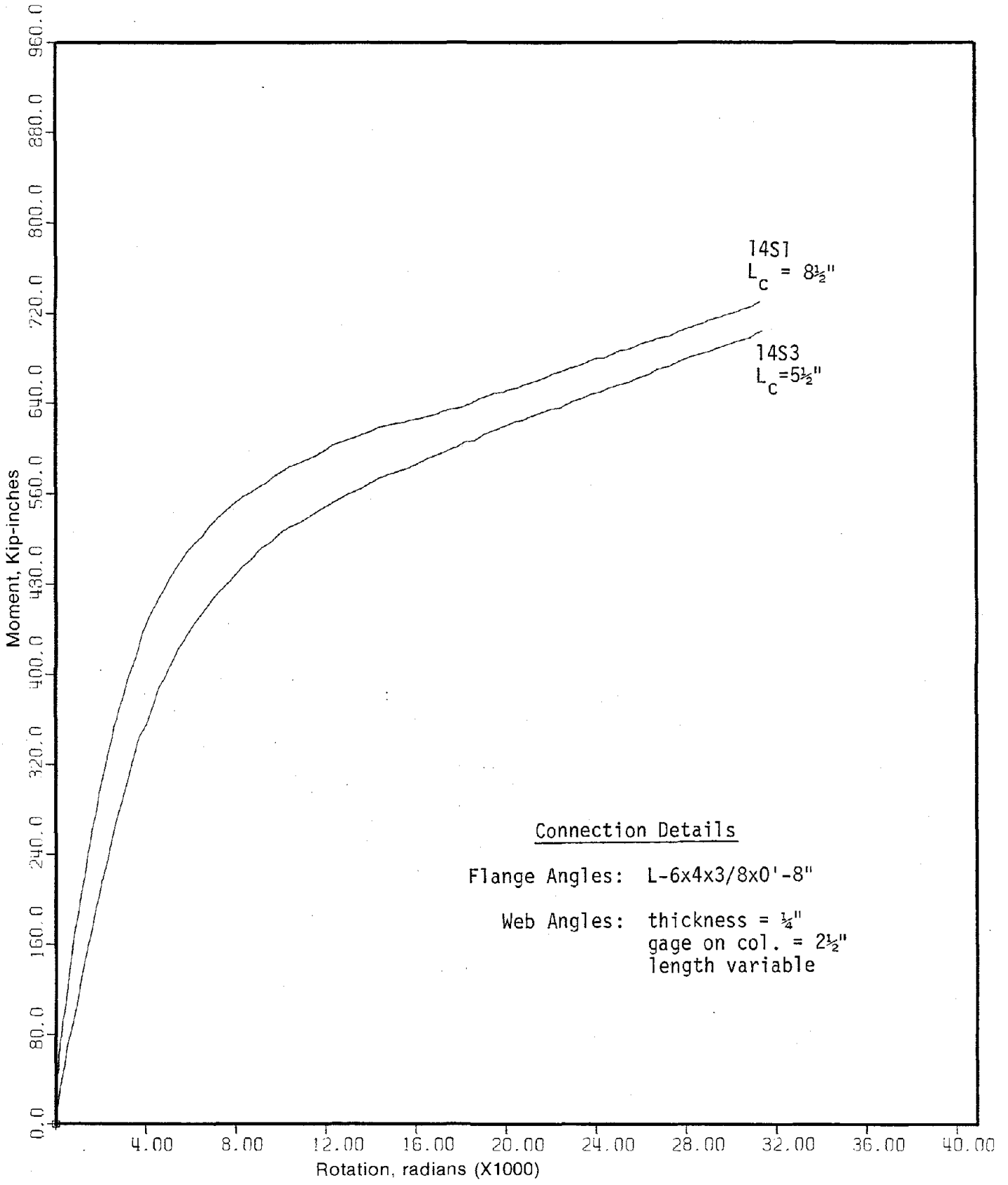

FIG. 3.9 EFFECT OF WEB ANGLE LENGTH ON STATIC MOMENT-ROTATION BEHAVIOR — W14X38 BEAM CONNECTION

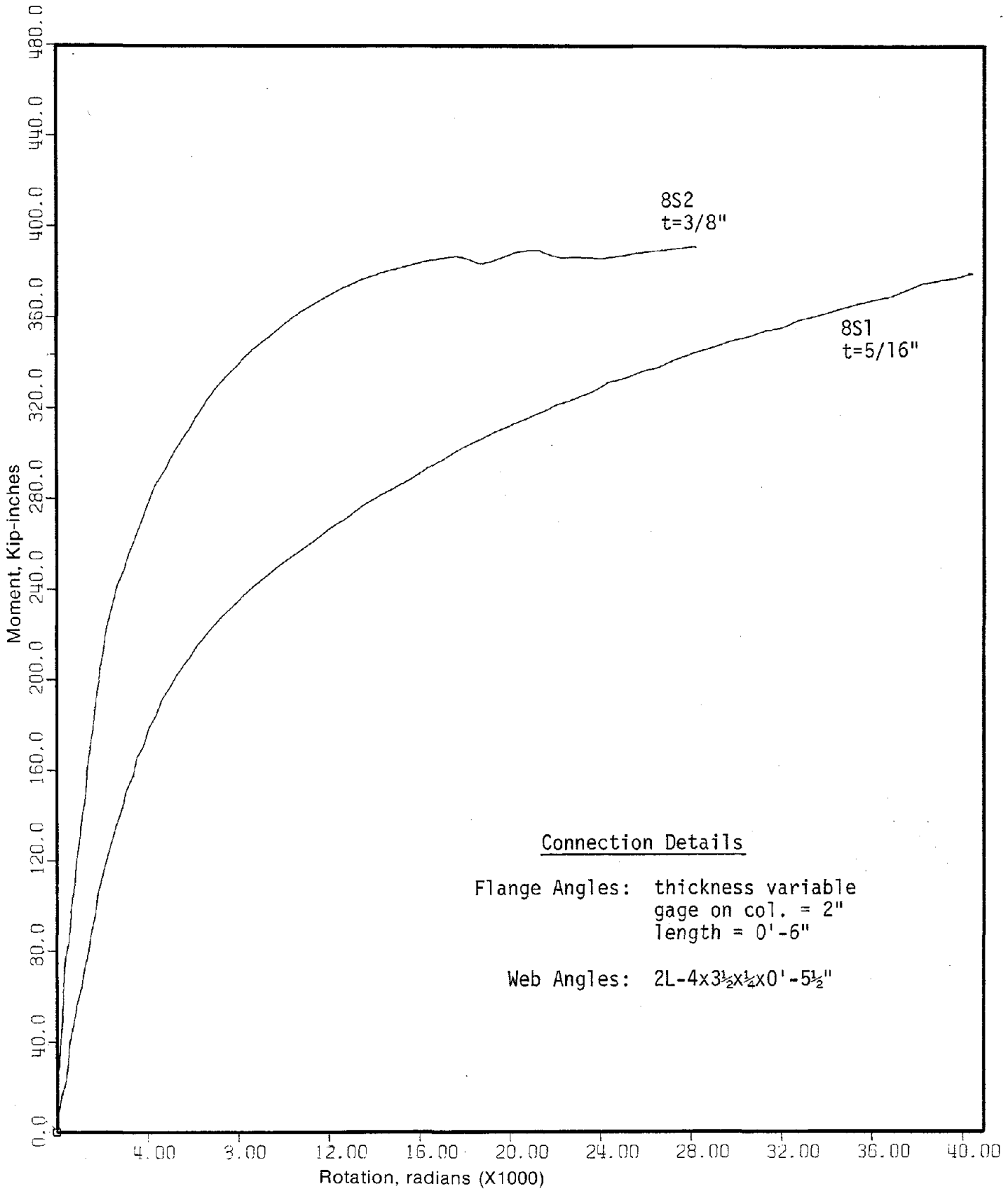

FIG. 3.10a EFFECT OF FLANGE ANGLE THICKNESS ON STATIC MOMENT-ROTATION BEHAVIOR — W8X21 BEAM CONNECTION (ANGLE GAGE = 2")

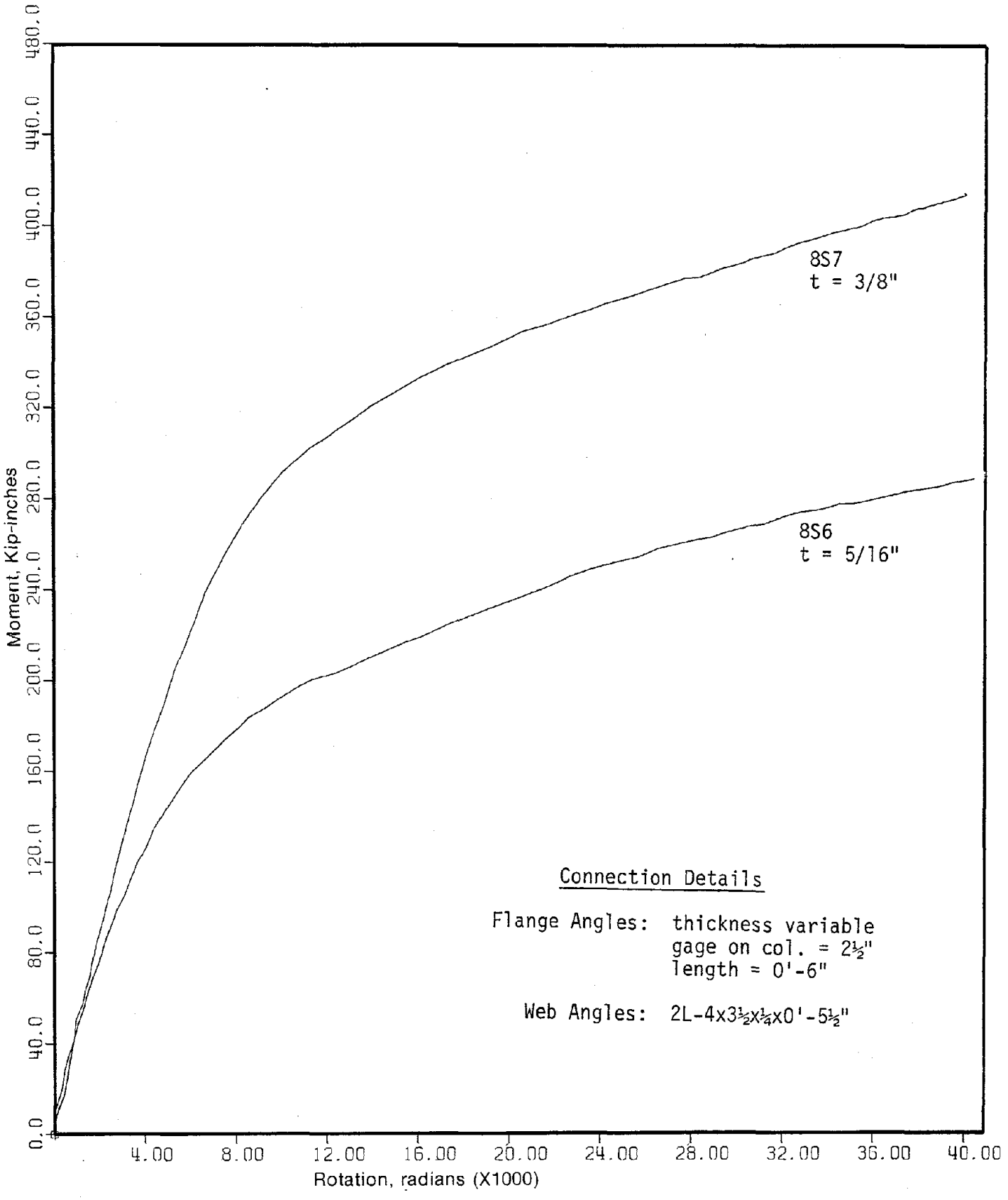

FIG. 3.10b EFFECT OF FLANGE ANGLE THICKNESS ON STATIC MOMENT-ROTATION BEHAVIOR — W8X21 BEAM CONNECTION (ANGLE GAGE = 2½")

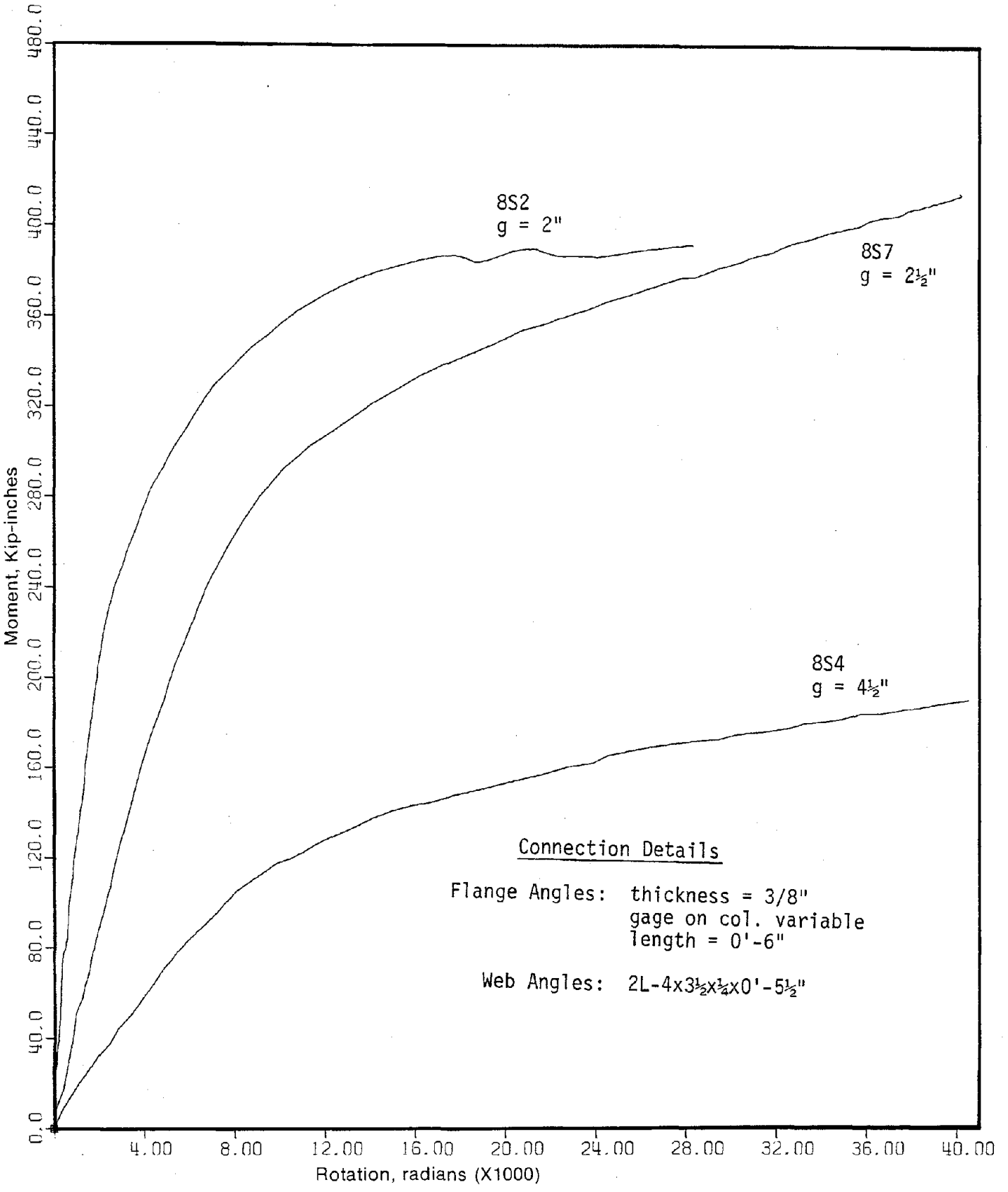

FIG. 3.11a EFFECT OF FLANGE ANGLE GAGE ON STATIC MOMENT-ROTATION BEHAVIOR — W8X21 BEAM CONNECTION (ANGLE THICKNESS = ⅜")

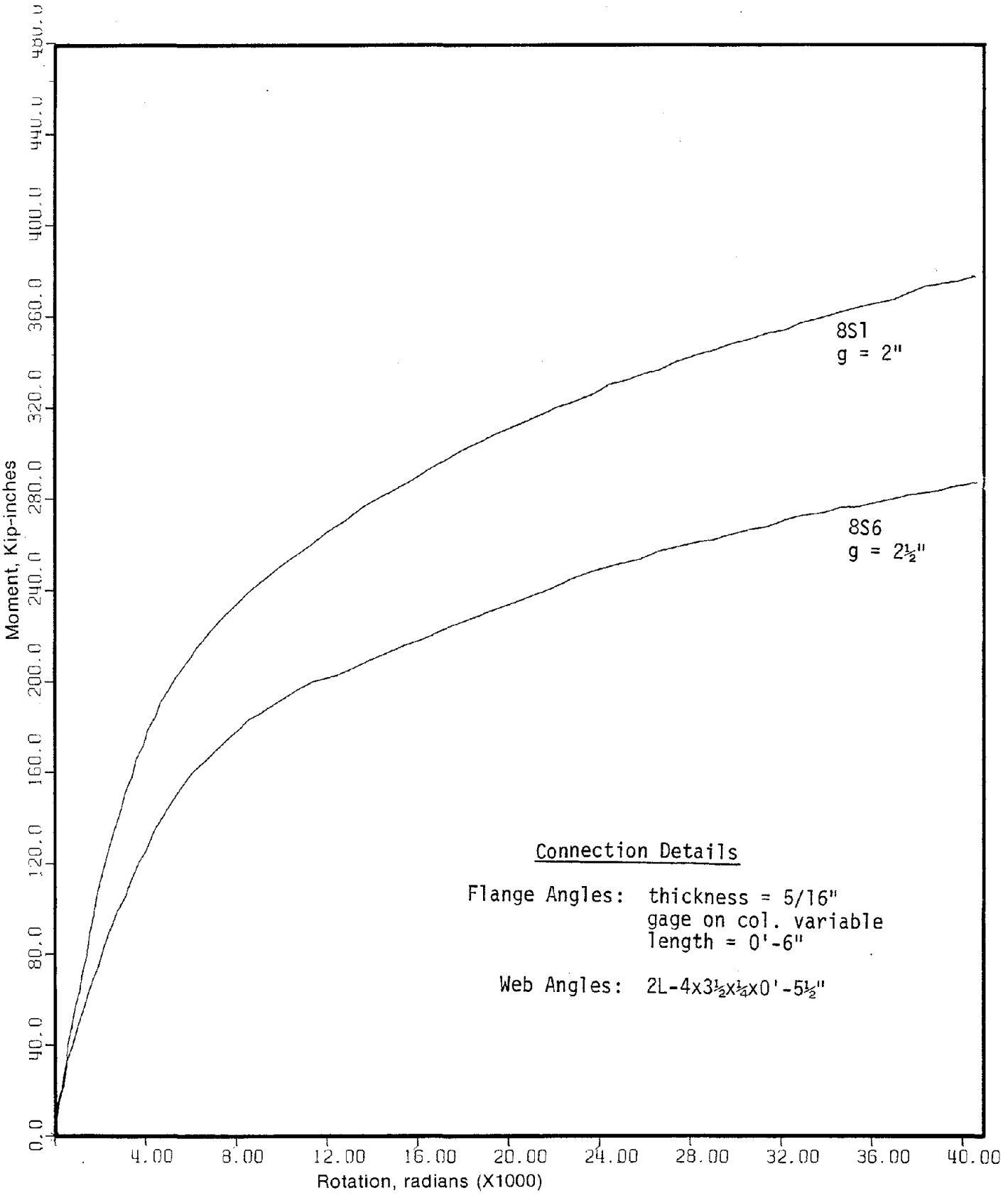

FIG. 3.11b EFFECT OF FLANGE ANGLE GAGE ON STATIC MOMENT-ROTATION BEHAVIOR — W8X21 BEAM CONNECTION (ANGLE THICKNESS — 5/16")

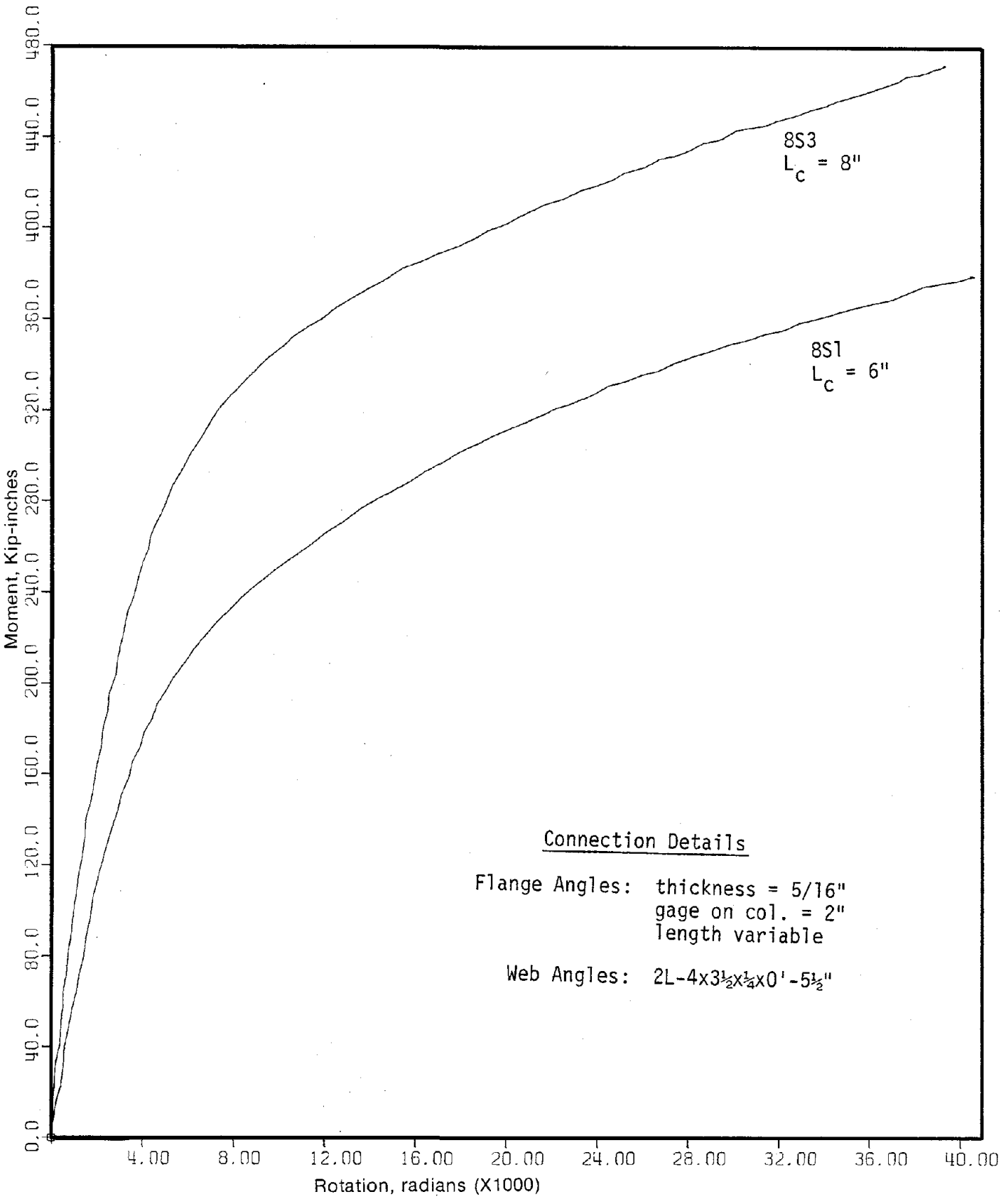

FIG. 3.12 EFFECT OF FLANGE ANGLE LENGTH ON STATIC MOMENT-ROTATION BEHAVIOR — W8X21 BEAM CONNECTION

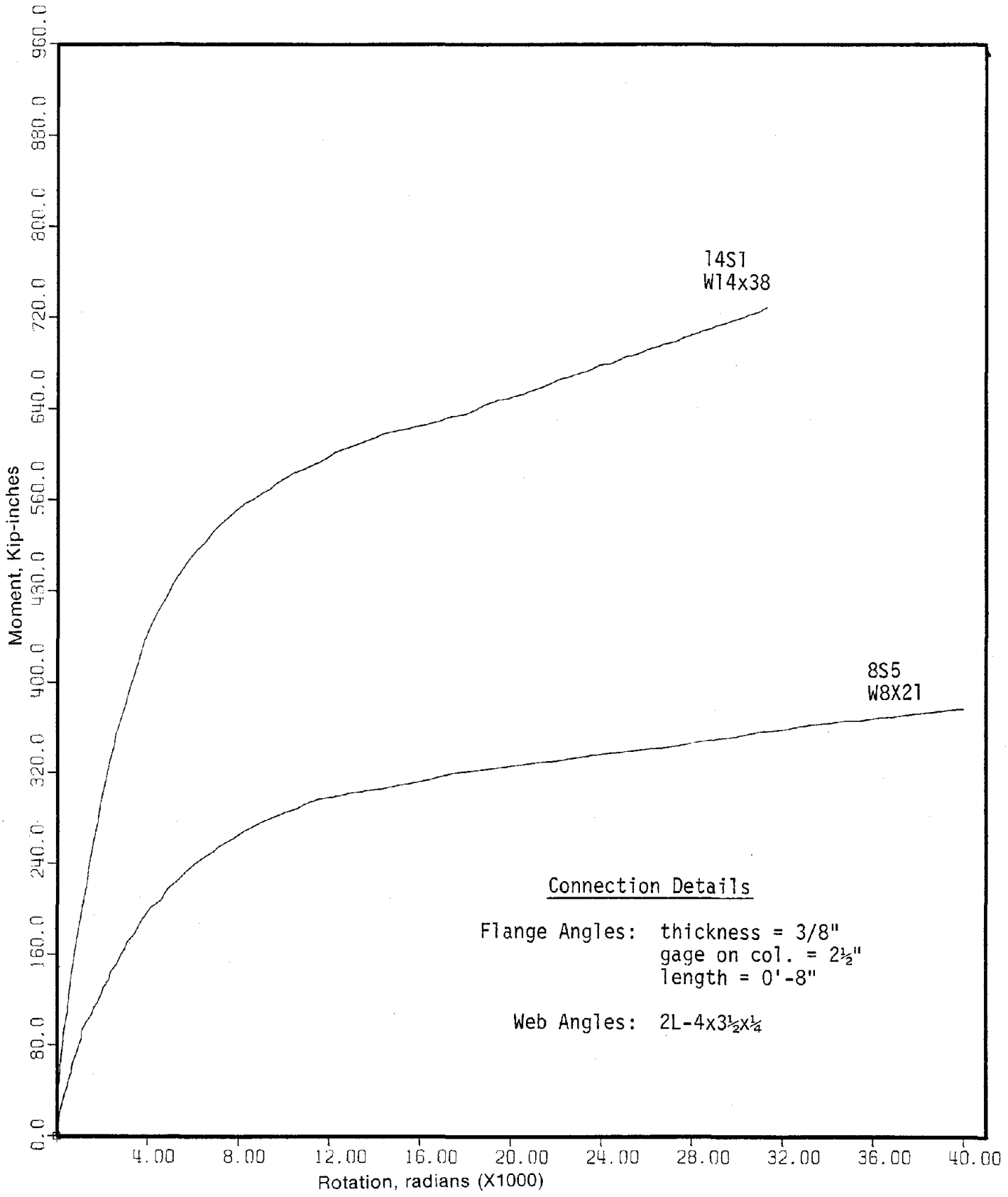

FIG. 3.13 COMPARISON OF STATIC MOMENT-ROTATION BEHAVIOR OF W14X38 and W8X21 BEAM CONNECTIONS

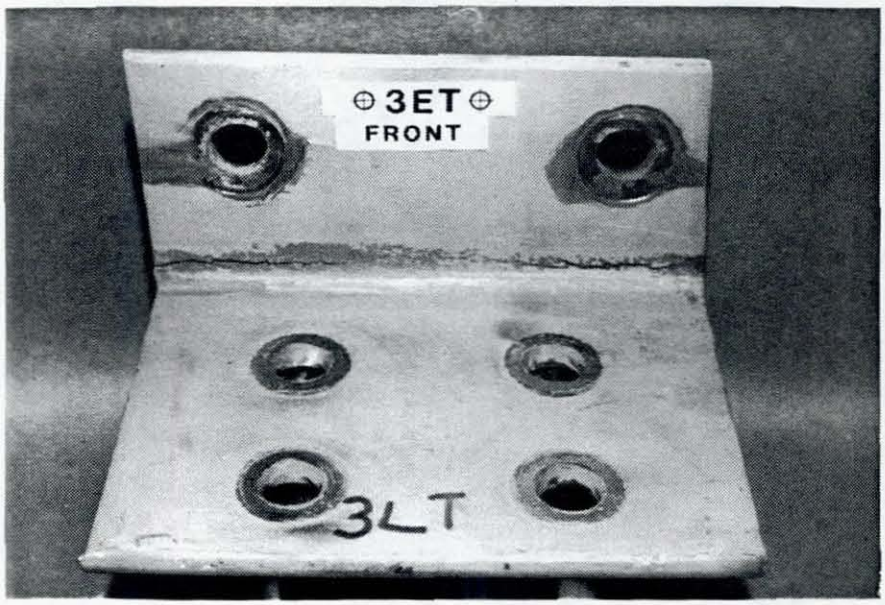

a. FRONT VIEW

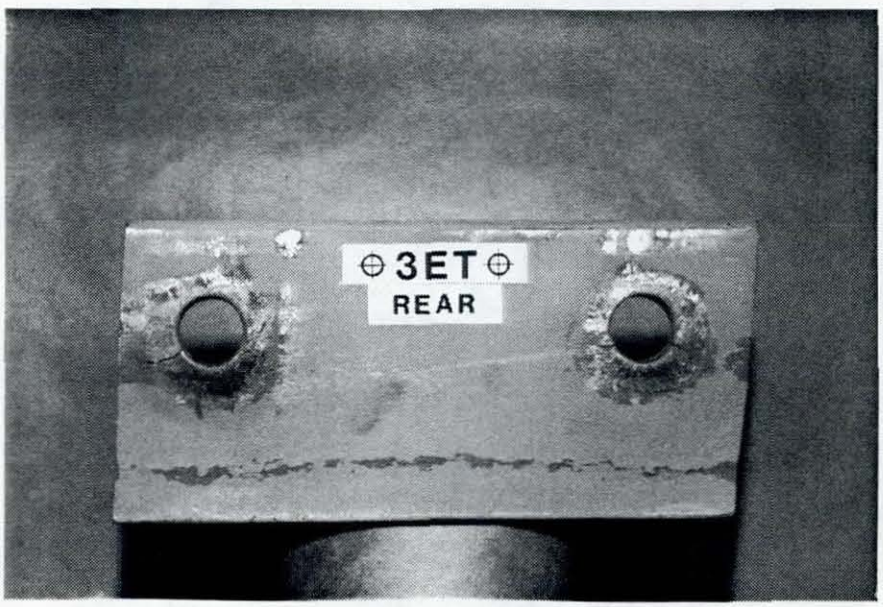

b. REAR VIEW

FIG. 3.14 FLANGE ANGLE FROM SPECIMEN 14C1 AFTER CYCLIC TEST

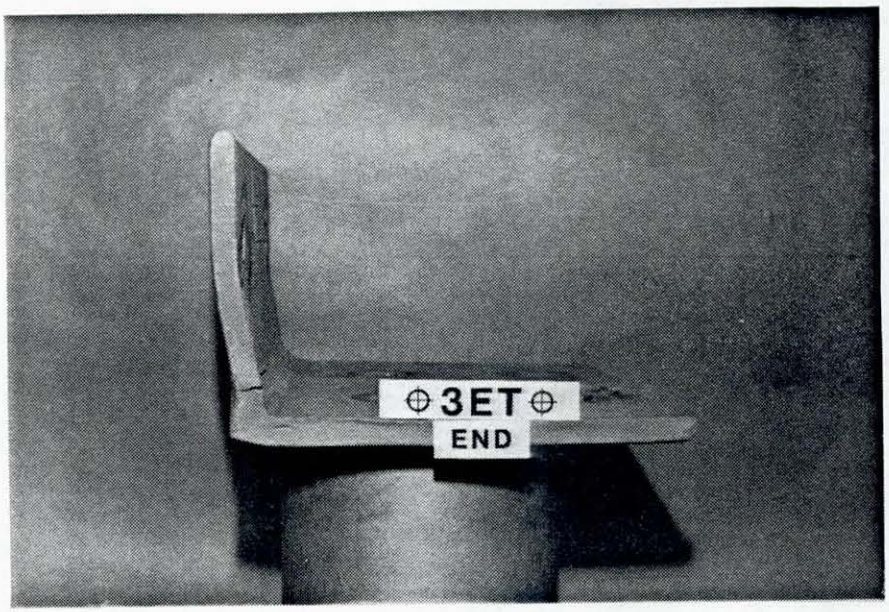

a. FLANGE ANGLE — END VIEW

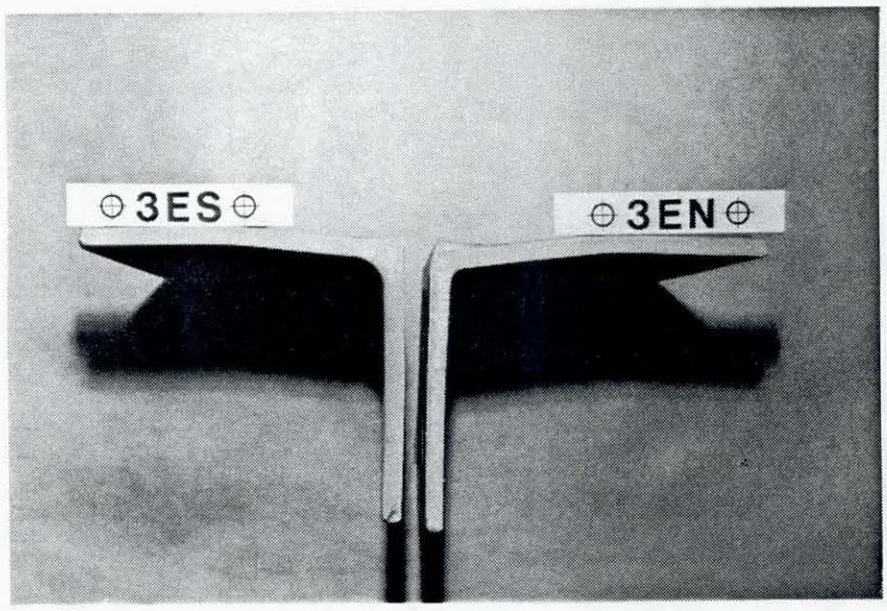

b. WEB ANGLES — END VIEW

FIG. 3.15 FLANGE AND WEB ANGLES FROM SPECIMEN 14C1 AFTER CYCLIC TEST.

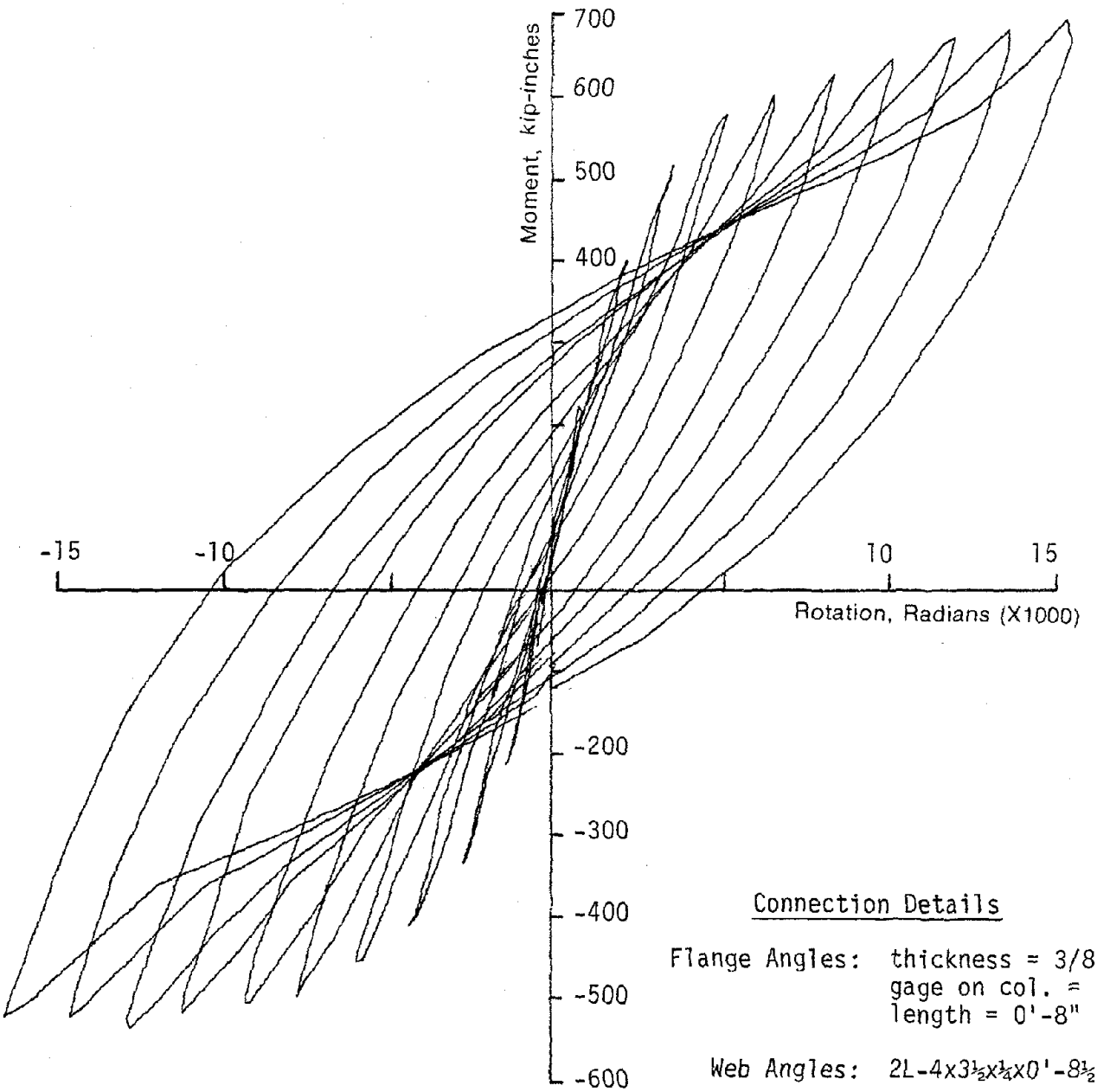

FIG. 3.16 STABLE HYSTERESIS LOOPS FOR SPECIMEN 14C1

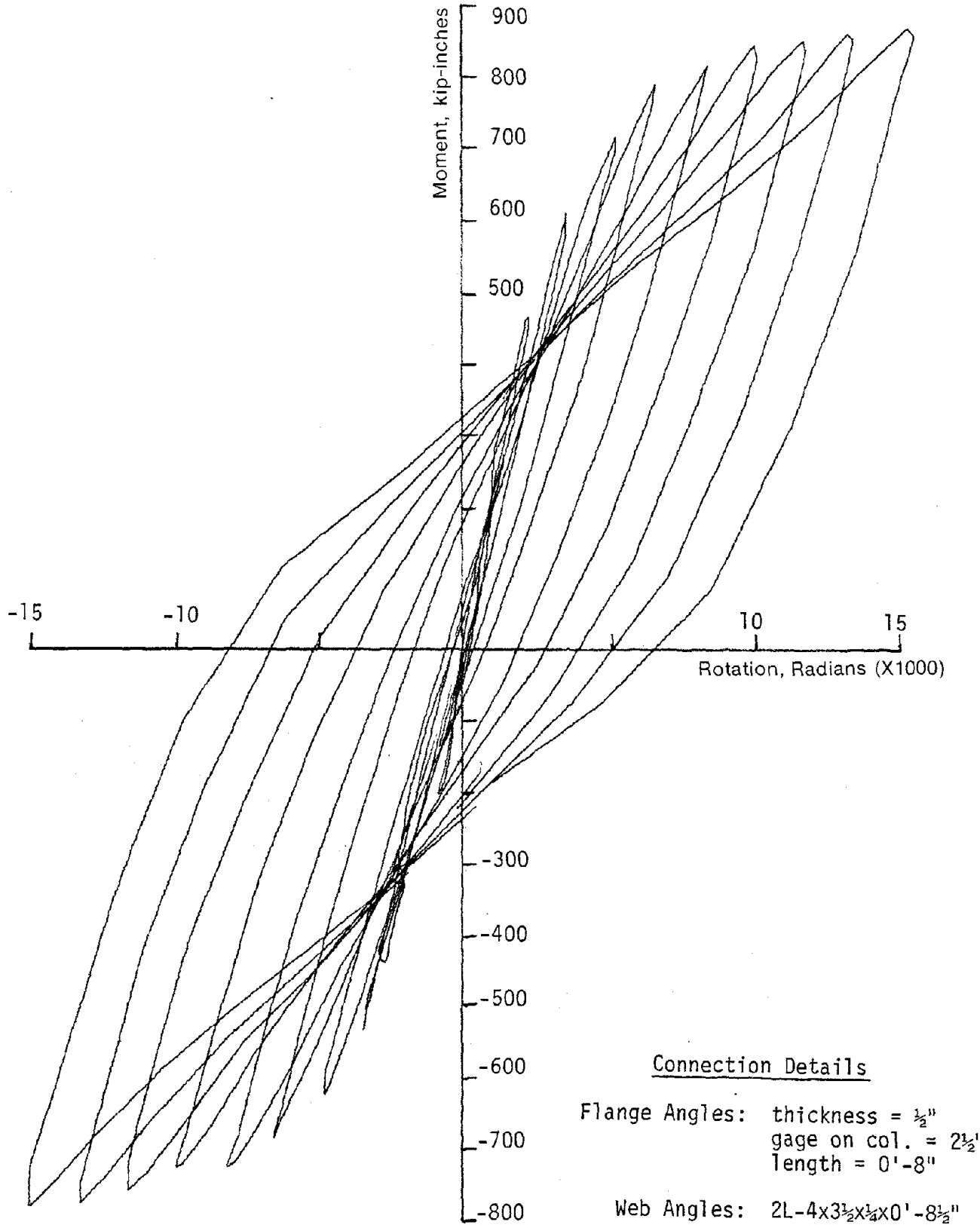

FIG. 3.17 STABLE HYSTERESIS LOOPS FOR SPECIMEN 14C2

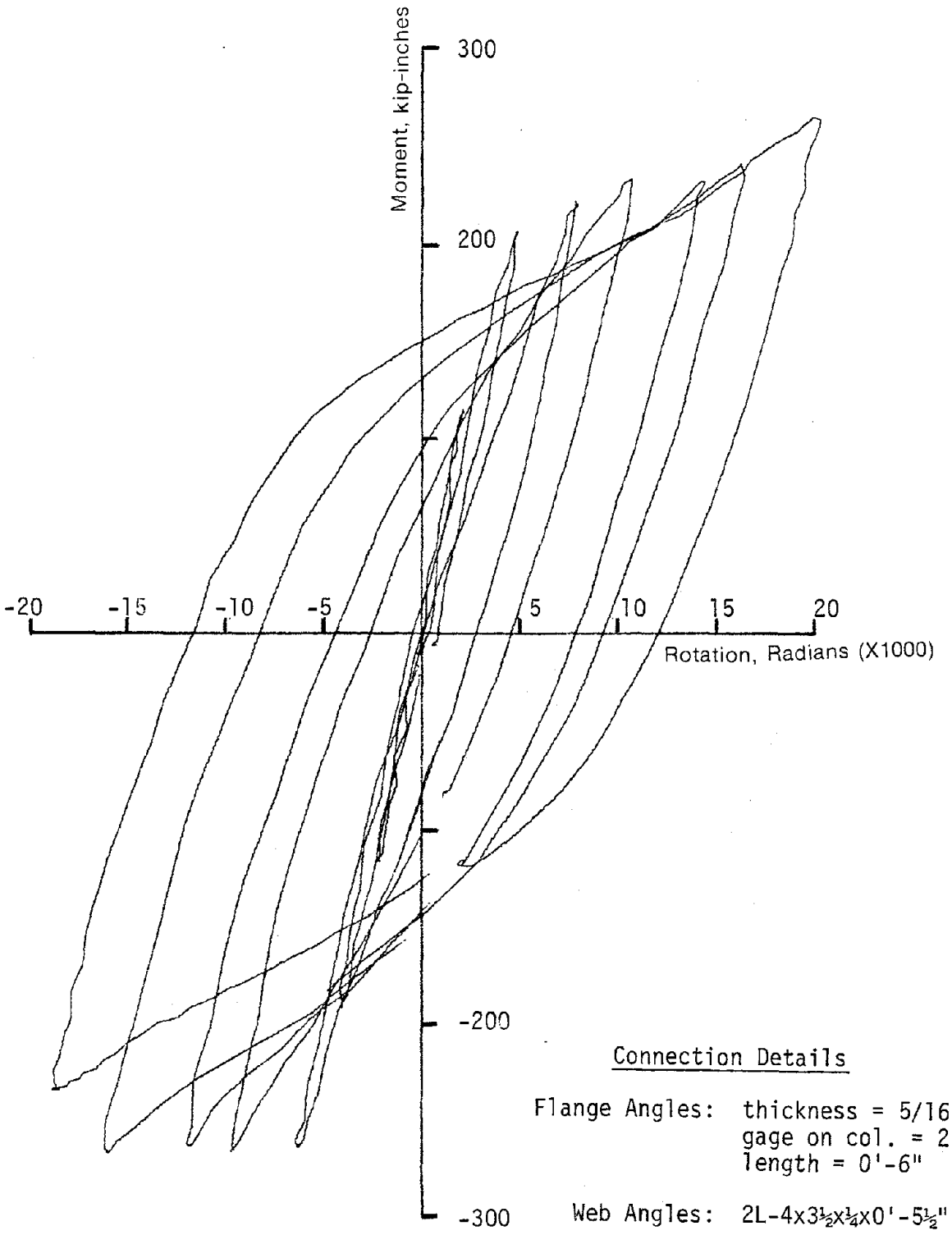

FIG. 3.18 STABLE HYSTERESIS LOOPS FOR SPECIMEN 8C1

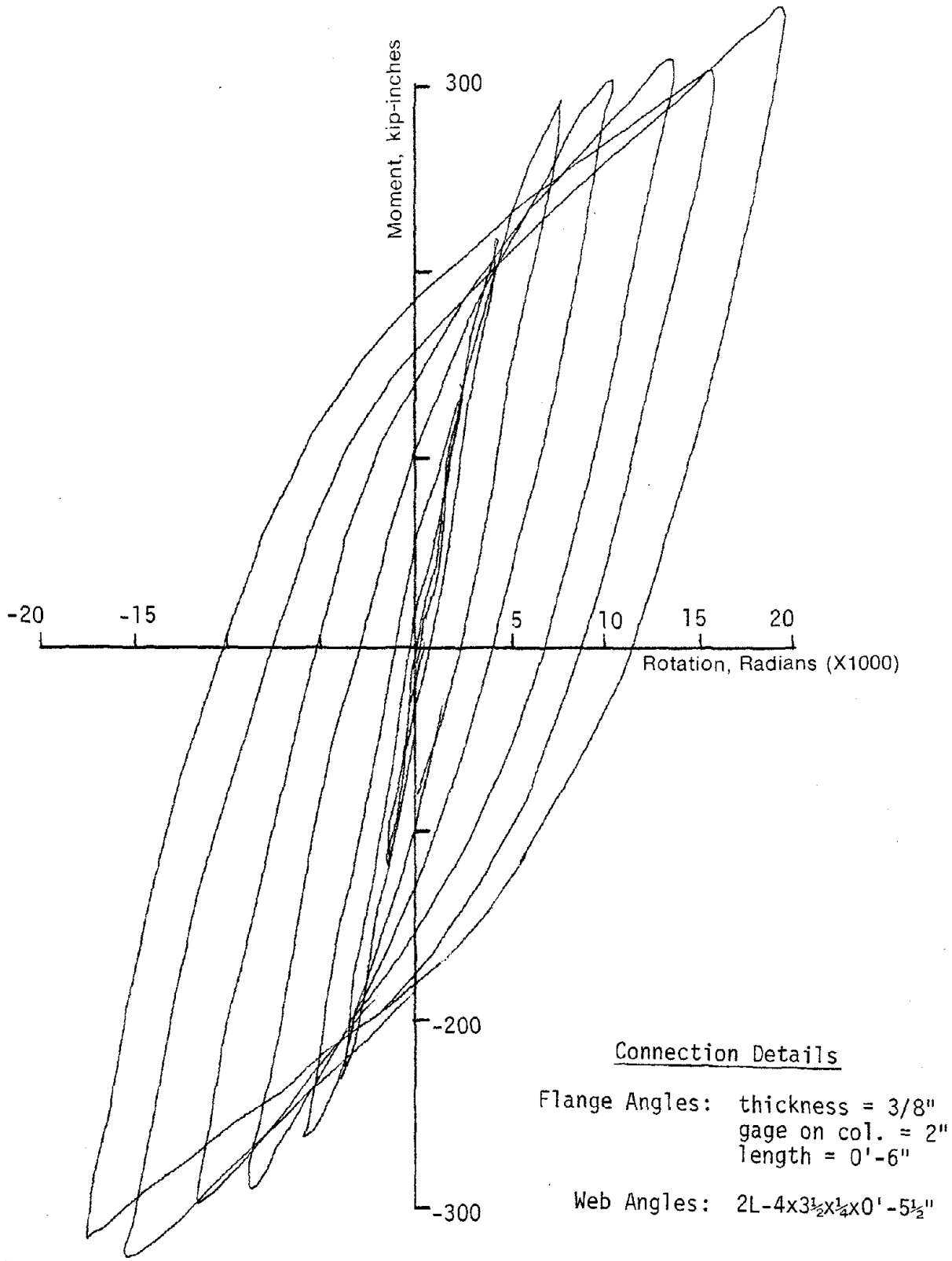

FIG. 3.19 STABLE HYSTERESIS LOOPS FOR SPECIMEN 8C2

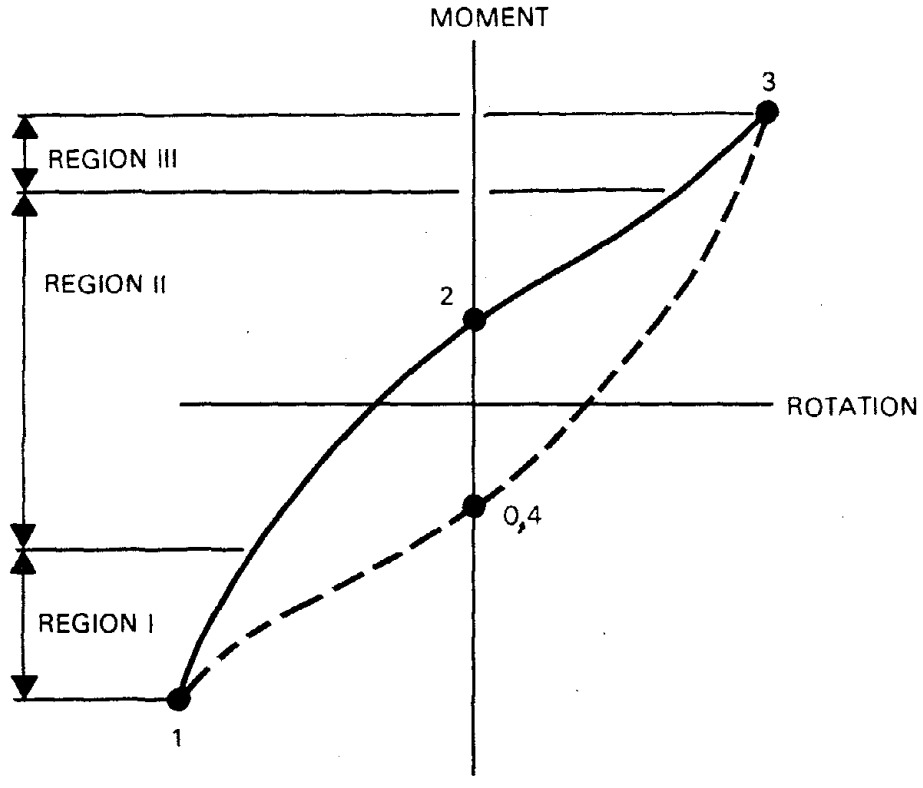

FIG. 3.20 TYPICAL MOMENT-ROTATION HYSTERESIS LOOP-CYCLIC TESTS

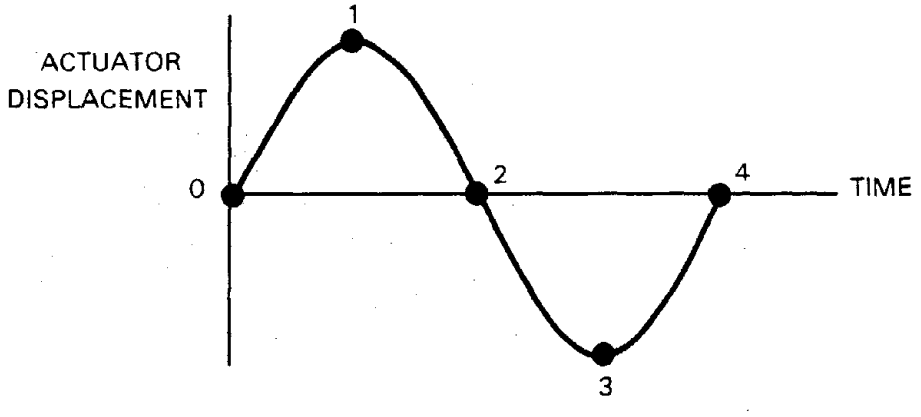

FIG. 3.21 TYPICAL TIME-ACTUATOR DISPLACEMENT CYCLE

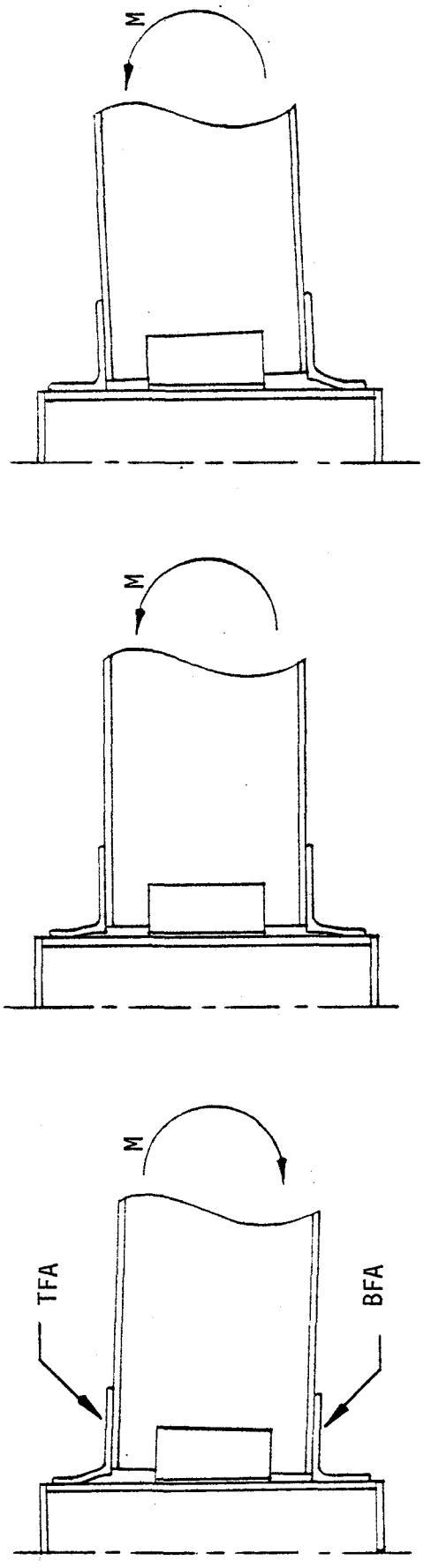

a. REGION I CONFIGURATION

b. REGION II CONFIGURATION

c. REGION III CONFIGURATION

FIG. 3.22 CONFIGURATIONS OF CONNECTION DURING ONE-HALF CYCLE

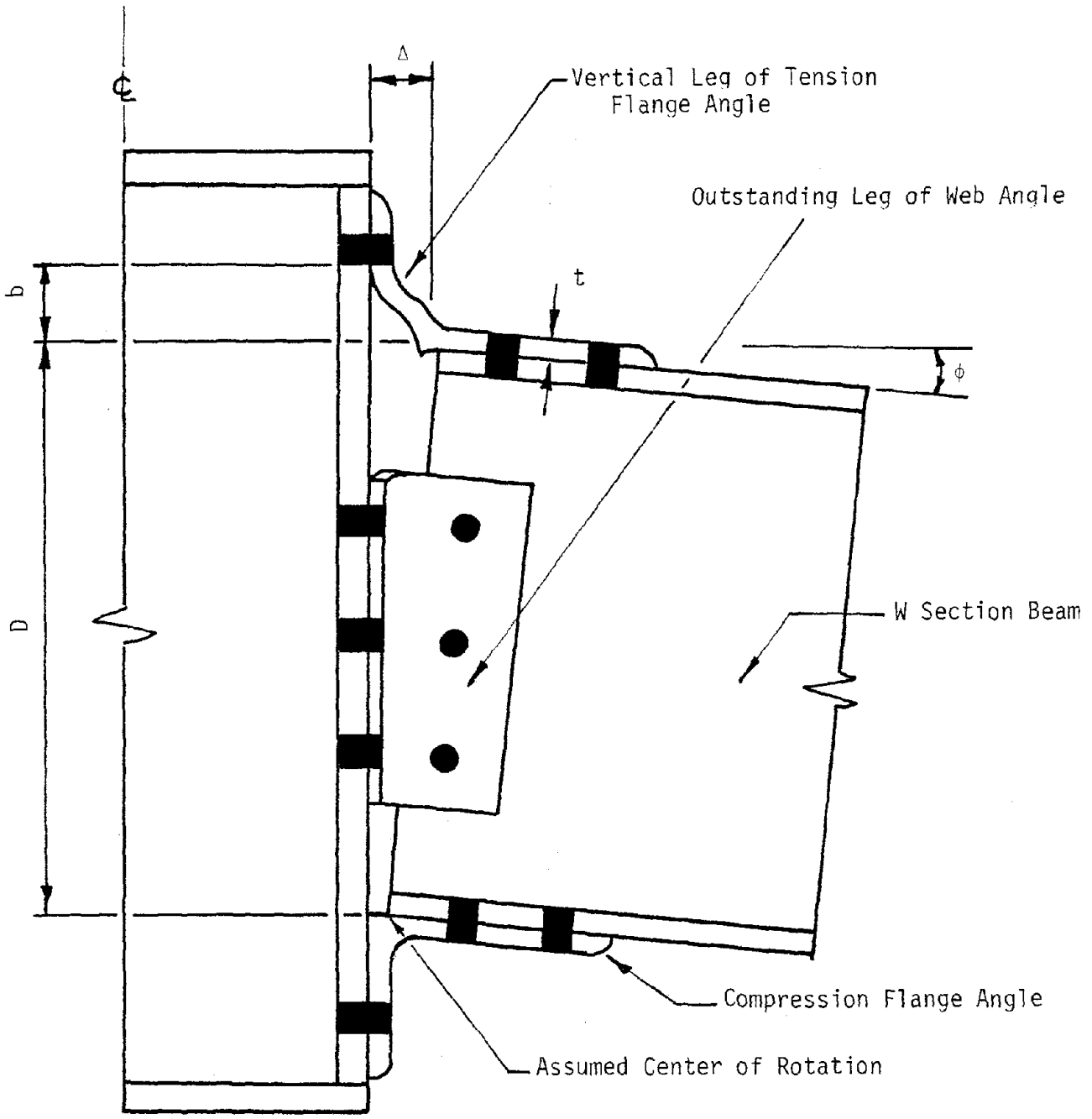

FIG. 4.1a ASSUMED BEHAVIOR OF BEAM TO COLUMN CONNECTION

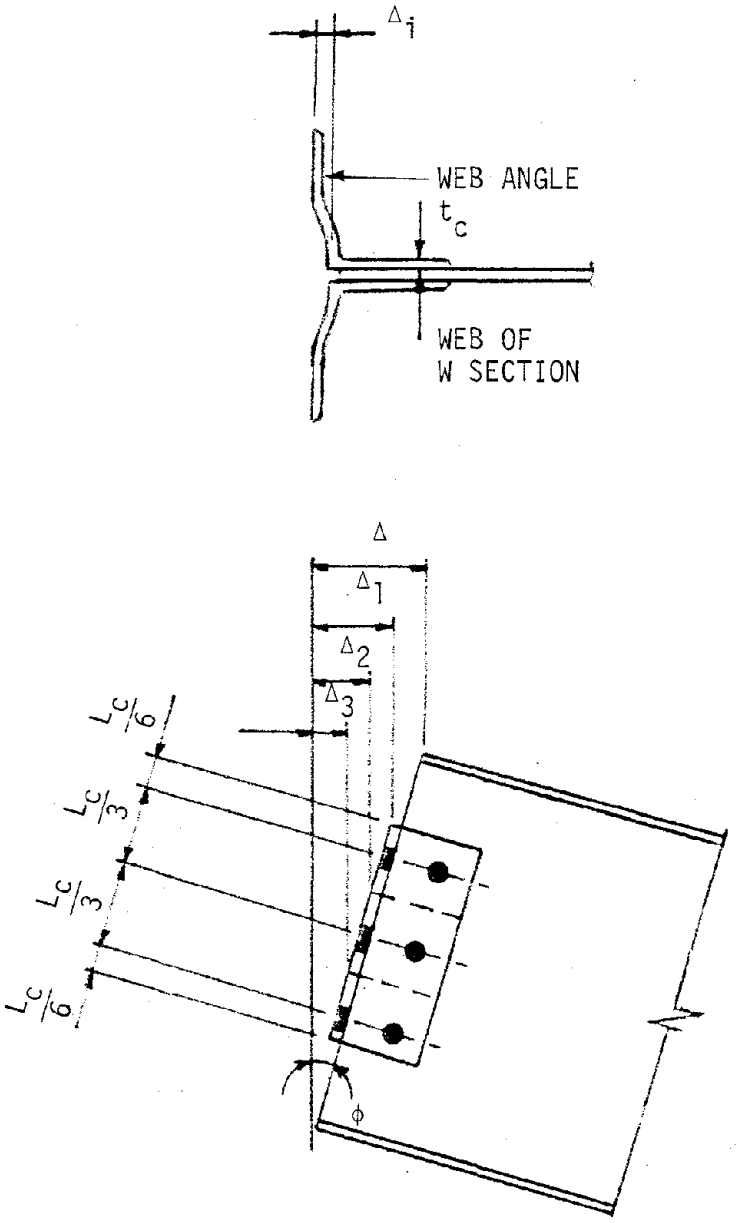

FIG. 4.1b BEAM MODEL FOR WEB ANGLES

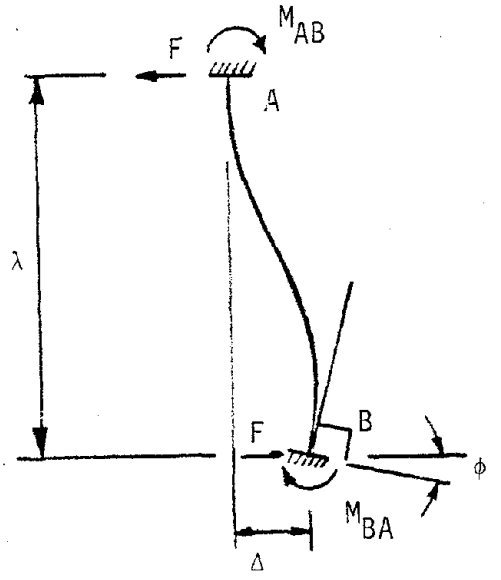

FIG. 4.2a IDEALIZED BEAM MODEL FOR FLANGE ANGLE

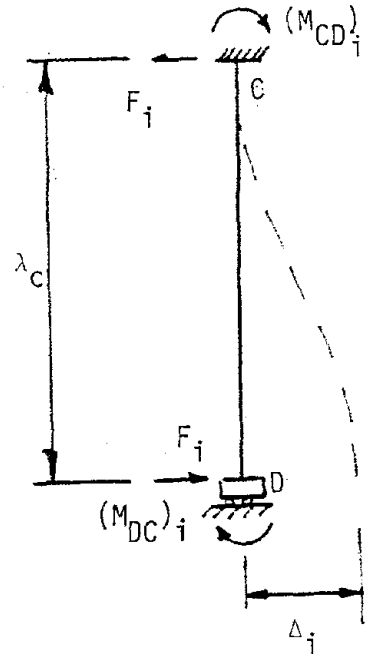

FIG. 4.2b IDEALIZED BEAM MODEL FOR WEB ANGLES

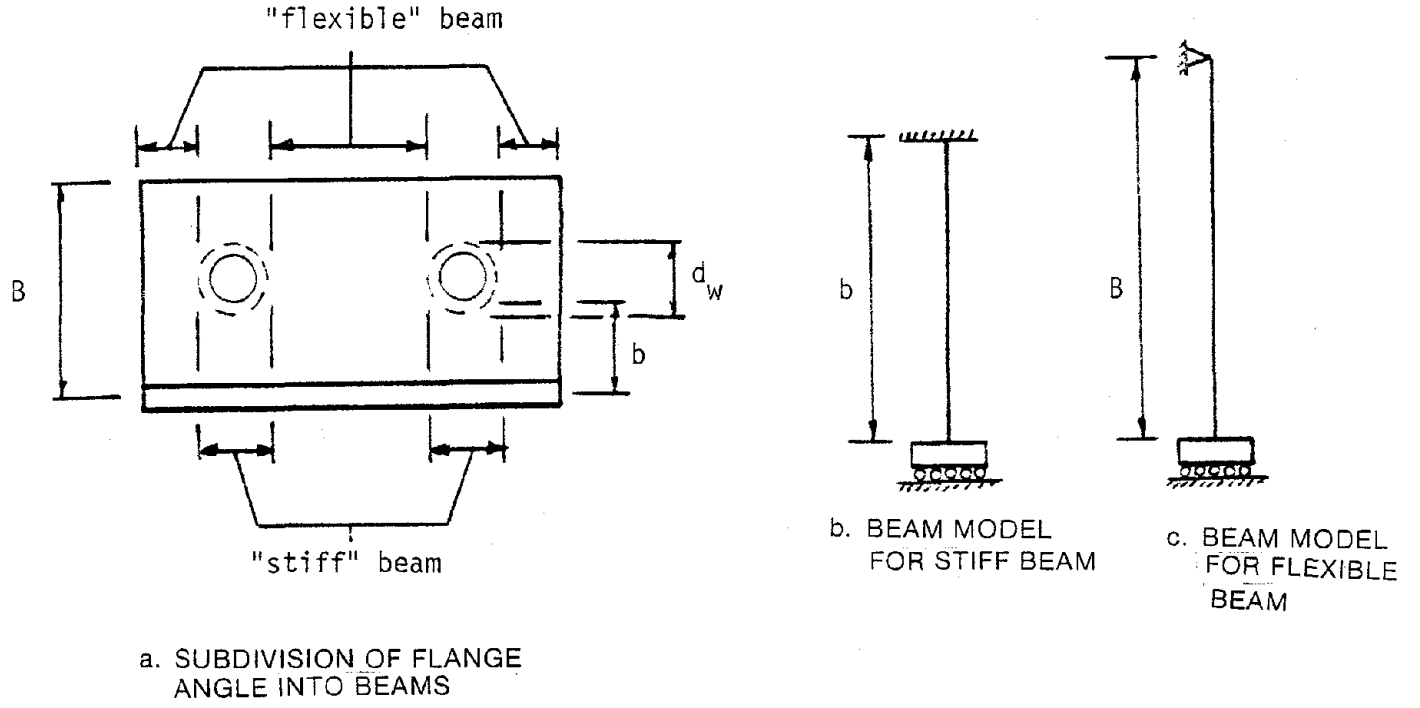

a. SUBDIVISION OF FLANGE ANGLE INTO BEAMS

b. BEAM MODEL FOR STIFF BEAM

c. BEAM MODEL FOR FLEXIBLE BEAM

FIG. 4.3 REFINED BEAM MODEL FOR FLANGE ANGLE

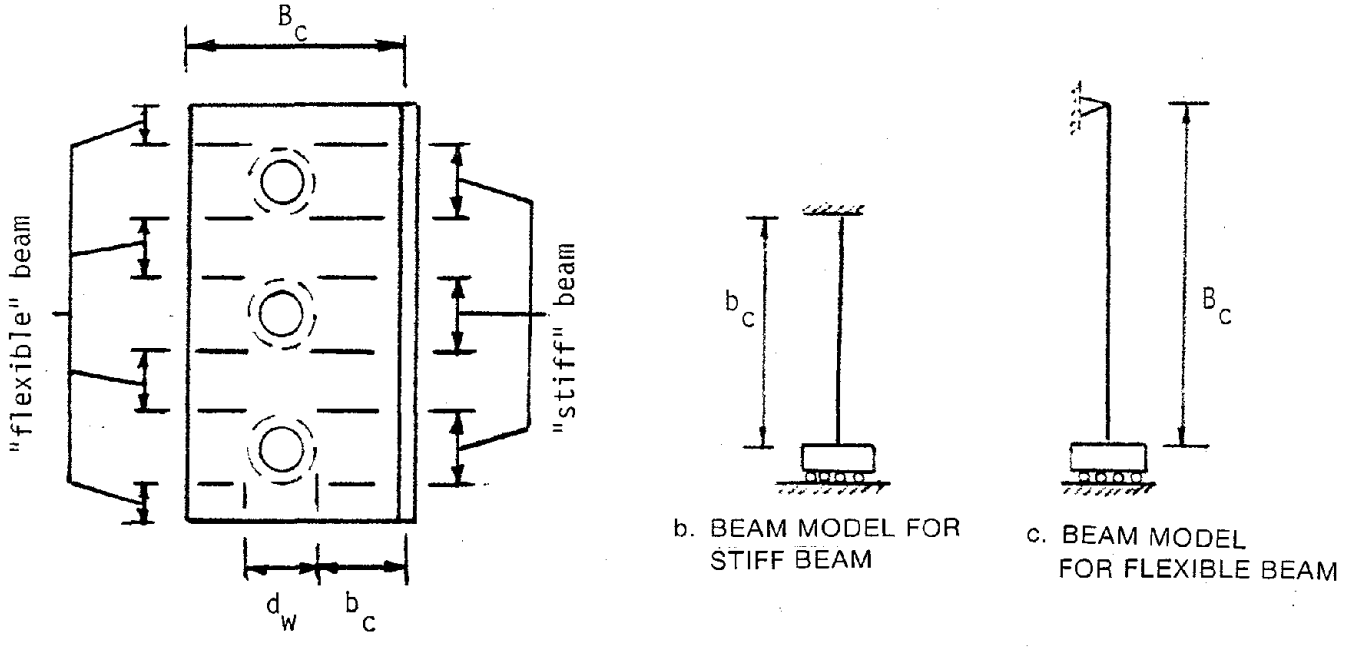

a. SUBDIVISION OF WEB ANGLE INTO BEAMS

b. BEAM MODEL FOR STIFF BEAM

c. BEAM MODEL FOR FLEXIBLE BEAM

FIG. 4.4 REFINED BEAM MODEL FOR WEB ANGLES

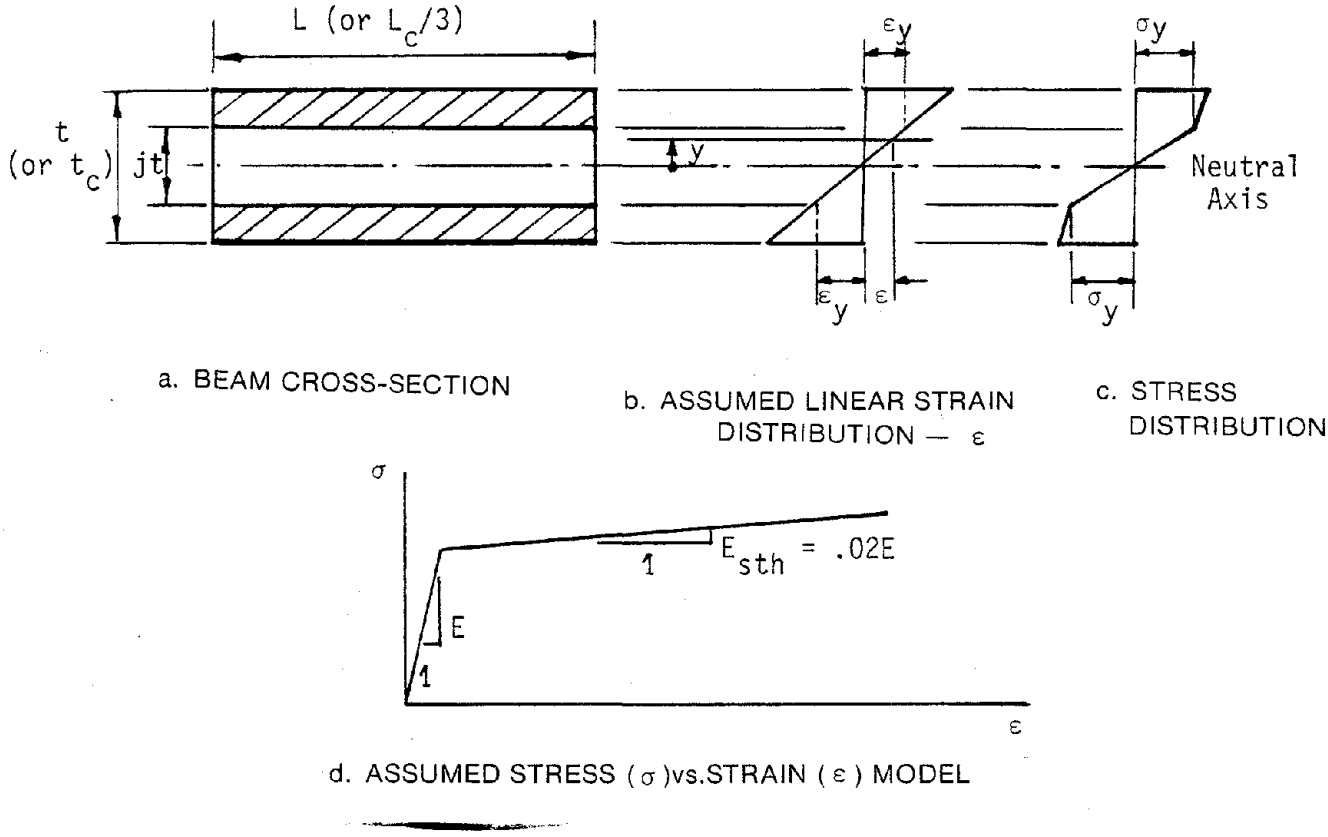

FIG. 4.5 ASSUMED MATERIAL BEHAVIOR FOR MODEL III

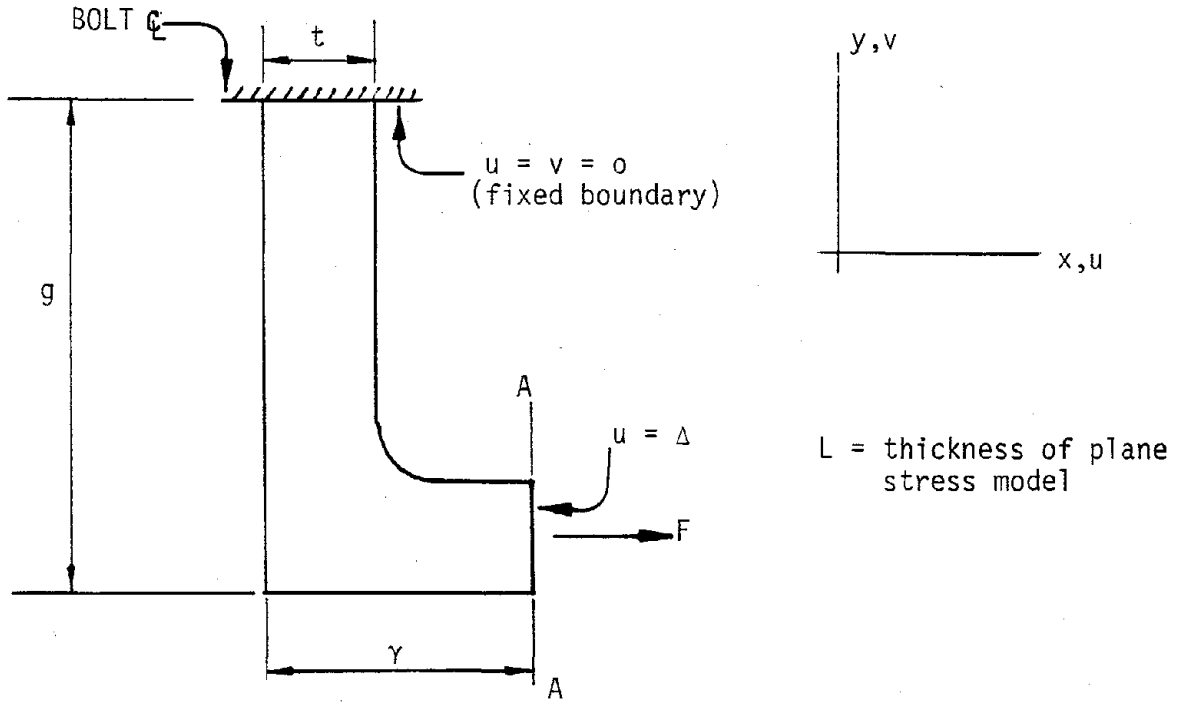

FIG. 4.6 MODEL IV — PLANE STRESS FINITE ELEMENT MODEL

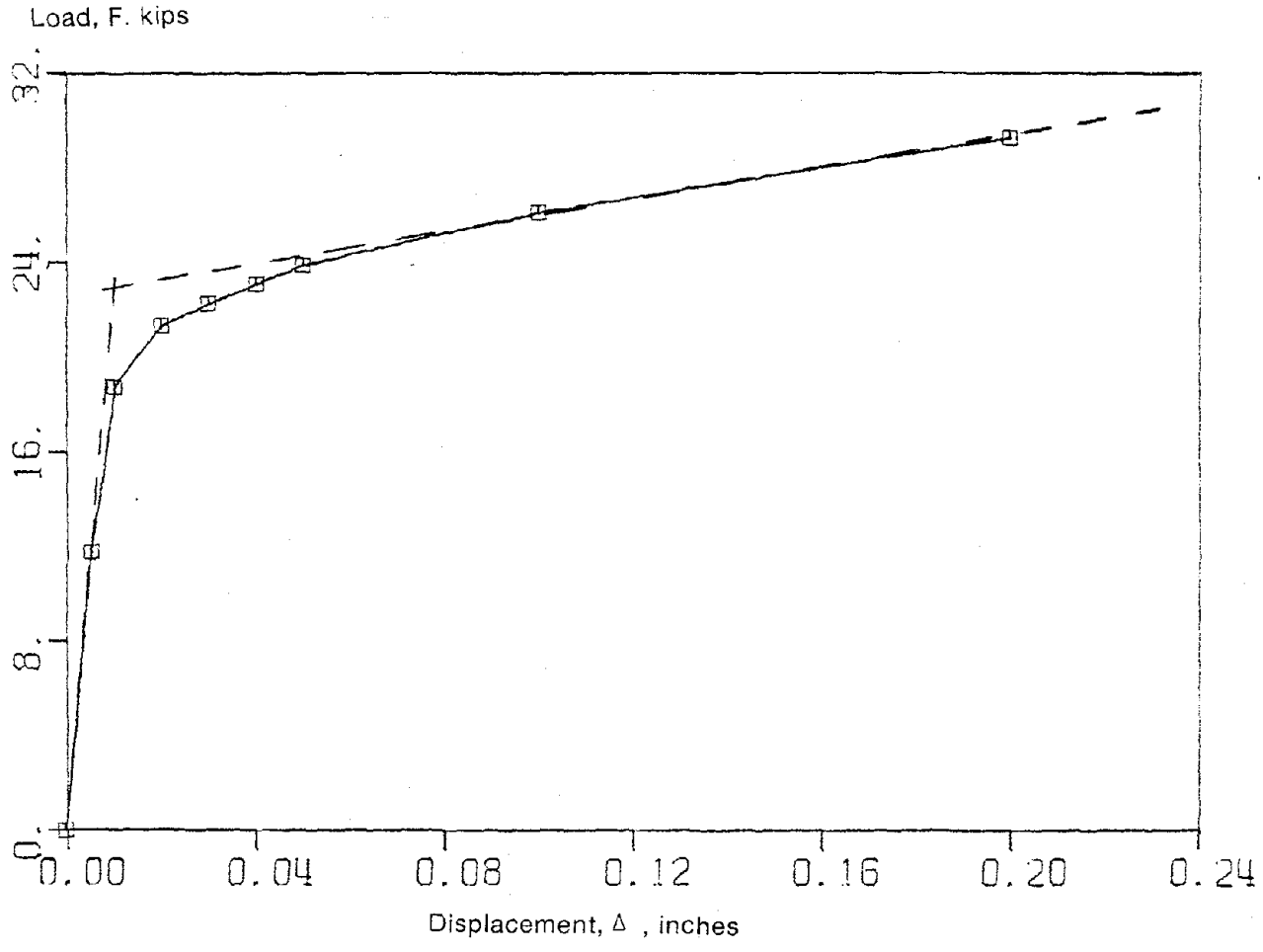

FIG. 4.7 LOAD VERSUS DISPLACEMENT CURVE FOR FLANGE ANGLE FOR MODEL IV.

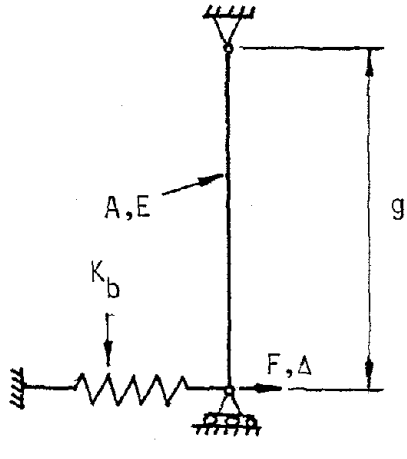

FIG. 4.8 MODEL V — DUAL SPRING MODEL

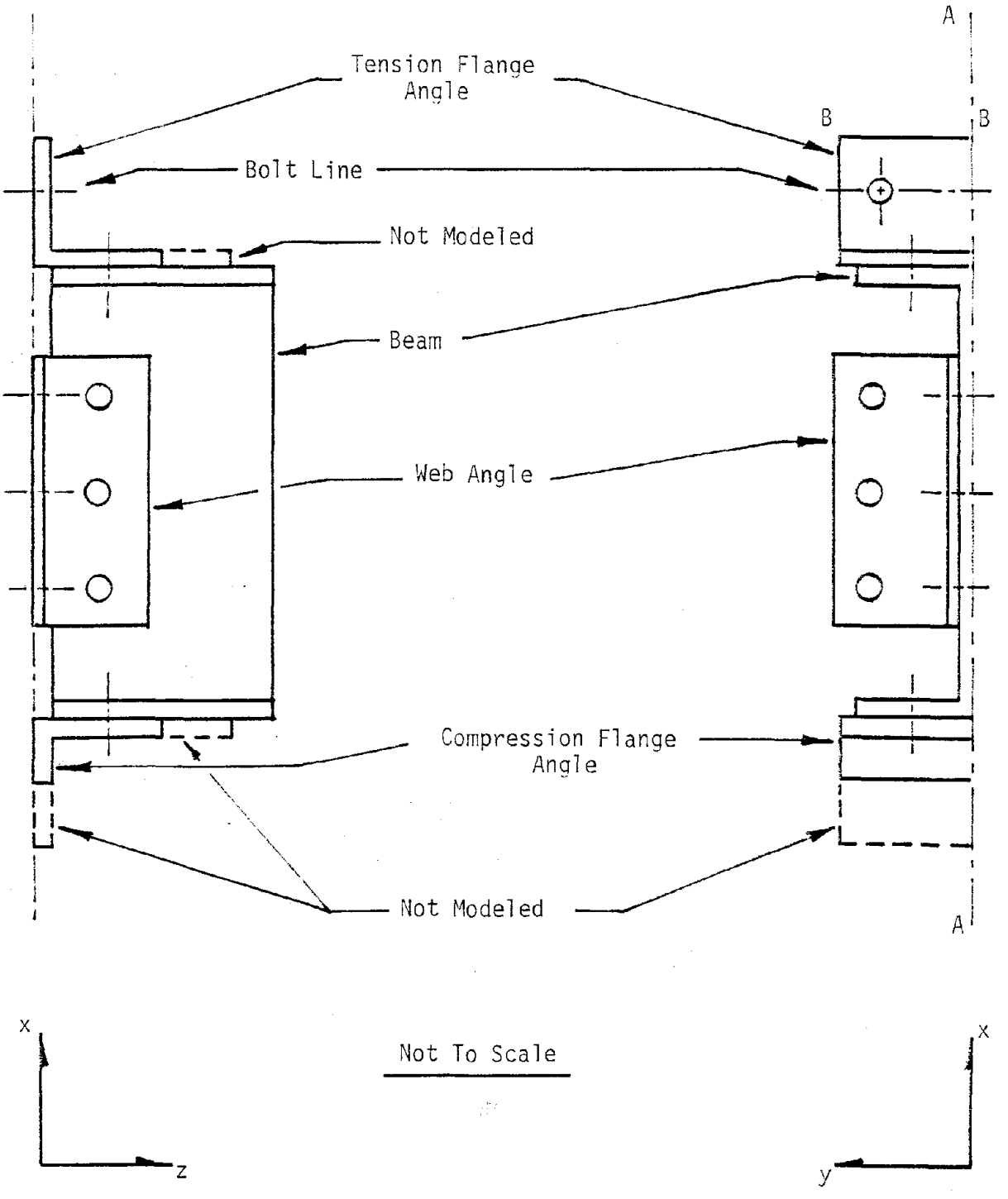

FIG. 4.9 HALF MODEL OF BEAM TO COLUMN CONNECTION MODEL VI

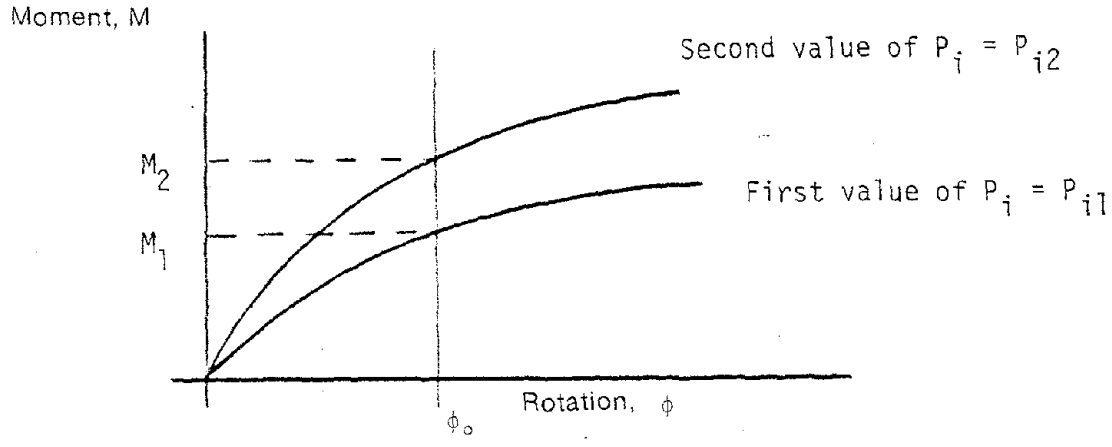

FIG. 4.10 MOMENT—ROTATION CURVES FOR TWO VALUES OF THE PARAMETER Pi

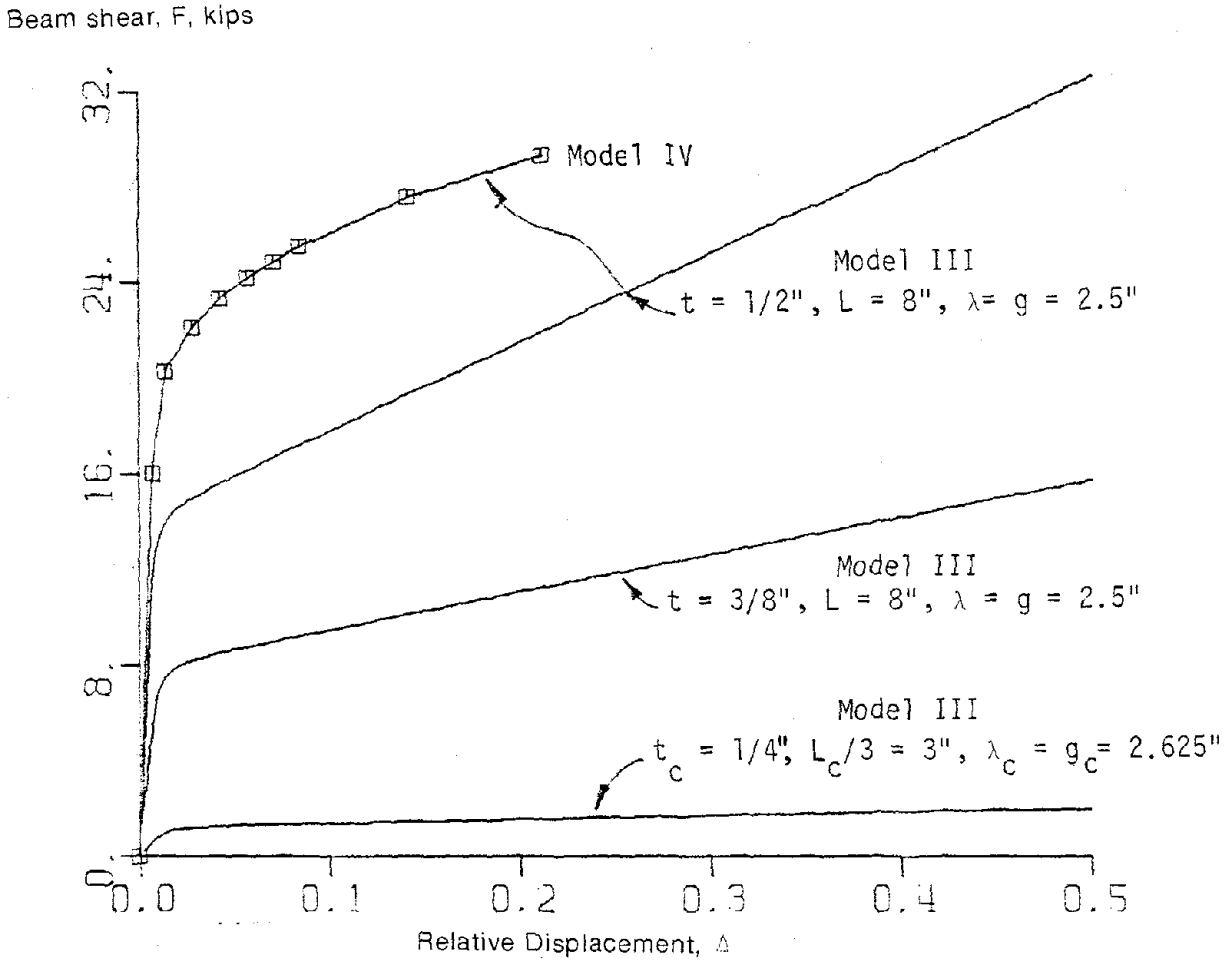

FIG. 4.11 RELATIONSHIP BETWEEN BEAM SHEAR, F, AND RELATIVE END DISPLACEMENT, Δ , FOR FLANGE AND WEB ANGLES

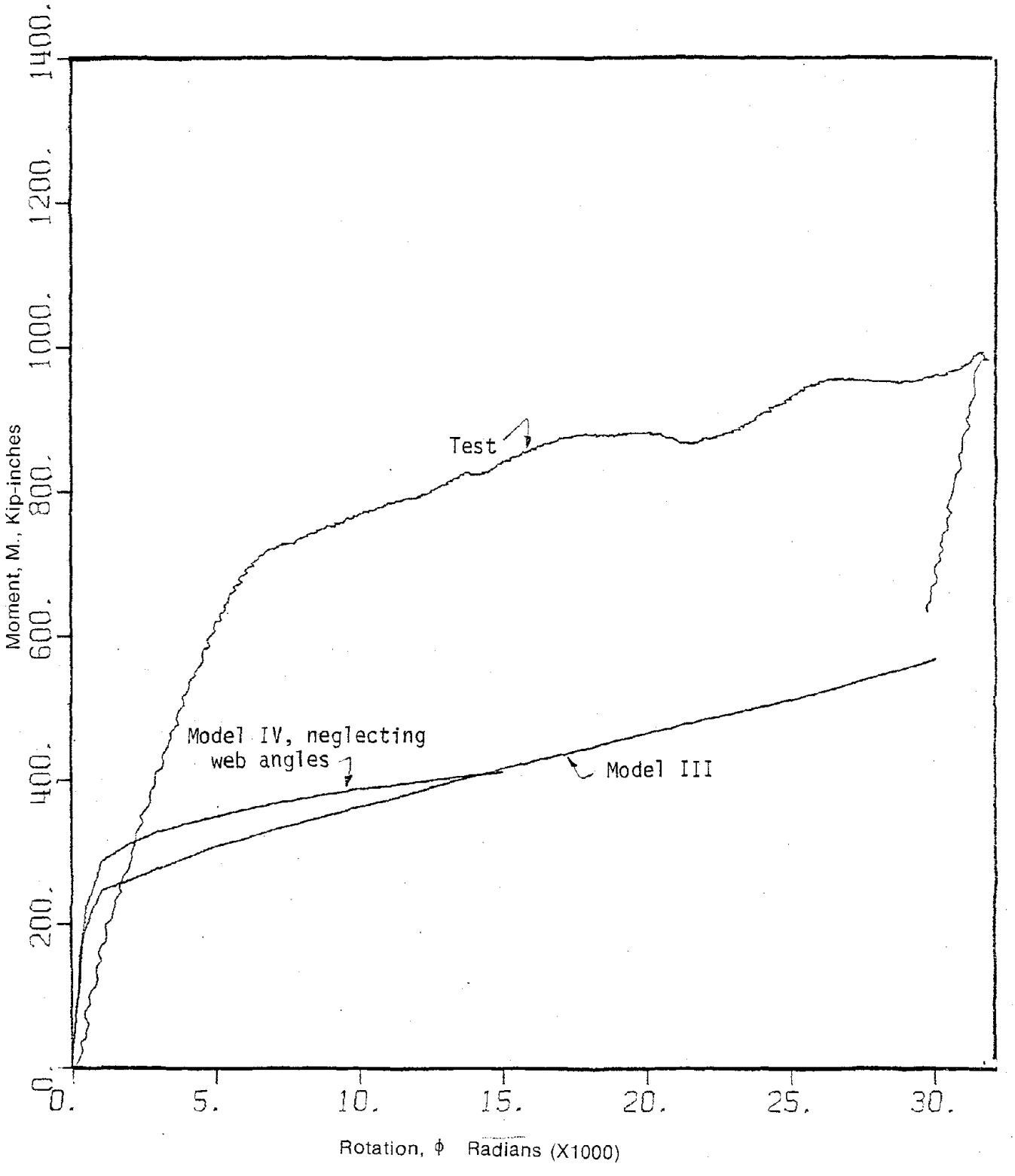

FIG. 4.12 COMPARISON OF MODEL III AND MODEL IV WITH TEST RESULTS FOR SPECIMEN 14S2

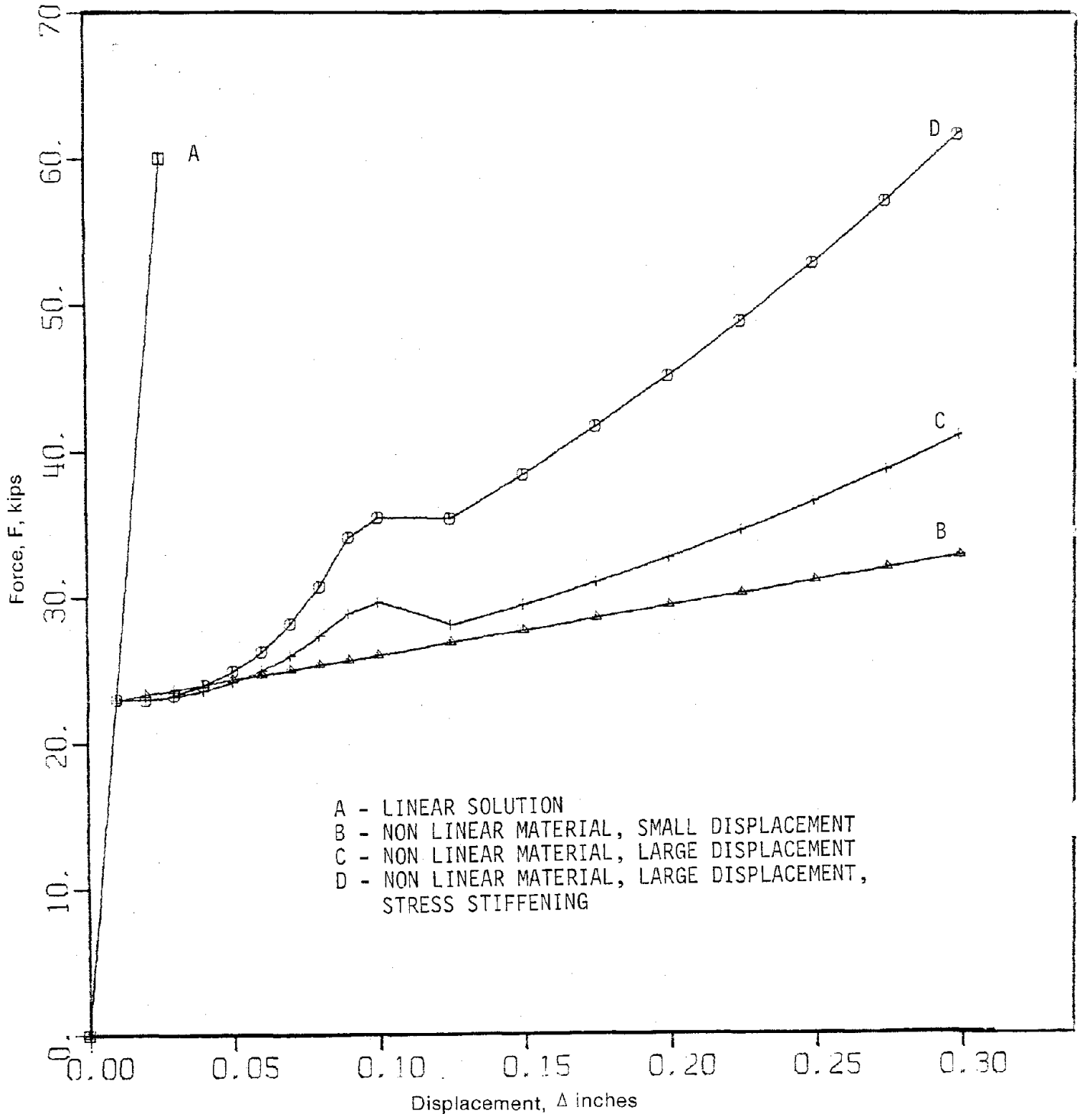

FIG. 4.13 RESULTS OF MODEL V ANALYSIS OF SPECIMEN 14S2 FLANGE ANGLE

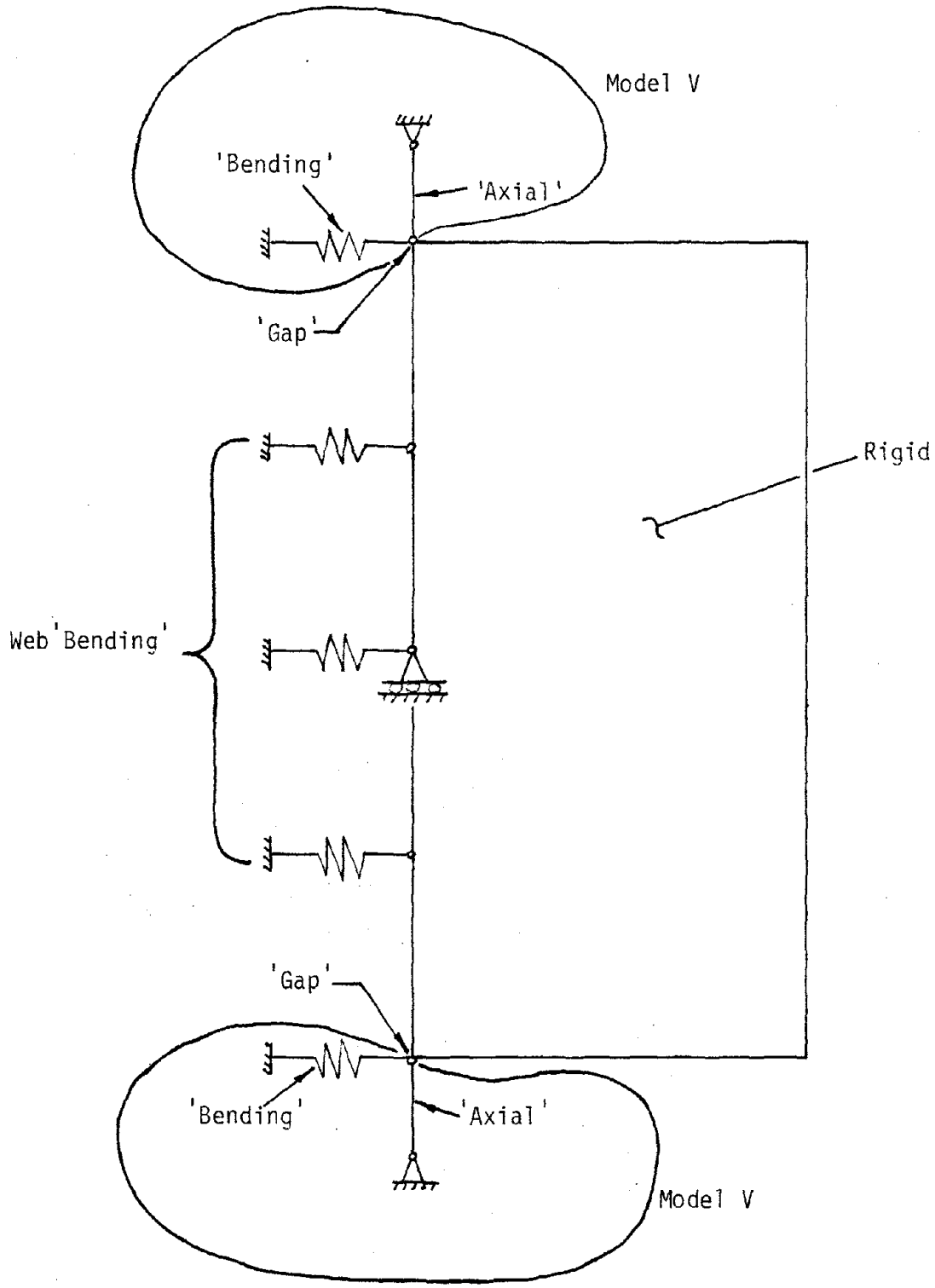

FIG. 4.14 OVERALL CONNECTION MODEL USING MODEL V FOR ANALYSIS BY ANSYS

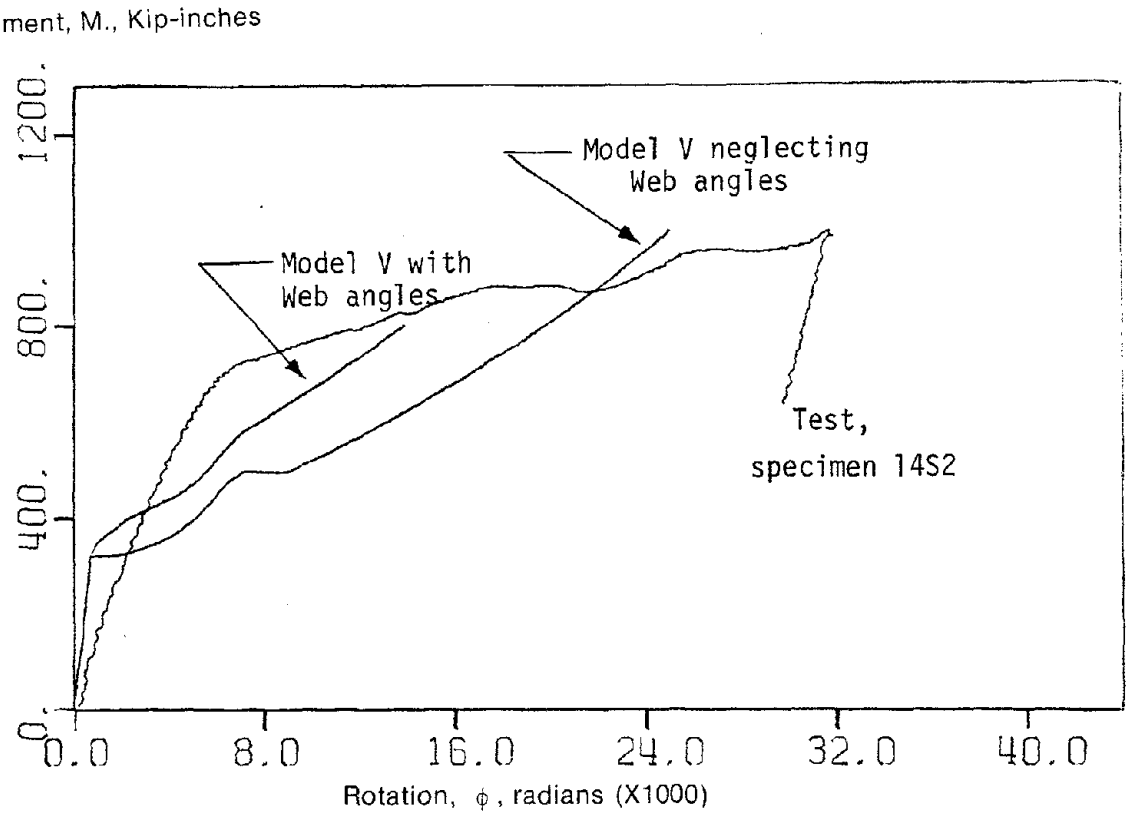

FIG. 4.15 COMPARISON OF TEST RESULTS WITH MOMENT-ROTATION BEHAVIOR PREDICTED BY MODEL V.

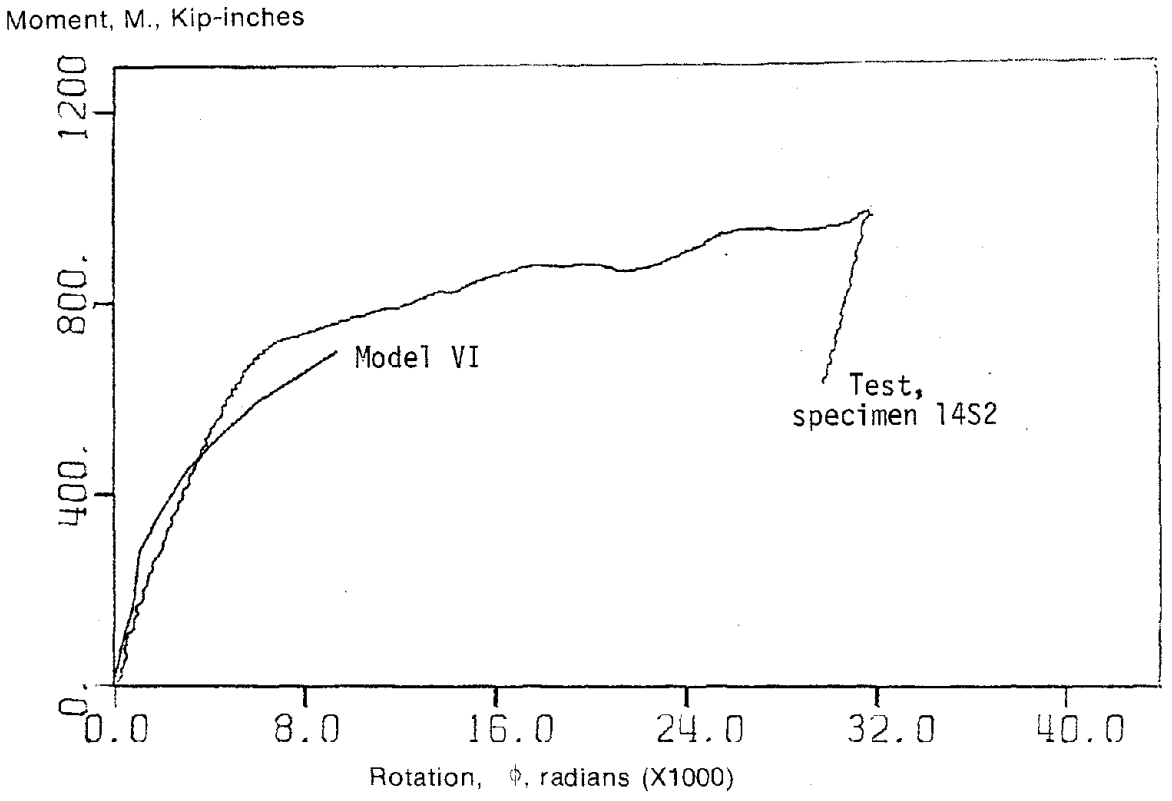

FIG. 4.16 COMPARISON OF TEST RESULTS WITH MOMENT-ROTATION BEHAVIOR PREDICTED BY MODEL VI

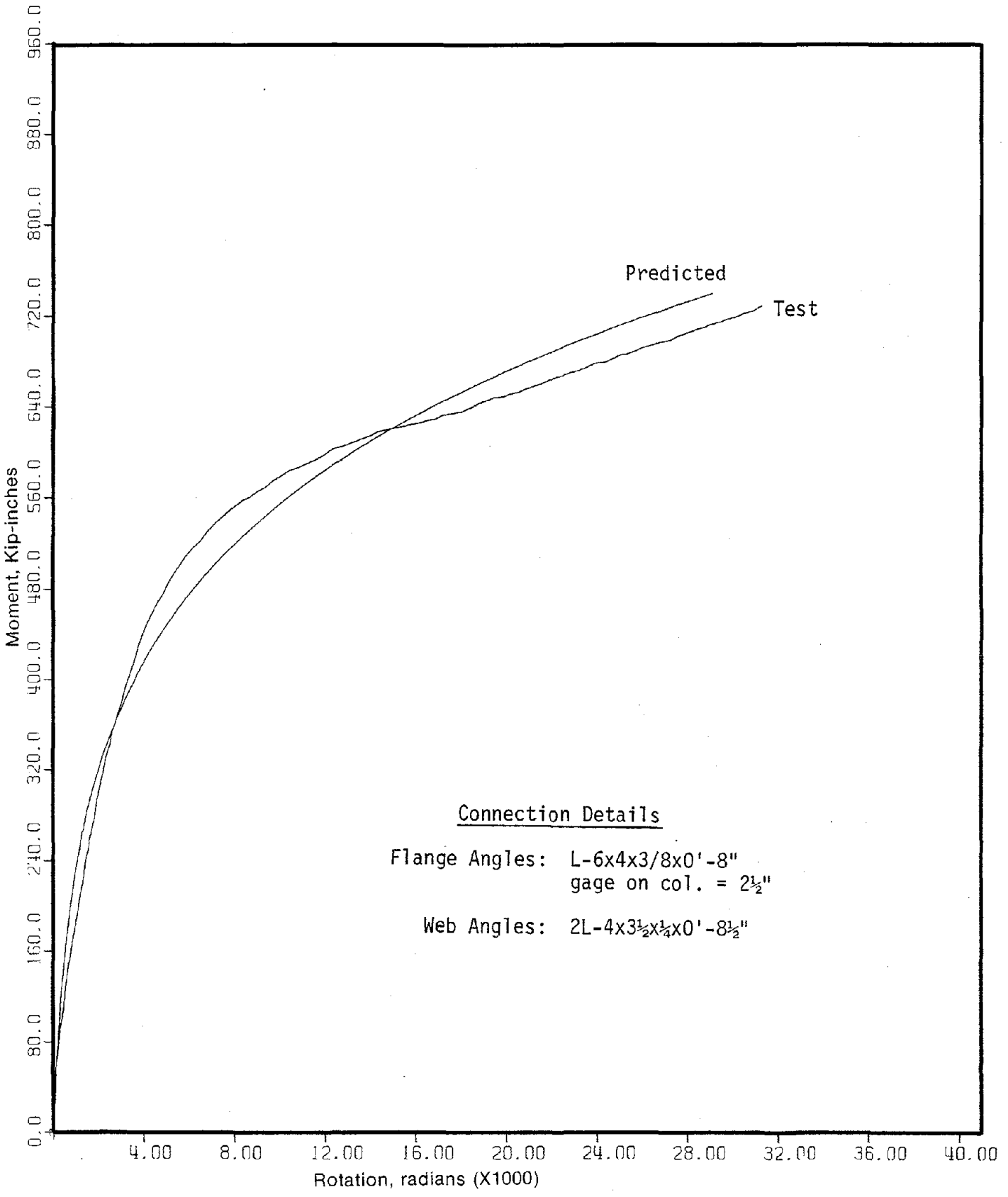

FIG. 4.17a COMPARISON OF MODEL VII WITH TEST RESULTS FOR SPECIMEN 14S1

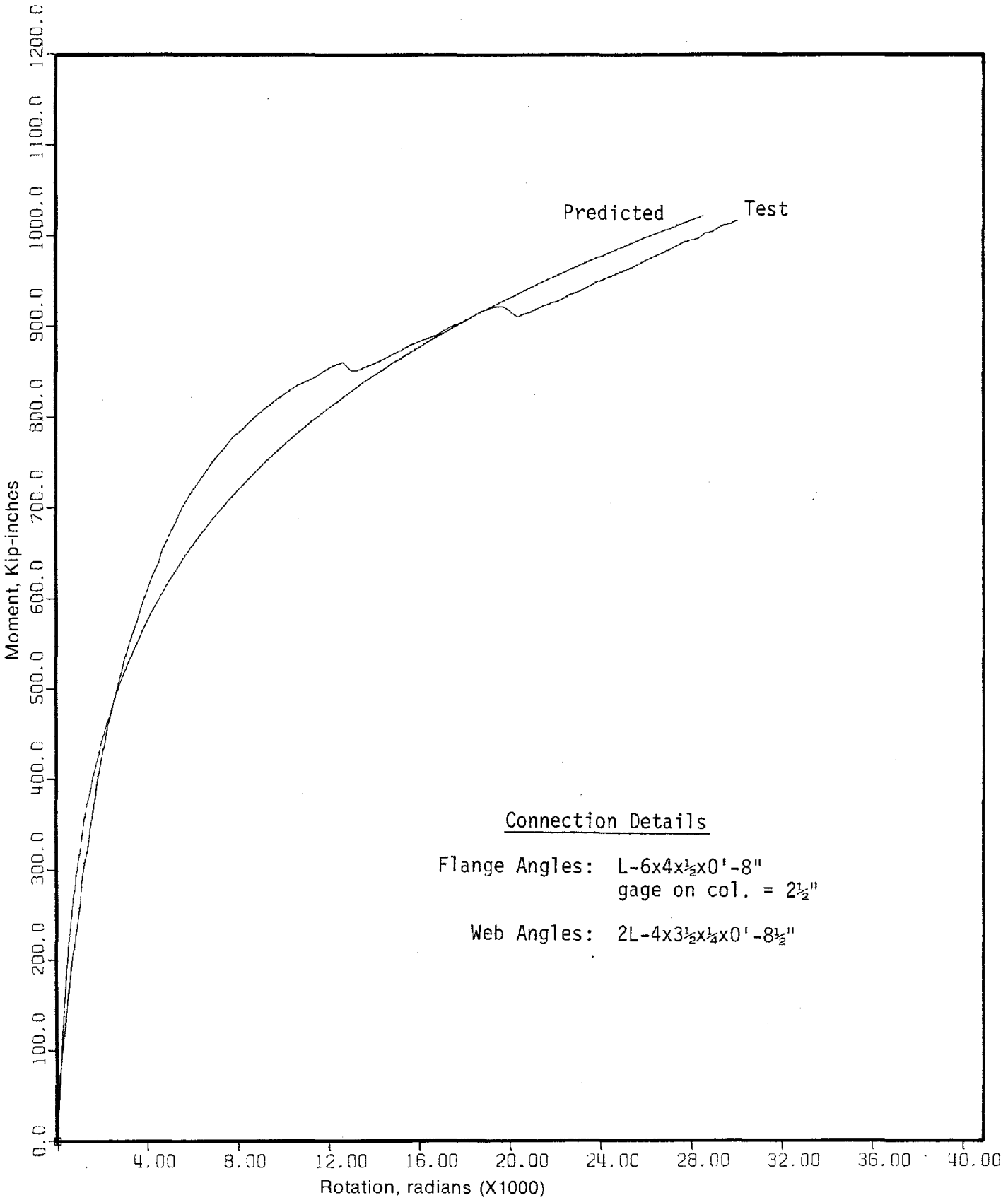

FIG. 4.17b COMPARISON OF MODEL VII WITH TEST RESULTS FOR SPECIMEN 14S2

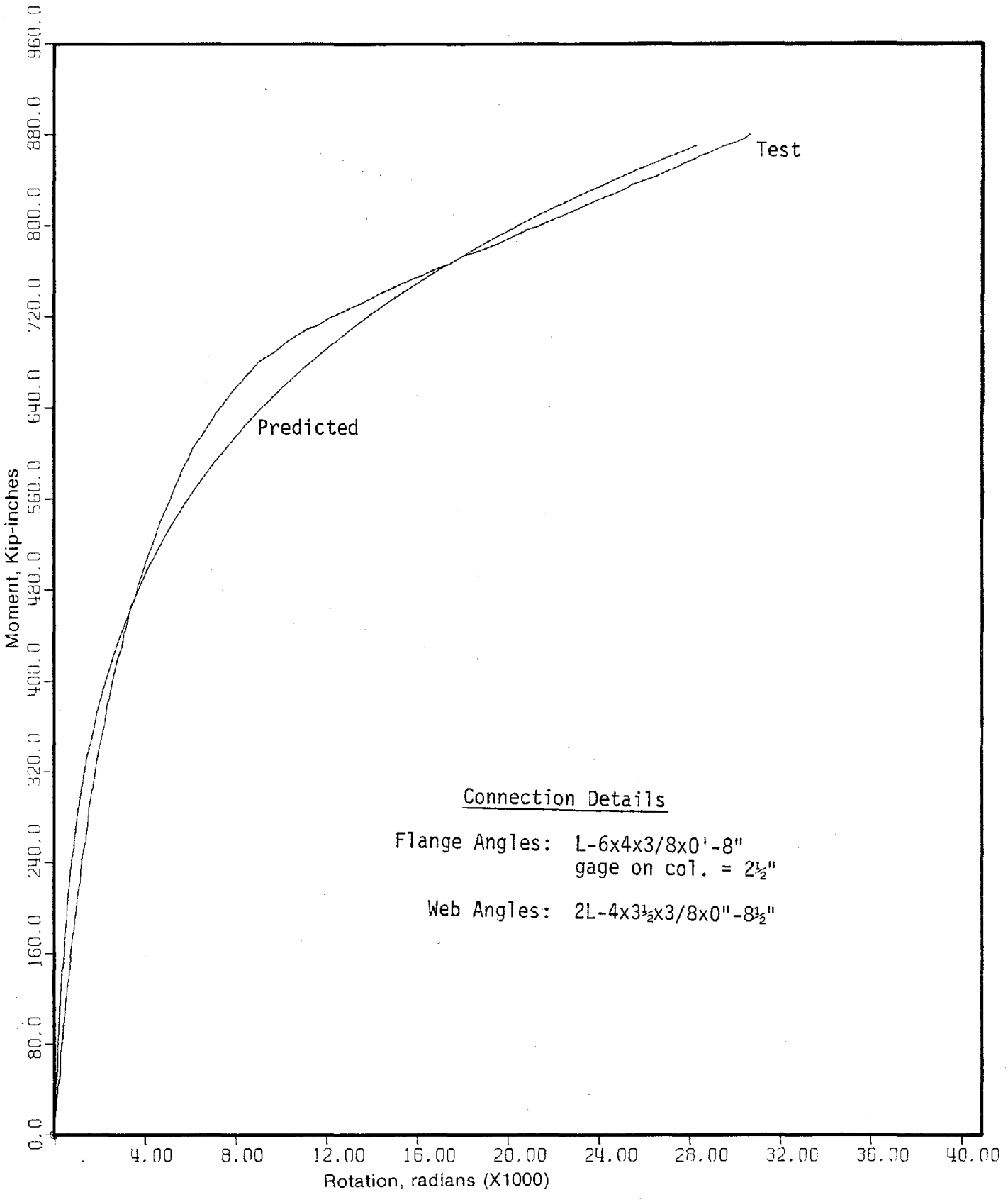

FIG. 4.17c COMPARISON OF MODEL VII WITH TEST RESULTS FOR SPECIMEN 14S4

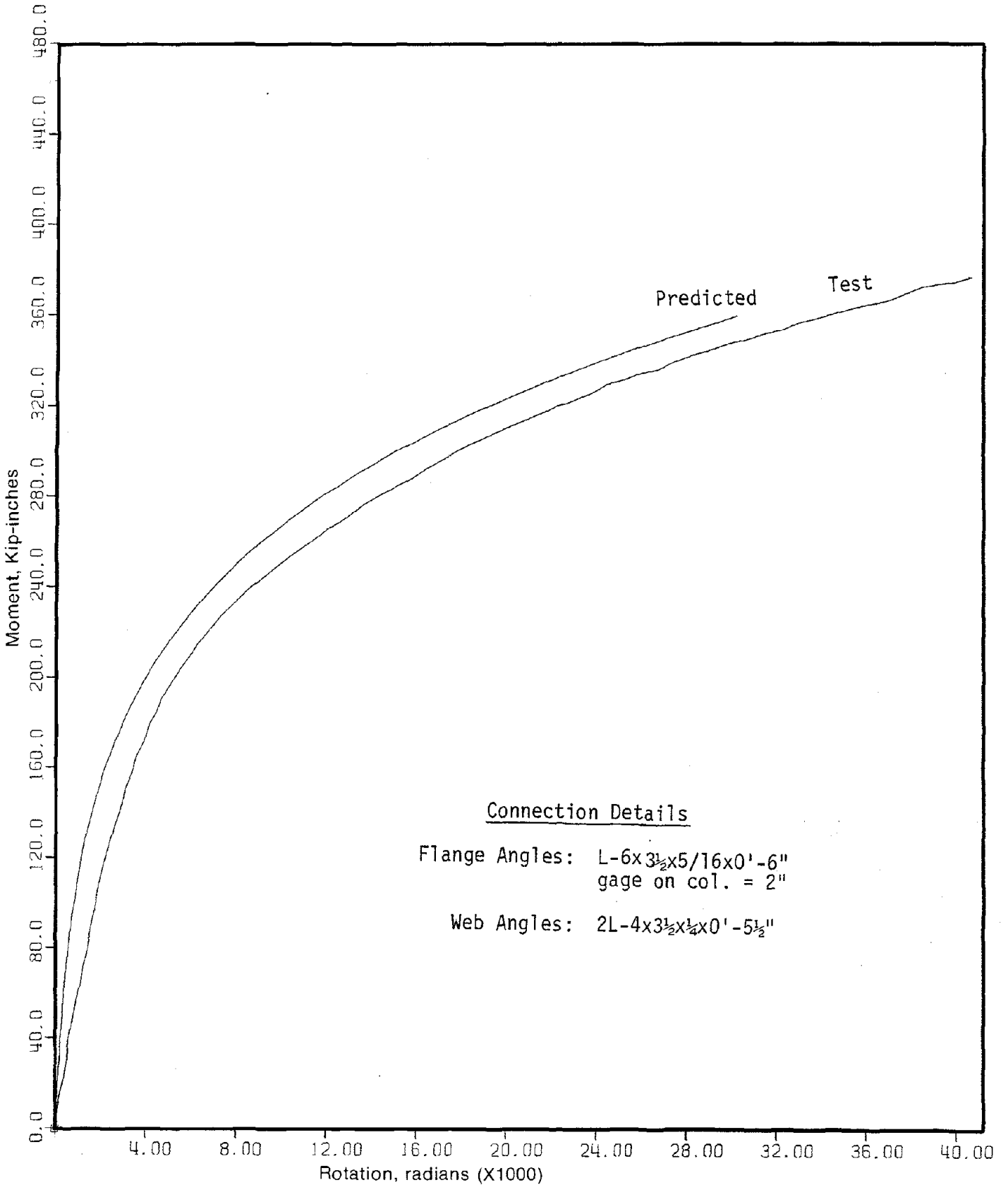

FIG. 4.17d COMPARISON OF MODEL VII WITH TEST RESULTS FOR SPECIMEN 8S1

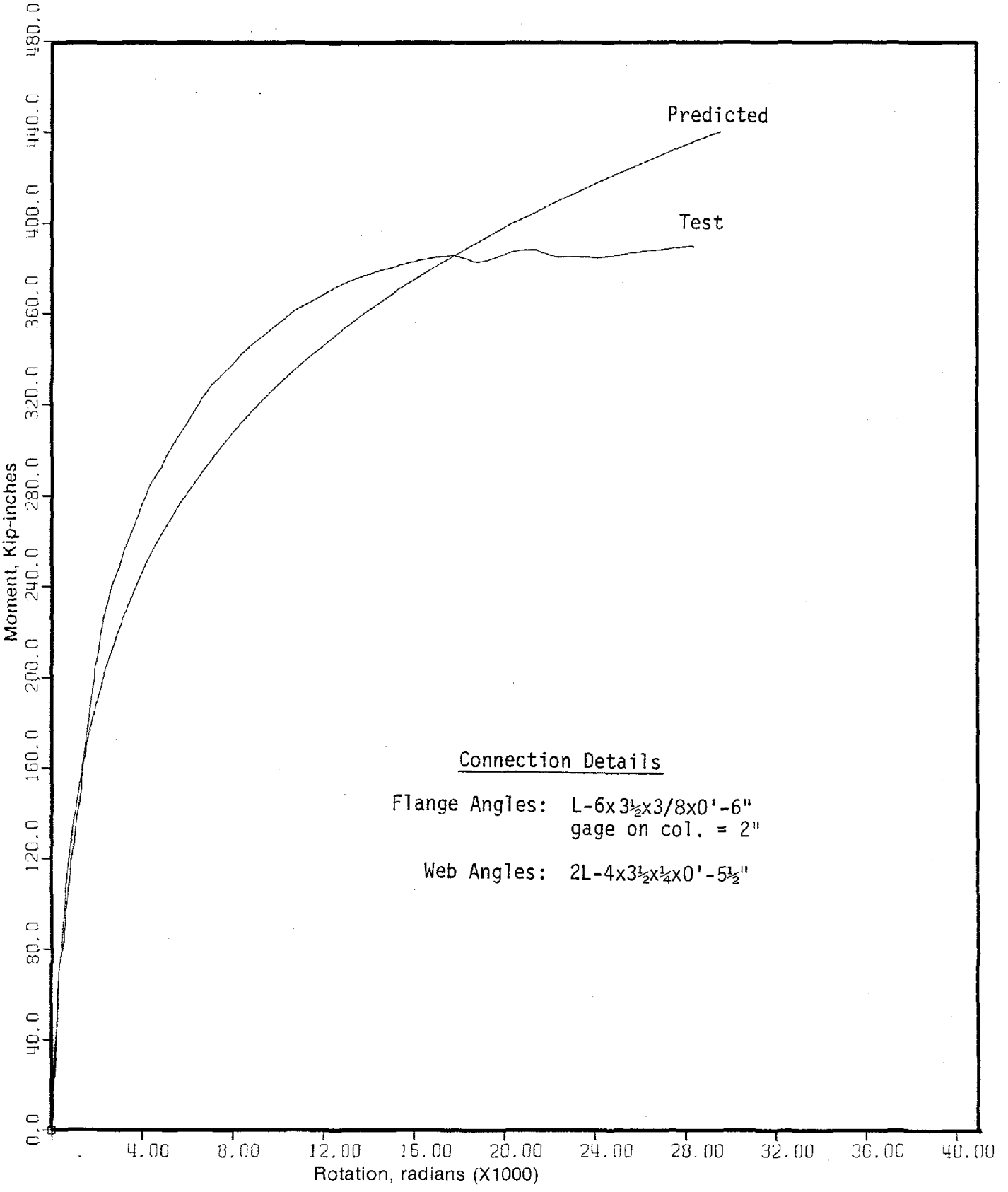

FIG. 4.17e COMPARISON OF MODEL VII WITH TEST RESULTS FOR SPECIMEN 8S2

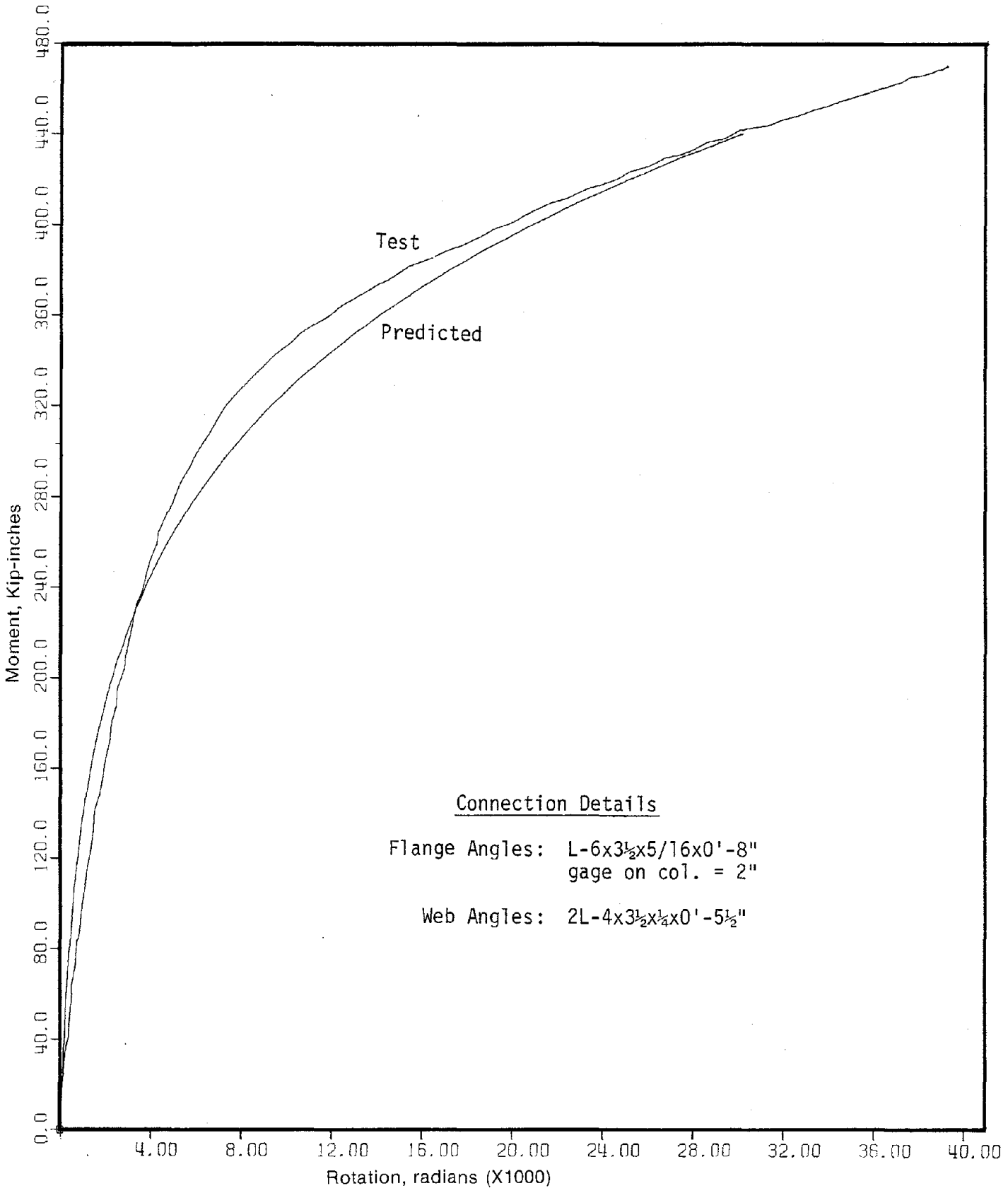

FIG. 4.17f COMPARISON OF MODEL VII WITH TEST RESULTS FOR SPECIMEN 8S3

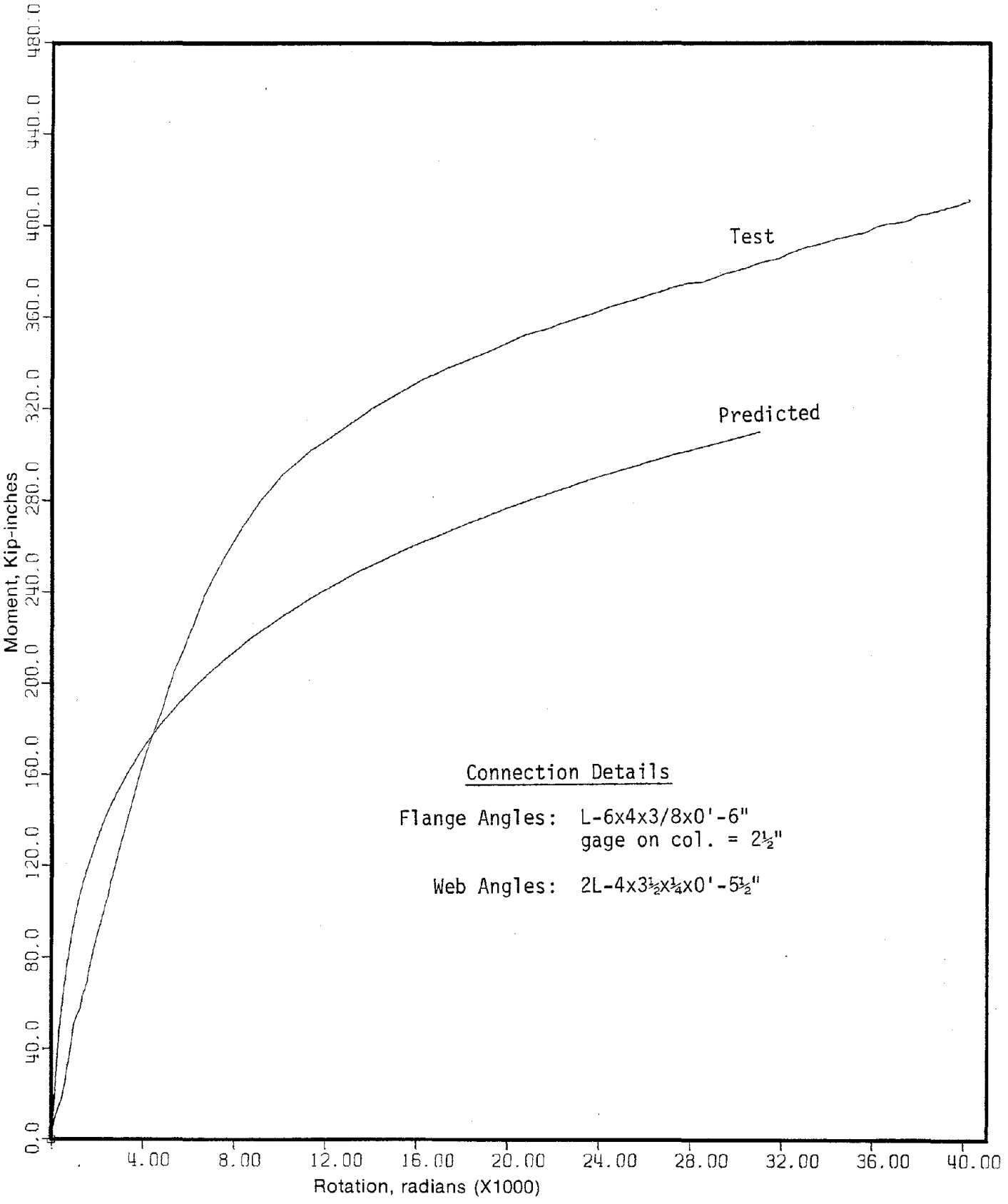

FIG. 4.17g COMPARISON OF MODEL VII WITH TEST RESULTS FOR SPECIMEN 8S7

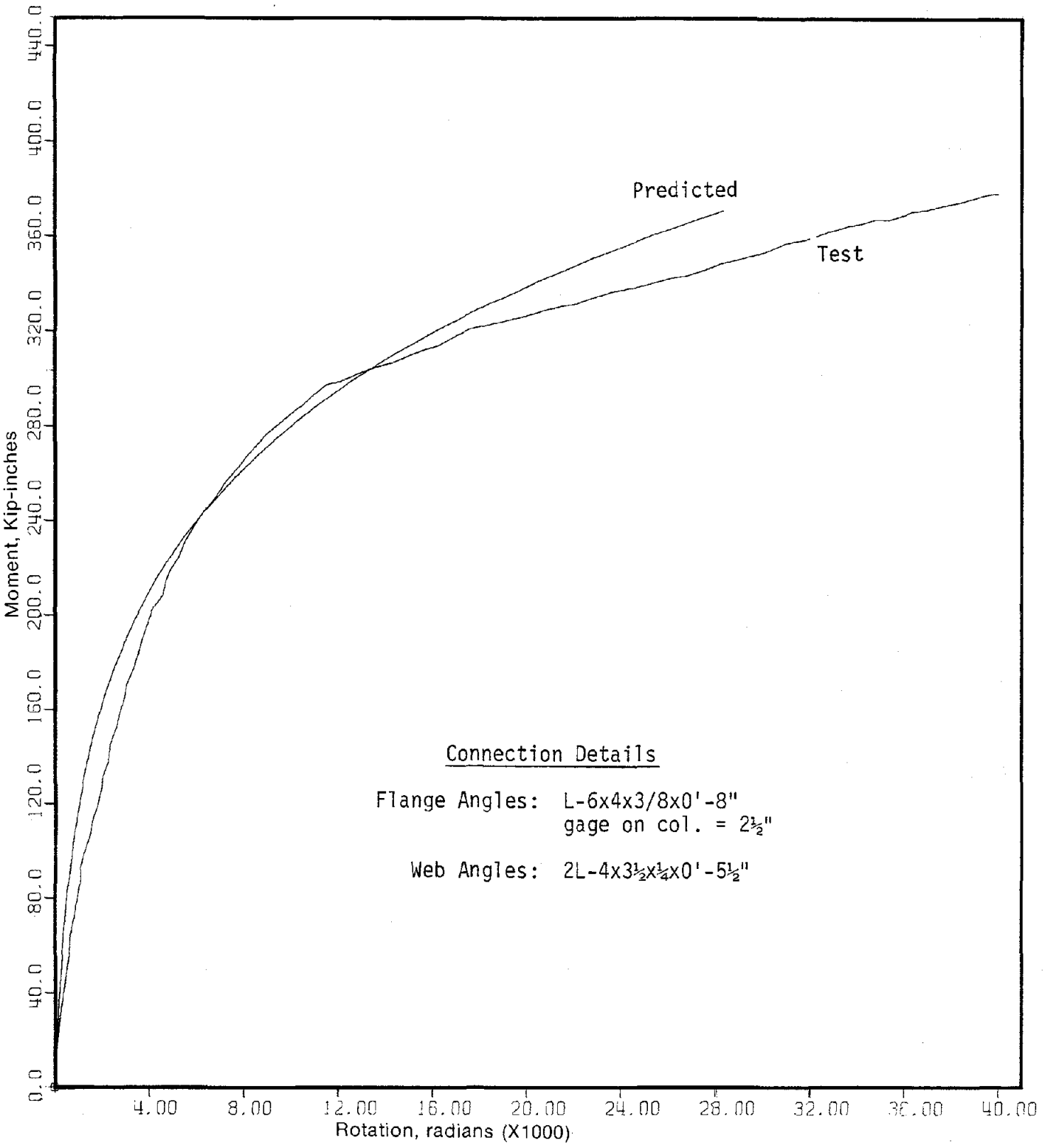

FIG. 4.17h COMPARISON OF MODEL VII WITH TEST RESULTS FOR SPECIMEN 8S5

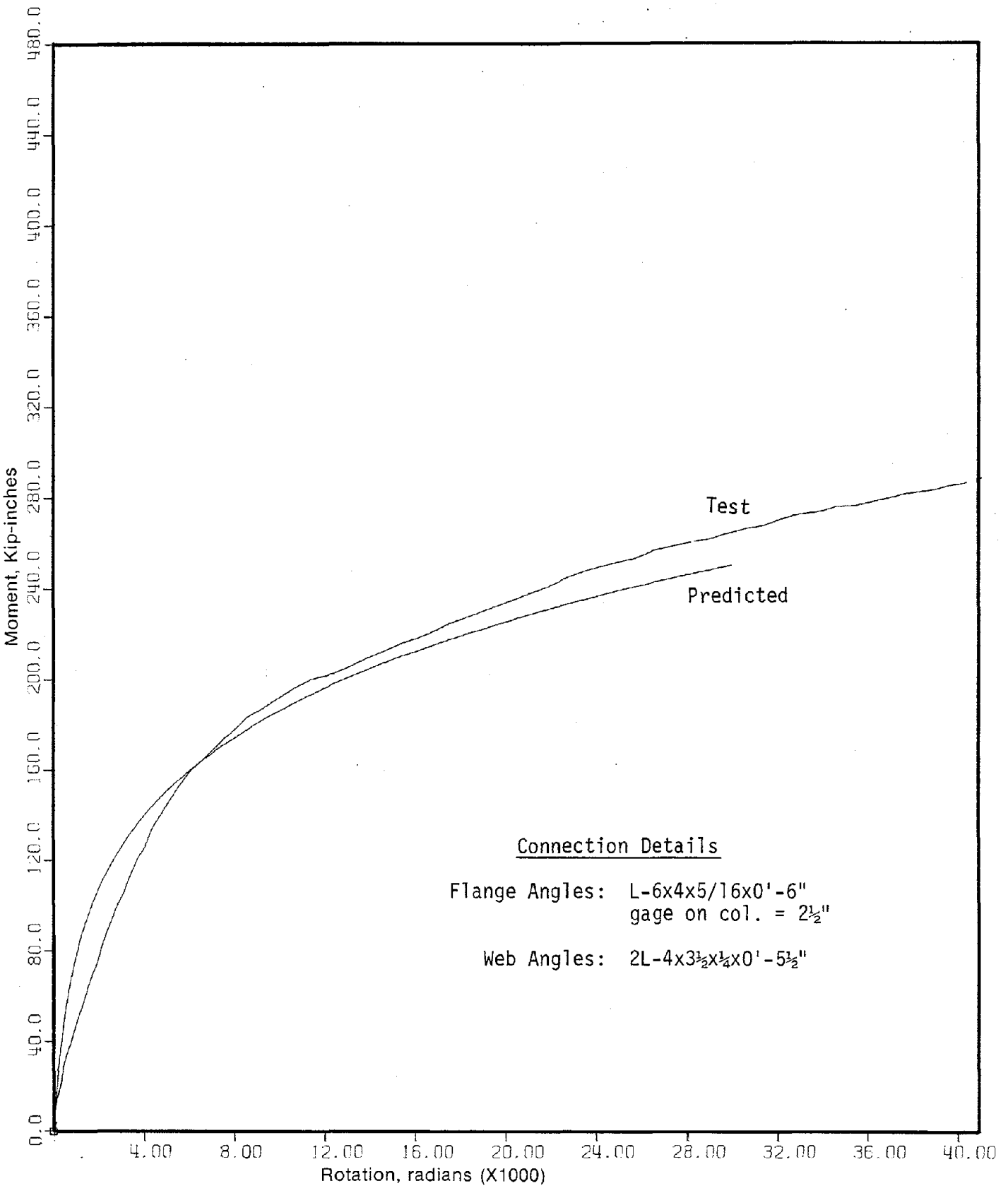

FIG. 4.17i COMPARISON OF MODEL VII WITH TEST RESULTS FOR SPECIMEN 8S6

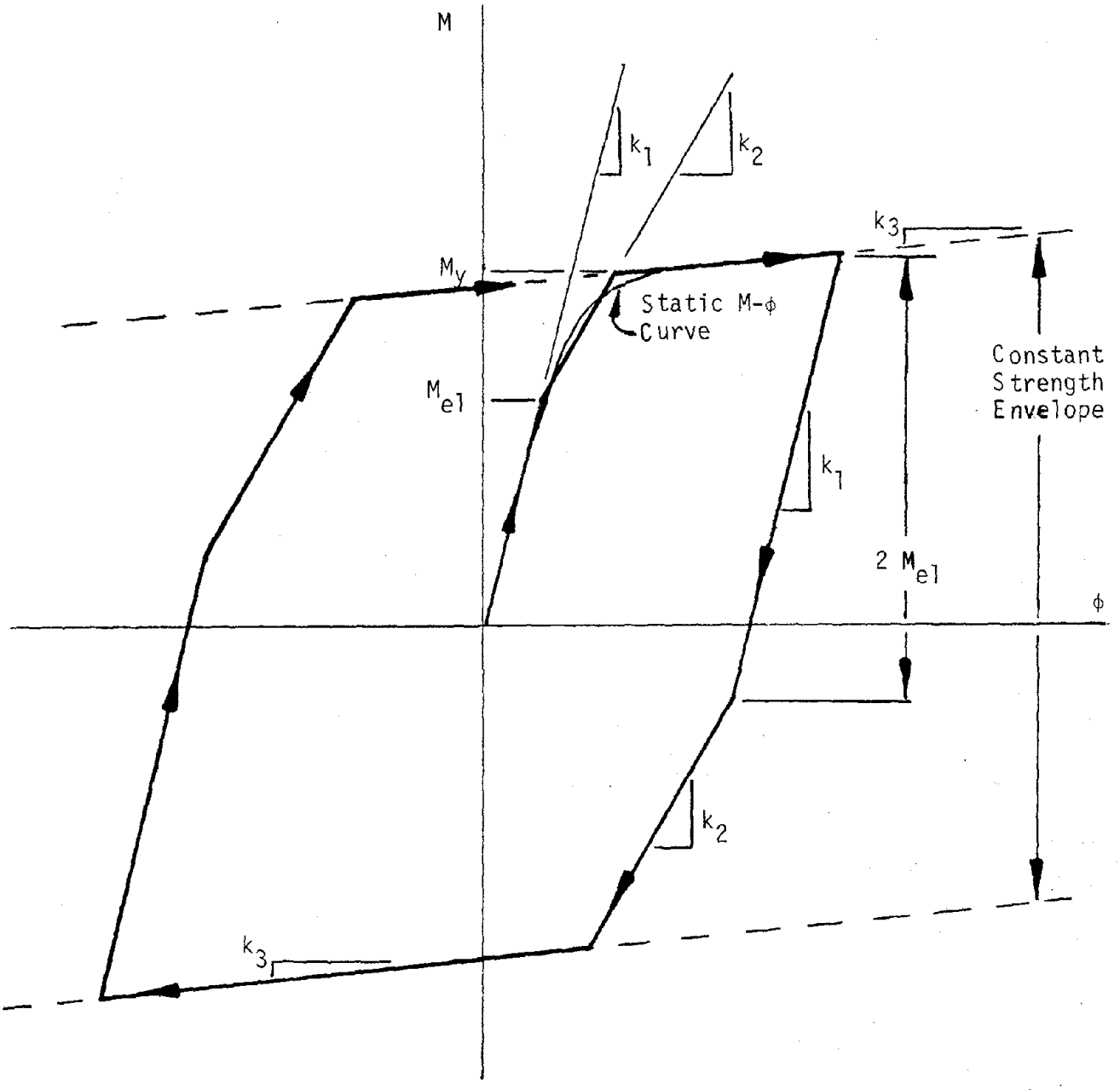

FIG. 4.18 TRI-LINEARIZED MOMENT-ROTATION HYSTERESIS LOOP

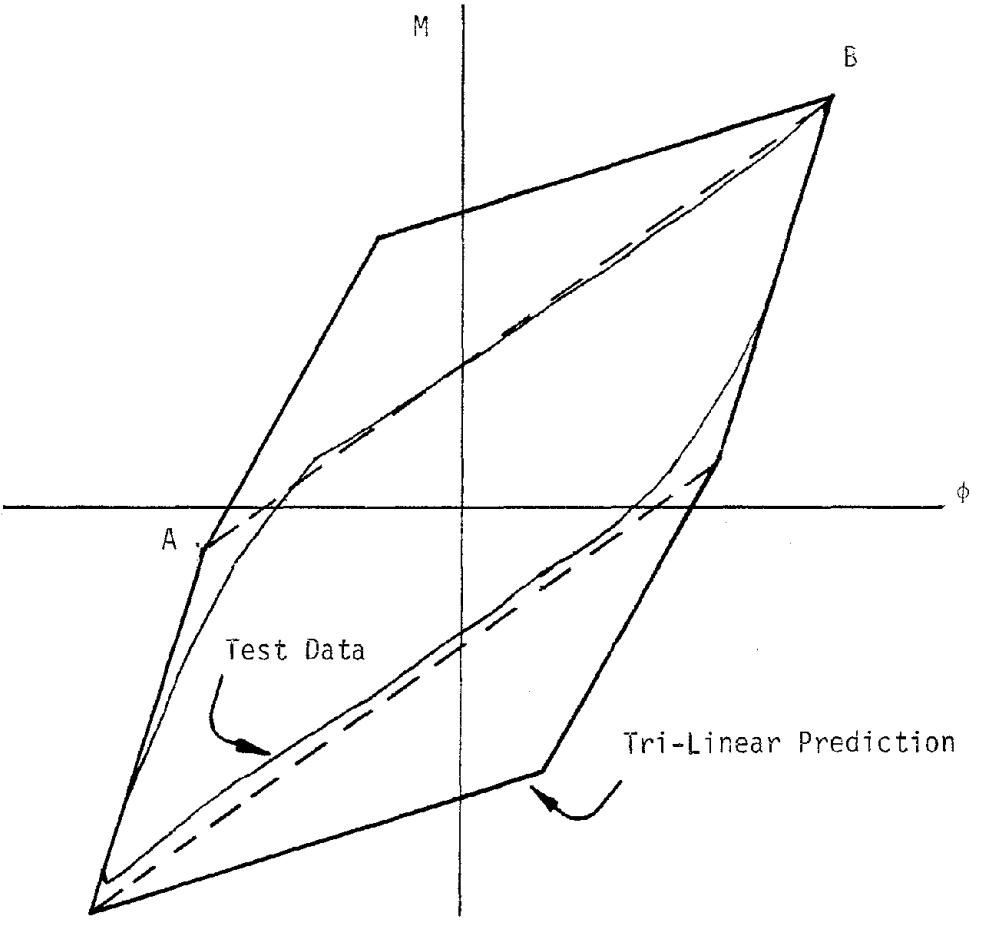

FIG. 4.19 COMPARISON OF TRI-LINEARIZED HYSTERESIS LOOP WITH SPECIMEN 14C2 TEST RESULTS